IMT School for Advanced Studies Lucca

Lucca, Italy

Investigation of Physiological and Pathological Conditions Using Electroencephalographic Connectivity Metrics

PhD Programme in Cognitive, Computational and Social Neurosciences

XXXII Cycle

By

Laura Sophie Imperatori

2019

The dissertation of Laura Sophie Imperatori is approved.

Programme Coordinator: Prof. Pietro Pietrini,
IMT School for Advanced Studies Lucca

Supervisor: Prof. Emiliano Ricciardi,
IMT School for Advanced Studies Lucca

Co-Supervisor: Dr. Giulio Bernardi,
IMT School for Advanced Studies Lucca

Erasmus+ Traineeship Supervisor: Dr. Robin A. A. Ince,
University of Glasgow

The dissertation of Laura Sophie Imperatori has been reviewed by:

Dr. Umberto Olcese,
University of Amsterdam

Dr. Denis A. Engemann,
French National Institute of Computer Science (INRIA)

IMT School for Advanced Studies Lucca

2019

Abstract

Functional connectivity (FC) metrics identify statistical (undirected) associations among distinct brain areas and therefore represent a powerful tool to investigate brain inter-regional interactions in distinct behavioural states. However, the application and interpretation of FC in electrophysiological data is impacted by important confounds related to the instantaneous propagation of electric fields generated by primary current sources to many of the on-scalp sensors – the so-called phenomenon of "volume conduction". Because of this linear mixing of different sources, common FC methods may lead to the identification of apparent couplings that do not reflect true brain inter-regional interactions. To overcome this problem, new FC metrics have been specifically designed to minimize the impact of volume conduction. Among these novel methods, the weighted Phase Lag Index (wPLI) and the weighted Symbolic Mutual Information (wSMI) attracted a growing interest during the last decade, and have been successfully applied to describe brain function in a wide range of different conditions, including states associated with altered levels of consciousness. In spite of the many promising applications and results, the two methods have never been characterized in detail, nor compared to investigate their potential similarities or differences. Given these premises, in the present thesis, my aim was to assess the properties of wPLI and wSMI in order to define their respective potential advantages and disadvantages, as well as to determine whether useful information could be gained through their combined application. To this aim I performed three distinct, complementary studies. In my first project, I simulated

realistic high-density EEG data based on imposed interaction dynamics between sources of interest to test the accuracy of wPLI and wSMI at detecting different types of linear and nonlinear functional interactions. Based on the resulting finding that they provide complementary information, I applied the two methods to the study of EEG data, collected in physiological and pathological states. In my second study, I analyzed power, wPLI and wSMI changes across distinct physiological stages of vigilance, specifically wakefulness (W), NREM and REM sleep in 24 healthy participants. Specifically, I explored the role of power- and FC-based features in identifying differences between all stages of interest (W, N2, N3, REM), stages characterized by higher (W+REM) and lower (N2+N3) probabilities of conscious experiences and differences in sensory disconnection (REM vs. W), using a cross-participant classification paradigm. Finally, in my third study, I applied the two methods for investigating the effects of motor rehabilitation on brain functional correlates in 16 multiple sclerosis patients. Obtained results demonstrated that wPLI and wSMI provide distinct and complementary information about functional brain dynamics and indicate that the conjoint use of these two methods may represent a powerful tool to investigate brain connectivity in physiological and pathological conditions.

Acknowledgements

I am grateful for the guidance I have received from both my three-year-long supervisor, Dr. Giulio Bernardi at the IMT School for Advanced Studies Lucca, and my one-year-long supervisor, Dr. Robin A. A. Ince at the University of Glasgow, who have both supported me in pursuing my research goals. I am very appreciative that both of them allowed me to follow my research interests independently, while at the same time responding to my questions and queries very promptly.

I would also like to thank the other co-authors of the two studies that have already been published and the study that I have presented at the World Sleep Congress 2019.

Firstly, I would like to thank both, Srivas Chennu and Andrés Canales-Johnson, at the Universities of Cambridge and Kent, whom I have been working with previously during my Master's thesis, Francesca Siclari, Lausanne University Hospital, where the EEG data of healthy participants was recorded, as well as Monica Betta, Luca Cecchetti, Emiliano Ricciardi and Pietro Pietrini, IMT Lucca, for their contributions to my first project (see chapter 2 that refers to the same-titled article, published in Scientific Reports (Imperatori et al., 2019)).

Secondly, I would like to thank Caterina Tramonti, Chiara Fanciullacci, Giuseppe Lamola and Carmelo Chisari, University Hospital of Pisa, for collecting the EEG data of and administering the rehabilitative training to the multiple sclerosis patients, Giada Lettieri and Luca Cecchetti for their additional MRI analyses and Emiliano Ricciardi for his feedback to my second article (published in the European Journal of Physical and Rehabilitation Medicine (Tramonti et al., 2018); see chapter 4).

Thirdly, I would like to thank Jacinthe Cathaldi, Monica Betta, Francesca Siclari and Emiliano Ricciardi for their respective roles in data collection and the provision of feedback to my last project, presented at the World Sleep Congress 2019 in Vancouver (see chapter 3).

Moreover, I am grateful for the positive feedback on my thesis from both reviewers, Umberto Olcese and Denis Engemann.

I am thankful for the financial support I have received in form of the PhD scholarship from IMT Lucca and the Erasmus+ traineeship grant from the European Union, as well as for my access to the computational clusters at IMT Lucca and the University of Glasgow, that have enabled me to pursue my research.

I am grateful for having been able to attend several international conferences and a summer school on "Consciousness: From Theory to Practice" with the leading consciousness researchers in the world at the Neuroscience School of Advanced Studies in Venice in 2018.

Finally, I wish to acknowledge the unwavering support and great love of my family and of Luke Milbourn, who have always encouraged me in everything I set out to do.

Vita

February 17, 1992	Born in Frankfurt, Germany
June 2010	Abitur Final mark: 1.0 Internatsschule Schloss Hansenberg, Geisenheim, Germany
October 2011 – June 2015	MSci & BA Honours Degree in Natural Sciences Tripos (Experimental and Theoretical Physics) Final mark: Class II.1 University of Cambridge, Cambridge, United Kingdom
November 2016	Admission to PhD Programme in Cognitive, Computational & Social Neurosciences IMT School for Advanced Studies Lucca, Lucca, Italy
February – September 2019	Erasmus+ Traineeship University of Glasgow, Glasgow, United Kingdom

Publications

1. **Imperatori, L. S.**, Betta, M., Cecchetti, L., Canales-Johnson, A., Ricciardi, E., Siclari, F., ... & Bernardi, G. (2019). EEG functional connectivity metrics wPLI and wSMI account for distinct types of brain functional interactions. Scientific Reports, 9(1), 8894.
2. ***Imperatori, L.S.**, *Tramonti, C., Fanciullacci, C., Lamola, G., Lettieri, G., Bernardi, G., ... & Chisari, C. (2018). Predictive value of EEG connectivity measures for motor training outcome in multiple sclerosis: an observational longitudinal study. *European Journal of Physical and Rehabilitation Medicine.* * Co-first Author (order changed for emphasis).
3. **Imperatori, L. S.**, Milbourn, L., & Garasic, M. D. (2018). Would the Use of Safe, Cost-Effective tDCS Tackle Rather than Cause Unfairness in Sports?. Journal of Cognitive Enhancement, 2(4), 377-387.

Presentations

1. "Cross-participant prediction of vigilance stages through the combined use of wPLI and wSMI EEG functional connectivity metrics"; **L.S. Imperatori**, J. Cataldi, M. Betta, E. Ricciardi, R. Ince, F. Siclari, G. Bernardi; World Sleep 2019, September 20-25 2019, Vancouver, Canada.

Abstracts accepted at (inter-)national Conferences

1. "Cross-participant prediction of vigilance stages through the combined use of wPLI and wSMI EEG functional connectivity metrics"; **L.S. Imperatori**, J. Cataldi, M. Betta, E. Ricciardi, R. Ince, F. Siclari, G. Bernardi; World Sleep 2019, September 20-25 2019, Vancouver, Canada.
2. "Integrity of corpus callosum is essential for the cross-hemispheric propagation of sleep slow waves: a high-density EEG study in split-brain patients"; G. Avvenuti, G. Handjaras, M. Betta, J. Cataldi, **L.S. Imperatori**, S. Lattanzi, B. Riedner, P. Pietrini, E. Ricciardi, G. Tononi, F. Siclari, G. Polonara, M. Fabri, M. Silvestrini, M. Bellesi, G. Bernardi; ; World Sleep 2019, September 20-25 2019, Vancouver, Canada.
3. "EEG connectivity measures wPLI and wSMI identify distinctive differences in brain functional interactions during wakefulness and sleep"; **L.S. Imperatori**, M Betta, E Ricciardi, P Pietrini, F Siclari, G Bernardi; 24th Congress of the European Sleep Research Society, September 25-28 2018, Basel, Switzerland.
4. "Predictive value of EEG-based functional connectivity measures on the outcome of a task-specific rehabilitative treatment in Multiple Sclerosis patients"; **L.S. Imperatori**, C Fanciullacci, C Tramonti, G Lettieri, L Cecchetti, G Bernardi, E Ricciardi, C Chisari; 19th World Congress of Psychophysiology, September 4-8, 2018, Lucca, Italy.
5. "EEG connectivity measures wPLI and wSMI identify distinct types of brain functional interactions"; **L.S. Imperatori**, M Betta, L Cecchetti, A Canales-Johnson, E Ricciardi, F Siclari, S Chennu, P Pietrini, G Bernardi; OHBM Meeting, June 17-21 2018, Singapore.
6. "La connettività funzionale è predittiva del recupero motorio in seguito ad un training task-specifico nella Sclerosi Multipla." C. Tramonti, **L.S. Imperatori**, C. Fanciullacci, S. Di Martino, G. Lamola, G. Lettieri, G. Bernardi, L. Cecchetti, E. Ricciardi, C. Chisari; XVIII Congresso Nazionale SIRN, April 5-7 2018, Trieste, Italy.
7. "Predictive value of EEG-based functional connectivity measures on the outcome of a task-specific rehabilitative treatment in Multiple Sclerosis patients"; **L.S. Imperatori**, C. Fanciullacci, C. Tramonti, S. Di Martino, G. Lettieri, L. Cecchetti, G. Bernardi, B. Rossi, E. Ricciardi, C. Chisari; XXV Annual SIPF Meeting, November 16-18 2017, Rome, Italy.

Contents

List of Figures

List of Tables

Abbreviations

AAFT Amplitude-Adjusted Fourier Transform. 26, 36, 37, 40

AP antero-posterior. 95, 96

AR auto-regressive. 20, 33

AUC Area under the Curve. 96

BBCB Berlin Brain Connectivity Benchmark. 17, 18, 33, 38, 43, 50

CC Cross-Correlation. 34, 35

CSD Current-Source Density. 22, 61, 95

ECoG Electrocorticography. 67, 145–149

EDSS Expanded Disability Status Scale. 93, 102

EEG Electroencephalography. 5, 14, 15, 18–22, 25, 27–29, 36, 41, 50, 52, 53, 124

FC Functional Connectivity. 2, 14, 15, 21, 27, 28, 50, 53, 54, 91, 104, 105

hd-EEG high-density Electroencephalography. 16, 17, 19, 28, 33, 42, 50, 53

ICA Independent Component Analysis. 29, 60, 94

II Interaction Information. 67, 149

INTERH inter-hemispheric. 95–98, 127, 131, 132, 139

LDA Linear Discriminant Analysis. 63, 66, 83

MCS Minimally Conscious State. 16, 54, 137, 138

MEG Magnetoencephalography. 5, 14, 15, 125

MI Mutual Information. 4, 66, 83, 149, 151

MS Multiple Sclerosis. 92, 93, 95, 100–103

N Independence Measure. 34, 35

NREM Non-rapid Eye Movement (Sleep). 12, 28, 53, 75

PID Partial Information Decomposition. 67, 84, 149, 152, 156

PSD Power-Spectral Density. 29, 62

REM Rapid Eye Movement (Sleep). 12, 75

SNR Signal-to-Noise-Ratio. 19, 24, 25, 27, 28, 33, 36, 38–43, 51

TOCT Task-Oriented Circuit Training. 92, 93, 95, 100–102

TUG Timed Up & Go. 94, 96–101

UWS Unresponsive Wakefulness Syndrome. 16, 54, 137, 138

wPLI weighted Phase Lag Index. 7, 8, 10, 15–17, 19, 21–23, 25, 28, 31, 33, 36–55, 62, 73, 74, 104–106

wSMI weighted Symbolic Mutual Information. 7, 9, 10, 15–17, 19, 21–23, 25, 28, 31, 33, 36, 38–41, 43–46, 48–55, 62, 104–106

Chapter 1

Introduction

1.1 Motivation for Investigating Brain Connectivity

The investigation of brain networks in different physiological and pathological conditions is a topic of growing interest in many branches of neuroscience (Sporns, 2011). The classical approach in neuroimaging is to compare uni-dimensional variables extracted from the same spatial location across different conditions. For example, in EEG studies we can compare the power measured at the same sensors across different conditions, while in fMRI we can compare the BOLD-responses in the same regions of interest across different conditions. This uni-dimensional approach has certainly helped us to learn more about brain function. However, as the brain is a multi-dimensional complex system (Stam, 2005), the interactions and co-dependencies between different brain regions (also referred to as 'connectivity') need to be taken into account as well.

1.1.1 Modes of Connectivity

The term connectivity can refer to several different and interrelated aspects of brain organisation (Horwitz, 2003; Sporns, 2007). The key three

modes of connectivity are structural, functional and effective (Friston, 1994). This distinction is applicable to neuronal networks at all time and spatial scales and at all potential levels of organisation (Varela et al., 2001), e.g. from mapping the "functional input connectivity" of individual neurons in vitro (Schubert et al., 2007) to functional networks obtained from seconds- or minute-long windows of neural activity in the macaque neocortex (Honey et al., 2007).

Structural connectivity

Structural connectivity refers to a network of anatomical (synaptic) connections between different neurons. While the physical pattern of anatomical connections is relatively stable at shorter time scales (seconds to minutes), they are likely to be subject to significant morphological change and plasticity at longer time scales (hours to days) (Sporns, 2015).

Structural connectivity analyses rely on either invasive tracing studies to find direct axonal connections (Köbbert et al., 2000) or on diffusion weighted imaging techniques, such as Diffusion Tensor Imaging, which is useful as whole-brain, in vivo markers of temporal changes in fibre tracts, but has a much lower spatial resolution (Hagmann et al., 2008).

Functional Connectivity

Functional Connectivity (FC) metrics identify statistical (undirected) associations among spatially distinct brain areas. As statistical patterns between neuronal elements fluctuate on multiple time scales, some as short as tens or hundreds of milliseconds, FC is highly time-dependent. Importantly, FC does not make any explicit reference to specific directional effects or to an underlying structural model unlike structural of effective connectivity (Friston, 1994). However, structural connectivity places constraints on which functional interactions occur in the network (Bullmore and Sporns, 2009).

Effective connectivity

Effective connectivity aims to infer causal effects of one neural component over another. Therefore, unlike to functional connectivity, directed neural networks are of interest. While causal effects can only be truly inferred through systematic perturbations of the system, approximations that rely on the assumption that causes must precede effects in time are also employed in time series analysis (Bastos and Schoffelen, 2016).

Some techniques for extracting effective connectivity require the specification of a model including structural parameters, for example Dynamic Bayesian Modelling. Most applications of Granger causality rely on a linear auto-regressive model fit to the data (Bastos and Schoffelen, 2016). On the contrary, transfer entropy is a generalised, model-free, information-theoretic approach to study delayed (directed) interactions between time series (Schreiber, 2000).

1.2 Common Functional Connectivity Metrics in Electrophysiology

Oscillatory synchronisation has been suggested as a key mechanism by which neural populations transmit information to form larger networks (Fries, 2005; Salinas and Sejnowski, 2001; Singer, 1993). Oscillations can be characterised by their frequencies (speed/ occurrences per second) and amplitudes (magnitudes of change w.r.t. their equilibrium positions). The phase of an oscillation can tell us the current position in the repeating cycle. Phase and power (proportional to the square of the signal's amplitude) are mostly independent measures and therefore likely reflect different neurophysiological dynamics, with phase being hypothesised to be sensitive to the timing of activity within a neural population and power to account for the number of neurons or spatial extent of the neural population (Cohen, 2014).

Therefore, statistical dependencies can be considered between the amplitudes and/or phases of the different signals. There are various different ways of assessing these statistical dependencies, or the synchronisa-

tion among spatially distinct brain areas. All of these approaches can be summarised under the term of functional "connectivity" metrics (Cohen, 2014). The best methods to capture brain oscillations non-invasively are electro- (EEG) and magnetoencephalography (MEG).

1.2.1 Phase-Based Metrics

The most common method of assessing linear correlations between EEG signals is coherence, computed as the cross-spectral density of two signals, which uses the Fourier transform of their cross- correlation (Sakkalis, 2011). The phase values are weighted by power values, implying that results from spectral coherence are likely to be influenced by strong increases or decreases in power. For example, if connectivity increases but power simultaneously decreases, spectral coherence may provide biased results (Lachaux et al., 1999).

As synchronisation between different brain areas is often only dependent on phase, the phase locking value (PLV) (Lachaux et al., 1999) has been developed to only detect phase synchronisations between two signals. However, both of these metrics are susceptible to volume conduction, which is explained in more detail in section 1.3.1.

1.2.2 Information-Theoretic Metrics

Mutual Information (MI) is a simple, yet robust method of detecting shared information between two variables (see Appendix C). It is computed based on the distributions of values within variables and the joint distribution of two (or more) variables. Mutual Information has the key advantage of being sensitive to linear as well as non-linear interactions, that standard correlation metrics would fail to identify. For example, a circle has a correlation coefficient of zero but a mutual information value greater than zero (Ince et al., 2017; Timme and Lapish, 2018). Although it is a widely used signal-processing technique, it does not have a straightforward neurophysiological interpretation (Cohen, 2014).

1.3 The problem with zero-lag connectivity

Electroencephalography (EEG) and Magnetoencephalography (MEG) represent popular neuroimaging modalities for the estimation of functional connectivity (FC) owing to their high temporal resolution, in the order of milliseconds. However, both EEG and MEG suffer from volume conduction, as sources in the brain generate large electromagnetic fields that are measured by more than one EEG electrode or MEG sensor, introducing spatial auto-correlation at the sensor level. Therefore, even though there can be physiological zero-lag connectivity (Gollo et al., 2014; Roelfsema et al., 1997), it cannot be unambiguously identified with EEG and MEG (see appendix A for more background information on M/EEG).

1.3.1 Volume Conduction

The 'volume conduction' phenomenon depends on the fact that electrical signals propagate throughout brain tissues reaching scalp electrodes in different locations. Therefore, at a given instant in time, the different EEG/MEG sensors capture a weighted sum of the activities of all brain sources. Moreover, signal propagation due to volume conduction is virtually instantaneous in comparison to the timescales of neural transmission within the brain. Thus, volume conduction enhances the degree of instantaneous coupling between channels independently of the actual brain source interaction. This leads to all channels to appear to be highly coupled with all others, even if only two interacting sources are simulated (Pizzella et al., 2014). More generally, a single detectable source (e.g., a set of synchronously firing pyramidal neurons) with a fixed amplitude and orientation induces field patterns on all sensors. In a noise-free case, this would imply that the covariance matrix across sensors has rank 1, i.e. that its column/row vectors are linearly dependent with respect to each other. This is illustrated by the widespread topographies of the auditory and somato-sensory evoked potentials, due to localised brain activations in the auditory and somato-sensory cortices respectively (Scherg et al., 2019). Any detectable (primary current) source is related to the movement of ions due to their chemical concen-

tration gradients (Hämäläinen et al., 1993). Passive Ohmic currents, also referred to as volume current, are set up in the surrounding medium to avoid a build-up of charge. The magnetic field is then generated by both the primary and volume currents. If the primary source and the surrounding conductivity distributions are known, the resulting electrical potential and magnetic field can be calculated from Maxwell's equations, that describe the spreading of all electromagnetic fields. [1]

The mathematical problem of projecting the relevant sources in the brain to the resulting field patterns in the sensor space is called the 'Forward Problem'. It provides an an answer to the question of what activity would look like on the scalp, given activation of one dipole in the brain (Cohen, 2014). For fields of physiological origin, frequencies are usually low (less than a few thousand Hz), such that magnetic induction (Faraday's law) has a negligible effect on the electric field, leading to the electro-quasistatic approximation of Maxwell's equations (Gratiy et al., 2017; Haus and Melcher, 1989; Plonsey and Heppner, 1967; Rosenfalck, 1969). [2]

In addition, the displacement current (including a time derivative) can be considered to be much smaller than the Ohmic currents and can therefore also be neglected, leading to the magneto-quasistatic approximation (Hämäläinen et al., 1993). [3]

The quasistatic approximation of Maxwell's equations then enables us to reduce the Forward Problem of the EEG to three steps: firstly to set up the current sources, secondly to solve Poisson's equation with the

[1] Interestingly, based on the physics underlying electromagnetism, MEG and EEG field distributions are mutually orthogonal. Moreover, MEG (in contrast to EEG) can only detect sources with currents that have a component tangential to the surface of a spherically symmetric conductor, while radial sources do not lead to a visible magnetic field outside the head. (Hämäläinen et al., 1993)

[2] Moreover, the macroscopic velocity u of ions in the brain and the magnetic fields of physiological origin are so low that the magnetic component of the Lorentz force $F = q(E + u \wedge B)$ is negligible, i.e. the magnetic field has a negligible effect on the motion of free charges as compared to the effect of the electric field. Neglecting the magnetic induction and the magnetic component of the Lorentz force results in considering the current density as independent of the magnetic field.

[3] The displacement current is responsible for the capacitive charging of neural membranes (Gratiy et al., 2017).

relevant boundary conditions to thirdly obtain the potentials at the scalp.

Importantly, at a boundary between different media (with different permittivities), field lines lines are diverted, i.e. electric fields spread tangentially at the skull-scalp boundary, which has a smearing effect (Nunez et al., 2006) on the surface potential distribution. The magnetic permeability of biological tissues is almost the same as that of empty space. Hence, the magnetic field is not distorted by scalp or skull (Singh, 2014).

Therefore, EEG, but not MEG, is also affected by the lateral spread of electrical fields through head tissues (cerebro-spinal fluid (CSF), skull, and scalp etc.), especially to neighbouring electrodes(Cohen, 2014), while magnetic fields pass through these tissues undisturbed.

However, the linear mixing of signals at the sensor level applies to both MEG and EEG and may therefore lead to the identification of apparent functional couplings that do not reflect true brain inter-regional interactions (Khadem and Hossein-Zadeh, 2014; Srinivasan et al., 2007; Vinck et al., 2011) for common methods of functional connectivity (FC) estimation, such as coherence or mutual information.

An additional potential confound with zero-lag connectivity in EEG stems from the common reference problem, which arises when a common reference channel is used for recording, which is typical of a large majority of EEG recording hardware. This leads to the presence of spurious zero-lag connectivity estimates depending on the strength of potentials fluctuations at the recording and reference sites (Bastos and Schoffelen, 2016).

1.4 Non-zero-lag-metrics

Two FC metrics, the weighted Phase Lag Index (wPLI; Vinck et al., 2011) and the weighted Symbolic Mutual Information (wSMI; King et al., 2013), represent examples of spectral (wPLI) and information-theoretic (wSMI) connectivity estimation methods that are increasingly applied to both EEG and MEG data (Canales-Johnson et al., 2017; Chennu et al., 2017, 2014, 2016; Comsa et al., 2019; Lau et al., 2012; Lee et al., 2017a,b; Ortiz et al., 2012; Parra et al., 2017; Robinson and Mandell, 2015; Simor et al.,

2018; Sitt et al., 2014; Tramonti et al., 2018; Xing et al., 2017).

These two connectivity metrics are modified versions of pre-existing methods (PLI (Stam et al., 2007; Vinck et al., 2011); SMI (King et al., 2013)) that minimise the contribution of '(almost-)zero-lag' interactions, potentially determined by volume conduction. These approaches are thus expected to allow identifying true time-lagged functional couplings (Cohen, 2015; Hipp et al., 2012; Palva and Palva, 2012; Peraza et al., 2012; Schoffelen and Gross, 2009) in the activity of underlying brain sources, while excluding apparent zero-lag connectivity driven by a mixture of real and spurious relationships (Gollo et al., 2014; Roelfsema et al., 1997).

1.4.1 Weighted Phase Lag Index

The wPLI measures the extent to which phase angle differences between two time series x(t) and y(t) are distributed towards positive or negative parts of the imaginary axis in the complex plane (similar to the PLI (Stam et al., 2007; Vinck et al., 2011)).

The underlying idea is that volume-conducted activity accounts for the greatest proportion of detected 0° or 180° phase differences between signals. Therefore, to obtain a conservative estimate for real, non-volume conducted activity, only phase angle distributions predominantly on the positive or negative side are considered.

The PLI is defined as the absolute value of the sum of the signs of the imaginary part of the complex cross-spectral density S_{xy} of two real-valued signals $x(t)$ and $y(t)$ at trial t.

$$\mathrm{PLI} = \left| \frac{\sum_{t=1}^{n} \mathrm{sgn}\left(\mathrm{imag}\left(s_{xy,t}\right)\right)}{n} \right| \tag{1.1}$$

While PLI is already insensitive to zero-lag interactions, the weighted Phase-Lag Index (Vinck et al., 2011) further addresses potential confounds caused by volume conduction, by scaling contributions of angle differences according to their distance from the real axis, as almost 'almost-zero-lag' interactions are considered as noise affecting real zero-lag in-

teractions:

$$\text{wPLI} = \left| \frac{\sum_{t=1}^{n} \left|\text{imag}\left(s_{xy,t}\right)\right| sgn\left(\text{imag}\left(s_{xy,t}\right)\right)}{\sum_{t=1}^{n} \left|\text{imag}\left(s_{xy,t}\right)\right|} \right| \tag{1.2}$$

The wPLI is based only on the imaginary component of the cross-spectrum, and thus implies robustness to noise compared to coherence, as uncorrelated noise sources cause an increase in signal power (Peraza et al., 2012).

1.4.2 Weighted Symbolic Mutual Information

The wSMI (King et al., 2013) evaluates the extent to which two EEG signals present non-random joint fluctuations, suggesting sharing of information.

The time series X and Y in all EEG channels are first transformed into sequences of discrete symbols $(\hat{X}, \hat{Y})$. The symbols are coded according to the trends in amplitudes of a specific predefined number of consecutive time points. If the kernel k is chosen to be 3, then the symbols are constituted by 3 elements, leading to $3! = 6$ different potential symbols in total (King et al., 2013; Sitt et al., 2014).

The temporal separation of elements that constitute a symbol can be predetermined to be τ frames, such that the maximum resolved frequency is $f_{\max} = \frac{f_s}{k\tau}$Hz, whereby f_s is the sampling frequency. The joint probability of each pair of symbols co-occurring in two different time series is computed to estimate the symbolic mutual information (SMI) shared across two signals.

To address volume conduction artifacts, the weighted symbolic mutual information disregards co-occurrences of identical or opposite-sign signals.

$$\text{wSMI}(\hat{X}, \hat{Y}) = \frac{1}{\log(k!)} \sum_{\hat{x} \in \hat{X}} \sum_{\hat{y} \in \hat{Y}} w(\hat{x}, \hat{y}) p(\hat{x}, \hat{y}) \log \frac{p(\hat{x}, \hat{y})}{p(\hat{x}) p(\hat{y})} \tag{1.3}$$

The wSMI can lead to negative values, given that it is a weighted mutual information measure, a form of weighted relative entropy (Kvålseth, 1991).

Other non-zero-lag-metrics

There are several other phase-based connectivity measures that ignore zero-phase-lag connectivity, including imaginary coherence (Nolte et al., 2004) and the phase-slope index (Nolte et al., 2008). These measures (including PLI and wPLI) are also insensitive to volume conduction, although in some cases they may still be susceptible to mixing sources (Peraza et al., 2012). While imaginary coherence (Nolte et al., 2004) was developed as a way to apply spectral coherence without concern for spurious connectivity due to volume conduction, the phase-slope index is mostly used to measure directed phase-based "effective" connectivity.[4]

1.5 Application of wPLI and wSMI to physiological and pathological conditions

Both wPLI and wSMI have been applied to explore brain functional dynamics associated with different behavioural states (Lau et al., 2012; Ortiz et al., 2012) or potential network-level alterations in pathological conditions (e.g., Alzheimer's disease (Parra et al., 2017), multiple sclerosis (Tramonti et al., 2018), schizophrenia (Robinson and Mandell, 2015) and social anxiety disorder (Xing et al., 2017)).

Interestingly, they have also been suggested to allow the identification of variations in functional integration accompanying changes in the level of consciousness (Chennu et al., 2017, 2014, 2016; King et al., 2013; Lee et al., 2017a,b; Sitt et al., 2014). For instance, King and colleagues (King et al., 2013) found that wSMI connectivity between centro-posterior areas and other brain regions is higher in healthy conscious individuals as compared to patients with unresponsive wakefulness syndrome (UWS) or in a minimally conscious state (MCS).

[4] The underlying idea is that if there is a directed functional connection from area A to area B with a fixed phase lag, the spectral representation of this phase lag will increase with increasing frequency. Thus, the phase-slope index measures whether the slope of the phase lag is consistently positive or negative over several adjacent frequency bins, whereby the sign of the slope indicates whether the net connectivity flows from region A to B or the reverse (Nolte et al., 2008).

Similarly, Chennu and colleagues (Chennu et al., 2017, 2014) showed that alpha-band wPLI-based functional networks differ between healthy individuals and patients with disorders of consciousness (UWS, MCS). In line with this, previous studies (Chennu et al., 2016; Lee et al., 2017b) also showed that propofol sedation in healthy individuals is associated with a decrease in alpha-band wPLI (Chennu et al., 2016) and a relative increase in delta-band wPLI connectivity (Lee et al., 2017b).

These observations across different conditions characterized by altered levels of consciousness are particularly interesting, as they suggest that wPLI and wSMI may offer general, relatively simple and reproducible indices of the current level of consciousness of an individual (Casali et al., 2013). An overview of metrics that have been suggested to allow tracking changes in the level of consciousness can be found in appendix B.

In spite of these promising findings, it had not been previously investigated whether the two methods provide a similar description of brain inter-regional relationships, or account instead for distinct types of functional interactions. In fact, wPLI (Vinck et al., 2011) is a measure of phase synchronisation that may account for linear interactions but is also expected to be sensitive to nonlinear couplings (David et al., 2004; West et al., 2016). On the contrary, wSMI (King et al., 2013) is thought to reveal nonlinear relationships due to its grounding in information theory (Ince et al., 2017).

However, the actual performance of the two methods at detecting distinct types of connectivity dynamics had never been directly compared in simulated or real experimental data. In addition, wPLI and wSMI have been mostly used to investigate pathological differences in the level of consciousness (between healthy participants and patients with disorders of consciousness; Chennu et al. (2017, 2014); King et al. (2013); Sitt et al. (2014)) and for the study of pharmacologically induced differences in the level of consciousness (anaesthesia; Chennu et al. (2016); Lee et al. (2017a,b)). The combination of the two metrics, wPLI and wSMI, had not been used previously to investigate differences in the levels of consciousness during sleep.

1.6 Aims

The principal aim of this work was to determine whether the two connectivity metrics, wPLI and wSMI, provide overlapping or complementary information about changes in brain functional dynamics across physiological and pathological conditions.

In chapter 2, I used simulated high-density (hd-)EEG data to investigate and compare the accuracy of wPLI and wSMI at identifying different types of functional interaction dynamics, including both linear and nonlinear dynamics. Moreover, in light of previous observations suggesting that the two methods may allow the detection of differences in the level of consciousness (Chennu et al., 2017, 2014, 2016; Comsa et al., 2019; King et al., 2013; Lee et al., 2017a,b; Sitt et al., 2014), I tested whether both wPLI and wSMI connectivity were also able to detect significant differences between wakefulness and deep (N3-)sleep, typically characterised by markedly different levels of consciousness (Nir et al., 2013), in EEG recordings of 12 healthy participants.

In chapter 3, I built on the findings of this simulation study and investigated whether the combined use of these two methods may unveil functional differences across distinct physiological stages of vigilance, including wakefulness, Non-rapid Eye Movement (Sleep) (NREM)- and Rapid Eye Movement (Sleep) (REM)-sleep. I studied the potential value of power-based and FC-indices wPLI and wSMI in the cross-participant prediction of four stages of vigilance (wakefulness, NREM (N2/N3), REM sleep) in the EEG recordings of 24 healthy participants. Furthermore, I investigated the relevance of FC-based features for the distinction between stages characterised by a higher probability of conscious experiences (e.g., perception or thoughts during wakefulness, and dreams during sleep) as compared to a lower probability of conscious experiences (in NREM-Sleep). To shed light on the possible functional basis of the typical sensory disconnection of sleep, I compared FC-derived features in REM-sleep and wakefulness, two stages characterized by vivid conscious experiences.

In chapter 4, I investigated the ability of wPLI and wSMI to track variations in brain integration in the pathological condition of multiple sclerosis in a cohort of 16 patients that underwent physical rehabilitation training.

In conclusion, the aim of this thesis was to investigate and compare the accuracy of wPLI and wSMI at identifying different types of functional interaction dynamics – both linear and nonlinear dynamics – in simulated hd-EEG data, where the ground-truth is known.

Building on this validation study, I then compared the performance of these two connectivity metrics at tracking changes in brain dynamics associated with a physiological (wakefulness/sleep) and a pathological condition (multiple sclerosis).

Chapter 2

EEG functional connectivity metrics wPLI and wSMI account for distinct types of brain functional interactions

2.1 Introduction

All the results shown in this chapter refer to the same-titled article, published in Scientific Reports (Imperatori et al., 2019).

Functional connectivity (FC) metrics identify statistical (undirected) associations among spatially distinct brain areas. EEG and MEG represent popular neuroimaging modalities for the estimation of FC due to their high temporal resolution, in the order of milliseconds.

However, both EEG and MEG suffer from volume conduction, as sources in the brain generate large electromagnetic fields that are measured by more than one EEG electrode or MEG sensor, introducing spatial auto-correlation at the sensor level. Because of this linear mixing of different sources on the same sensor, common methods for FC estima-

tion, such as coherence or mutual information, may lead to the identification of apparent functional couplings that do not reflect true brain interregional interactions (Khadem and Hossein-Zadeh, 2014; Srinivasan et al., 2007; Vinck et al., 2011).

To overcome this problem, several new FC methods have been specifically designed to minimize the impact of volume conduction effects. In particular, the weighted Phase Lag Index (wPLI; Vinck et al. (2011)) and the weighted Symbolic Mutual Information (wSMI; King et al. (2013)), represent examples of spectral (wPLI) and information-theoretic (wSMI) connectivity estimation methods that are increasingly applied to both EEG and MEG data (Canales-Johnson et al., 2017; Chennu et al., 2017, 2014, 2016; Comsa et al., 2019; Lau et al., 2012; Lee et al., 2017a,b; Ortiz et al., 2012; Parra et al., 2017; Robinson and Mandell, 2015; Simor et al., 2018; Sitt et al., 2014; Tramonti et al., 2018; Xing et al., 2017).

These two connectivity metrics are modified versions of pre-existing methods (PLI (Stam et al., 2007; Vinck et al., 2011); SMI (King et al., 2013)) that minimise the contribution of '(almost-)zero-lag' interactions, potentially determined by volume conduction. These approaches are thus expected to allow identifying true time-lagged functional couplings (Cohen, 2015; Hipp et al., 2012; Palva and Palva, 2012; Peraza et al., 2012; Schoffelen and Gross, 2009) in the activity of underlying brain sources, while excluding apparent zero-lag connectivity driven by a mixture of real and spurious relationships (Gollo et al., 2014; Roelfsema et al., 1997).

Both wPLI and wSMI have been applied to explore brain functional dynamics associated with different behavioural states (Lau et al., 2012; Ortiz et al., 2012) or potential network-level alterations in pathological conditions (e.g., Alzheimer's disease (Parra et al., 2017), multiple sclerosis (Tramonti et al., 2018), schizophrenia (Robinson and Mandell, 2015) and social anxiety disorder (Xing et al., 2017)).

Interestingly, they have also been suggested to allow the identification of variations in functional integration accompanying changes in the level of consciousness (Chennu et al., 2017, 2014, 2016; King et al., 2013; Lee et al., 2017a,b; Sitt et al., 2014). King and colleagues (King et al., 2013) found that wSMI connectivity between centro-posterior areas and other

brain regions is higher in healthy conscious individuals as compared to patients with Unresponsive Wakefulness Syndrome (UWS) or in a Minimally Conscious State (MCS).

Similarly, Chennu and colleagues (Chennu et al., 2017, 2014) showed that alpha-band wPLI-based functional networks differ between healthy individuals and patients with disorders of consciousness (UWS, MCS). In line with this, previous studies (Chennu et al., 2016; Lee et al., 2017b) also showed that propofol sedation in healthy individuals is associated with a decrease in alpha-band wPLI (Chennu et al., 2016) and a relative increase in delta-band wPLI connectivity (Lee et al., 2017b).

These observations across different conditions characterized by altered levels of consciousness are particularly interesting, as they suggest that wPLI and wSMI may offer general, relatively simple and reproducible indices of the current level of consciousness of an individual (Casali et al., 2013).

In spite of these promising findings, it is currently unclear whether the two methods provide a similar description of brain inter-regional relationships, or account instead for distinct types of functional interactions. In fact, wPLI (Vinck et al., 2011) is a measure of phase synchronisation that may account for linear interactions but is also expected to be sensitive to nonlinear couplings (David et al., 2004; West et al., 2016). On the contrary, wSMI (King et al., 2013) is thought to reveal nonlinear relationships due to its grounding in information theory (Ince et al., 2017).

However, the actual performance of the two methods at detecting distinct types of connectivity dynamics has never been directly compared in simulated or real experimental data. Therefore, here we used simulated high-density Electroencephalography (hd-EEG) data to specifically investigate and compare the accuracy of wPLI and wSMI in identifying different types of interaction dynamics, including both linear and nonlinear dependencies.

In addition, to evaluate the potential impact of differences between the two methods on the analysis of real experimental data, we tested wPLI and wSMI on hd-EEG recordings collected from human participants in distinct behavioural states, namely wakefulness and deep (N3-)

sleep, typically characterised by markedly different levels of consciousness (Nir et al., 2013). In light of previous observations suggesting that the two methods may allow the detection of differences in the level of consciousness (Chennu et al., 2017, 2014, 2016; Comsa et al., 2019; King et al., 2013; Lee et al., 2017a,b; Sitt et al., 2014), we expected both wPLI and wSMI connectivity to differ between wakefulness and N3-sleep.

However, here we also asked whether the two connectivity metrics provide overlapping or complementary information about changes in brain functional dynamics across the two vigilance states.

2.2 Methods

2.2.1 Simulation of hd-EEG data

The MATLAB-based Berlin Brain Connectivity Benchmark (BBCB) framework (Haufe and Ewald, 2016) was used to simulate realistic hd-EEG recordings (108 channels, 500Hz, 120s). In particular, the simulated electrical activity was generated by imposing bivariate relationships between two cortical sources, which were then projected at scalp level using a biophysically realistic model of electrical current propagation in the head. The adopted model was based on the standard ICBM152 anatomical template (Huang et al., 2016) and included 6 tissue types: scalp, skull, air cavities, gray matter, white matter and cerebrospinal fluid (CSF). A finite element model (FEM) was solved to generate the lead field.

We modelled both intra- and inter-hemispheric interactions between pairs of cortical sources (see Fig. 1, including corresponding MNI coordinates [1]. The first source was placed either in the left (LIPL) or right (RIPL) inferior parietal lobule, while the second source was kept in the right middle frontal gyrus (RMFG).

The choice of these locations was motivated by previous neuroimaging studies showing that resting state activity of these areas is modulated

[1] The MNI coordinate system is a normalised coordinate system, described in (Evans et al., 1993; Mazziotta et al., 2001), to map the location of brain structures, independent from individual differences in size and shape, facilitating comparisons across time points, subjects, groups and sites.

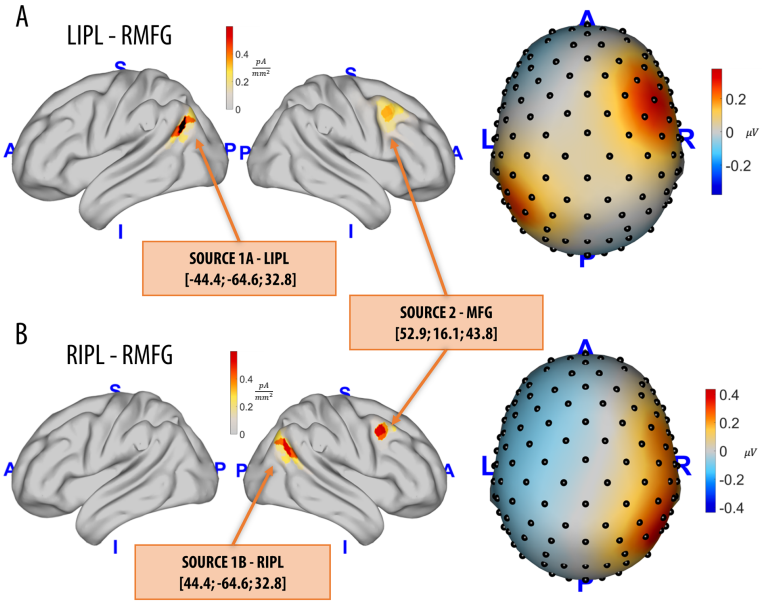

Figure 1: From modelling source dynamics to EEG field patterns. Intra- and inter-hemispheric interactions between two source pairs were modelled: the first source was placed either in left (LIPL) or right (RIPL) inferior parietal lobule, while the second source was kept in the right middle frontal gyrus (RMFG). The orientation of the neuronal current at each node is defined as the normal vector w. r. t. the mesh surface at that node, i.e. field spreads were calculated assuming perpendicular source orientations. Source amplitudes are shown using a lateral view of the brain, while resulting EEG field potentials are plotted using a top view of the scalp. The brain images were plotted based on the Matlab scripts provided in the BBCB toolbox (Haufe and Ewald, 2016)

by conscious perception and attention (Maksimow et al., 2005; Martuzzi et al., 2010; Vanhaudenhuyse et al., 2011, 2009).

Moreover, studies that employed wPLI and wSMI to investigate functional connectivity in different states of consciousness specifically suggested that a key correlate of such changes may be represented by variations in the strength of interactions across posterior and anterior brain areas (Blain-Moraes et al., 2014; Chennu et al., 2016; Comsa et al., 2019). For the sake of simplicity, only two interacting sources at a time were considered: a) LIPL-RMFG (inter-hemispheric) and b) RIPL-RMFG (intra-hemispheric).

Nine different coupling relationships between the two sources, which differed in the type and relative degree of linear and nonlinear components, were modelled. For each pair of source locations (LIPL-RMFG and RIPL-RMFG) and each type of simulated source coupling dynamics we also modelled 100 different Signal-to-Noise Ratios; from 0.01 to 1, with steps of 0.01), which describe the weighting of simulated source signals with respect to simulated background activity.

As detailed below, 100 different background noise patterns were obtained for each considered Signal-to-Noise-Ratio (SNR). Brain noise $n_b(t)$ was generated by placing 500 mutually statistically independent time-series characterised by $1/f$-shaped power (pink noise) and random phase spectra at an equal number of random locations sampled from the entire cortical surface. Moreover, spatially and temporally uncorrelated sensor noise $n_s(t)$ was sampled from a univariate standard normal distribution. The overall noise contribution was defined as noise $n(t)$:

$$n(t) = 0.9\frac{n_b(t)}{\|n_b(t)\|_F} + 0.1\frac{n_s(t)}{\|n_s(t)\|_F}, \tag{2.1}$$

where $\|n_b(t)\|_F$ the Frobenius norm. The simulated hd-EEG recording was generated according to:

$$x^{int}(t) = \alpha\frac{s^{int}(t)}{\left\|s^{int}(t)\right\|_F} + (1-\alpha)\frac{n(t)}{\|\tilde{n}(t)\|_F}, \tag{2.2}$$

where s^{int} corresponds to the signal contribution of the sources of interest to the EEG scalp signal (i..e. $s^{int}(t)$ is the projected source interaction to

the EEG sensors through multiplication of the lead field with the source time courses, mapped to two patches of the cortical surface). The parameter α is related to the signal-to-noise and $\tilde{n}$(t) is the filtered version of $n(t)$ in the frequency-range of interest (8-12Hz for linear dynamics, 0.5-12Hz for the non-linear dynamics).

2.2.2 Source Interaction Dynamics

For each source pairing (LIPL-RMFG, RIPL-RMFG), nine different coupling relationships were simulated by modelling the time-series of the two sources based on linear (auto-regressive (AR) model) and nonlinear (Hénon (Hénon, 1976), Ikeda (Ikeda, 1979), Rössler (Rössler, 1979), Lorenz (Lorenz, 1963)) dynamical systems.

2.2.3 Linear interactions

The time courses of the two sources were modelled using bivariate linear autoregressive (AR) models of order 5:

$$\begin{bmatrix} z_1(t) \\ z_2(t) \end{bmatrix} = \sum_{p=1}^{P} \begin{bmatrix} a_{11}(p) & a_{12}(p) \\ a_{21}(p) & a_{22}(p) \end{bmatrix} \begin{bmatrix} z_1(t-p) \\ z_2(t-p) \end{bmatrix} + \begin{bmatrix} \varepsilon_1(t) \\ \varepsilon_2(t) \end{bmatrix} \tag{2.3}$$

where $a_{ij}(p)$, $i, j \in 1,2$, $p \in 1,..,P$ are linear autoregressive (AR) model coefficients, and $\epsilon_i(t)$, $i \in 1,2$ are uncorrelated standard normal distributed noise variables. The off-diagonal entry $a_{12}(p)$ was set to zero, while $a_{21}(p)$ was set to 0.5. Thus, interactions arise from a unidirectional time-delayed influence of z_1 on z_2.

The generated time series were bandpass-filtered in the alpha band (8-12 Hz) using an acausal third-order Butterworth filter with zero phase-delay (Haufe and Ewald, 2016). We decided to simulate alpha oscillations with a clearly defined sender-receiver relationship, as they are also a key feature of brain activity in physiological wakefulness (Sadaghiani and Kleinschmidt, 2016).

2.2.4 Nonlinear interactions

Several distinct non-linear dynamics were selected in order to represent a wide-range of possible functional interactions. Among the chosen dynamics, the Hénon map and the Rössler systems have previously been employed by Wang et al. (2014) to test different functional connectivity measures.

The time courses of the two sources were modelled by considering each one as a time-varying state variable of a specific dynamical system. We considered four different nonlinear systems: two defined by two-dimensional non-iterated maps (Hénon (1976) and Ikeda (1979)) and two represented by three-dimensional nonlinear ordinary differential equation systems (Rössler (1979) and Lorenz (1963) dynamics).

Dynamical systems describe the motion of a point in a multidimensional state space, where the starting point is defined by the initial conditions of the system. For each system all potential combinations of variables were considered as representing different interaction dynamics, i.e. Hénon (x,y), Ikeda (x,y), Rössler (x,y), Rössler (x,z), Rössler (y,z), Lorenz (x,y), Lorenz (x,z) and Lorenz (y,z).

The MATLAB-based Chaotic Systems Toolbox was used to compute the time series for the selected nonlinear systems, and the respective parameters were chosen to achieve complex chaotic behaviour: Hénon map [a=1.4; b=0.3], Ikeda map [$\mu = 0.9$], Rössler dynamics [a=0.2, b=0.2, c=5.7, $x_0 = 0.1$, $y_0 = 0.1$, $z_0 = 0.1$, h=0.1], Lorenz dynamics [σ=10, β=28, ρ=8/3, $x_0 = 0.1$, $y_0 = 0.1$, $z_0 = 0.1$, h=0.1]. Due to the complex nature of these dynamics, they have not been limited to a specific frequency band.

2.2.5 Connectivity Analysis

The simulated EEG datasets (108 channels, 500Hz, 120 s) generated for each coupling model were divided into 60 non-overlapping 2 s-epochs (Colclough et al., 2016; King et al., 2013; Vinck et al., 2011). Then, FC was computed for each epoch and pair of electrodes. While wPLI and wSMI could be theoretically applied to source-modelled EEG data, they are most commonly applied at scalp-level, and for this reason all present

analyses were performed by computing connectivity values between pairs of scalp EEG-sensors.

Before computing connectivity measures, a Current-Source Density (CSD) transform (Kayser and Tenke, 2006) was applied to the EEG data, as in previous works (King et al., 2013; Vinck et al., 2011). This method provides a reference-independent signal and acts as a spatial filter, leading to a relatively improved spatial resolution (Nunez et al., 2006).

Analyses were focused on the 0.5-12 Hz frequency range for the broadband computations and on delta- (0.5-4Hz), theta- (4-8Hz) and alpha-bands (8-12Hz) for the frequency-band-resolved analyes.

wPLI

wPLI was computed using the Fieldtrip toolbox (Oostenveld et al., 2011) (multi-taper method fast Fourier transform, single Hanning taper (Vinck et al., 2011) 0.5 Hz frequency resolution). The mean value across the frequency-bins in the frequency range of interest was computed to obtain a single wPLI coupling value (Broadband 0.5-12Hz; Delta 0.5-4Hz; Theta 4-8Hz; Alpha 8-12Hz).

wSMI

We chose the kernel k to be 3, implying that the symbols are constituted of three elements, leading to 3!=6 different potential symbols in total (King et al., 2013; Sitt et al., 2014).

The temporal separation of elements that constitute a symbol was set to be $\tau = 14$ frames ($\tau_t = 28ms$), such that the maximum resolved frequency was $f_{\max} = \frac{f_s}{k\tau} = \frac{500\text{Hz}}{3\times14} = 11.9\text{Hz}$.

Prior to wSMI computation, the signal was low-pass-filtered using the `ft_preproc_lowpass` FieldTrip function with an additional mirror padding (`ft_preproc_padding`) of 1s before and after each individual epoch to avoid potential filter edge-artifacts. For the analysis in frequency bands, a bandpass-filter (`ft_preproc_bandpass`) was used with the same padding scheme.

2.2.6 Statistical Procedure for Simulated Data

The accuracy of wPLI and wSMI was evaluated at whole-brain and topographic levels, respectively indicating

- the ability to detect the presence of statistical dependencies in the overall (median) connectivity across all pairs of electrodes (see figs. 1 and 2), and
- the ability to detect a significant interaction between the pairs of electrodes spatially closest to the actual brain sources among all pairs of electrodes.

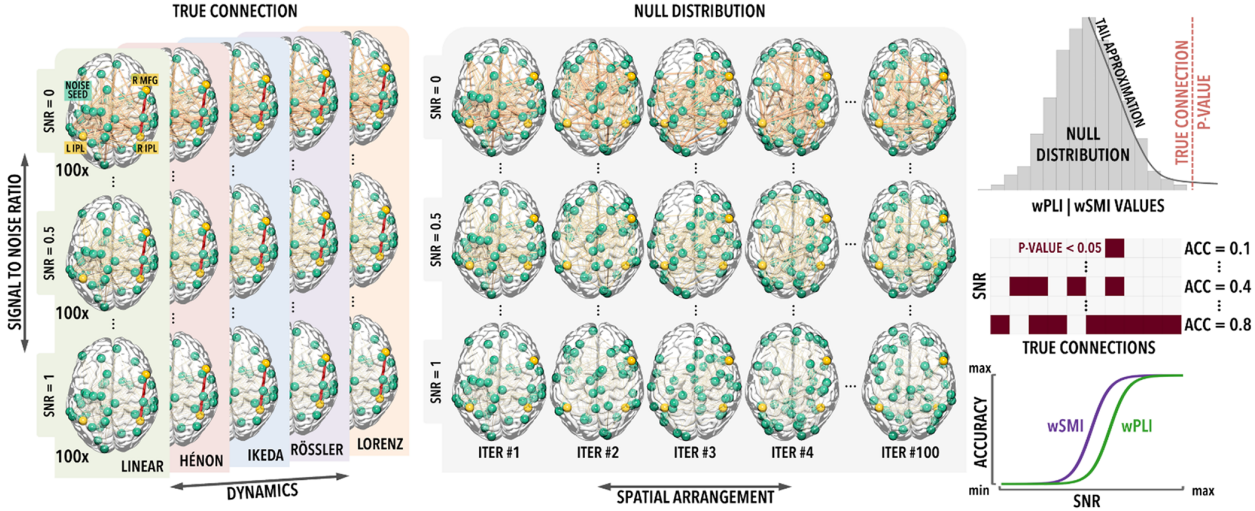

Figure 2: Outline of the methodological design for the assessment of whole-brain accuracy. The source locations LIPL, RIPL and RMFG are marked as yellow dots in the brain plots, while the red line indicates a true interaction between two of the sources (RIPL-RMFG). For each SNR in the range 0.01-1.00 (0.01 steps; N=100) different spatial distributions (N=100) of random background noise (marked as green dots) were generated in combination with true interactions between the source pairs and projected at scalp level. The corresponding null distributions were obtained through time-point-shuffling of the original interacting source-level timeseries. The same procedure has been applied to all interaction dynamics and tested source pairs (intra/inter-hemispheric). The brain images were rendered using Surf Ice (vers. 5 May 2016, 64-bit).

2.2.7 Whole-brain accuracy

For each source pairing (LIPL-RMFG, RIPL-RMFG), tested interaction dynamics and SNR, the whole-brain detection accuracy of wPLI and wSMI was computed as the proportion of cases (N=100 datasets differing by their respective spatial noise distributions), in which the whole-brain median connectivity value (across all electrode-pairs) of simulated EEG data passed the 95th percentile of a null distribution obtained after time-point-shuffling of the original source-level timeseries (N=100 permutations; Fig. 2, Algorithm 1).

Algorithm 1: Whole-Brain Accuracy

Result: Whole-Brain Accuracy

Generate different spatial distributions (N=100) of random background noise - with either real underlying interactions or surrogate interactions between the chosen source pairs;
for *SNR=0.01:0.01:1* **do**
    for *NoiseDistribution=1:1:100* **do**
        Test whole-brain connectivity value (Acc_{true}) obtained from EEG dataset with given noise distribution but real interaction dynamics against 95% threshold of null distribution (Acc_{perm}) of whole-brain connectivity values obtained from EEG datasets with randomised interaction dynamics (use generalised Pareto distribution to model the tail of the null distribution);
    end
    if $Acc_{true} > Acc_{perm}$ **then**
        Assign a score of 1.
    else
        Assign a score of 0.
    end
    Take the sum over all scores and divide by the number of tested noise distributions to obtain the whole-brain accuracy at each SNR;
end

To account for the small number of permutations, a generalised Pareto distribution was used to model the tail of the null distribution, using the PALM (Permutation Analysis of Linear Models) software (Winkler et al., 2014). Of note, we chose to focus on a time-point-shuffling procedure instead of phase-shuffling, since the latter can introduce spurious interdependences between time-series, especially for the Rössler dynamics (Maiwald et al., 2008).

A null distribution was also generated by phase-shuffling the original time-series using the Amplitude-Adjusted Fourier Transform (AAFT) procedure (see algorithm 2 (Theiler et al., 1992, 1991)). With the expected exception of the Rössler dynamics, the two approaches provided similar results (see Fig. 7).

Algorithm 2: Amplitude-Adjusted Fourier Transform

Result: Surrogate data with preserved linear structure and amplitude distribution and randomised temporal relationships

1 Scale the data to a Gaussian distribution (Gaussianization);
2 Perform Fourier Transform and assign random phase to each frequency. (The phase must be conjugate symmetric around the centre frequency in order to obtain a real, surrogate dataset.);
3 Perform inverse Fourier Transforms;
4 Do an inverse transformation of the first Gaussian transformation (de-Gaussianization).

2.2.8 Topographic accuracy

For each source location pairing, interaction dynamics and SNR, the topographic accuracy was defined as the proportion of simulated EEG datasets (N=100 differing by their respective spatial noise distributions), in which the connectivity between the two electrodes spatially closest to the cortical sources (minimum Euclidean distance) passed the 95th percentile of all other electrode pairings (N=5777) in each simulated EEG-recording with the same underlying brain noise (Algorithm 3).

Algorithm 3: Topographic Accuracy

Result: Topographic Accuracy

Generate different spatial distributions (N=100) of random background noise with real underlying interactions between the chosen source pairs;
for *SNR=0.01:0.01:1* **do**
  for *NoiseDistribution=1:1:100* **do**
    Test connectivity value (Acc_{source}) between the two electrodes spatially closest to the sources (Euclidean distance) against 95% threshold of null distribution of all other connectivity values;
  end
  if $Acc_{true} > Acc_{perm}$ **then**
    Assign a score of 1.
  else
    Assign a score of 0.
  end
  Take the sum over all scores and divide by the number of tested noise distributions to obtain the topographic accuracy at each SNR;
end

In summary, for both approaches, a threshold corresponding to the 95th percentile of the respective null-distributions (surrogate data for whole-brain connectivity, and connectivity of all electrode-pairs in topographic analysis) was regarded as the limit for the detection of significant FC interactions ($\alpha = 0.05$).

The mean total accuracy of wPLI and wSMI was computed as the mean of accuracies obtained across all SNRs. Non-parametric permutation tests (N=10000, $p < 0.05$) were used to compare the performance of the two metrics at each SNR and for mean accuracy. Specifically, for each examined condition, the difference in mean accuracy between wPLI and wSMI was compared with a null distribution obtained by randomly 'reassigning' to the two metrics the values of accuracy determined for the different SNR configurations. A similar procedure was used to compare performance of wPLI and wSMI for different spatial distributions of noise at each SNR.

2.2.9 Experimental hd-EEG recordings

To verify whether potential differences between wPLI- and wSMI-based FC measures in recognizing distinct interaction dynamics have actual implications for the analysis of real experimental data, an additional investigation was performed on hd-EEG recordings (257 channels, Electrical Geodeisics Inc.; 500 Hz) obtained in different behavioural states.

Specifically, data were obtained from 12 healthy volunteers (25 ± 4 yrs, 6F) during distinct states of vigilance: relaxed wakefulness with eyes closed (W) and deep (N3-)sleep. The data was recorded as part of a larger project aimed at exploring the effects of changes in visual experiences during wakefulness on NREM-sleep features (Bernardi et al., 2019a) [2].

Brain activity during N3-sleep was extracted from an overnight EEG recording in the sleep laboratory, whereas wakefulness data consisted of six minutes of eyes-closed resting-state activity obtained at 8am the following morning, when homeostatic sleep pressure is expected to be at its minimum (Borbély, 1982).

All continuous wake and N3-sleep recordings were band-pass filtered between 0.5 and 45 Hz (NetStation 5, EGI), and the first and last 5-s of data were discarded to account for filter-related edge-artifacts. Bad

[2] The collection of experimental EEG data in wakefulness and sleep was approved by the ethical committee of the Canton of Vaud (Switzerland) and performed in accordance with relevant guidelines and regulations. Written informed consent was obtained from each subject.

channels were identified upon visual inspection and interpolated using spherical splines: we removed 31.5 ± 12.9 electrodes (corresponding to $12.3 \pm 5.0\%$ of all electrodes) in sleep recordings, and 30.8 ± 8.6 electrodes ($12.0 \pm 3.4\%$) in wakefulness recordings.

Sleep scoring was performed using standard procedures (Iber, 2007) and all $30s$ epochs containing N3-sleep were extracted and concatenated. EEG recordings during wakefulness were divided into non-overlapping $5s$ segments and visually inspected to identify and reject clear artifacts. Overall, $27.3 \pm 13.8\%$ of all epochs were discarded due to artifacts, while in deep sleep no epochs were discarded. Indeed, large artifacts caused by eye movements, movements or muscular activity are typically absent or greatly reduced while in deep sleep.

For both wakefulness and sleep data, a procedure based on Independent Component Analysis (ICA) was used to remove residual ocular, muscular, and cardiac artifacts (Delorme and Makeig, 2004).

For each subject, we randomly extracted and analyzed the minimum common number (across subjects) of artifact-free 2s-long epochs of wakefulness data, corresponding to 70 segments (i.e. 140s; the first 0.5s and the last 0.5s of each 5s segment were discarded). The same amount of data (i.e. 70 2s-epochs; 140s) was randomly selected from N3-sleep that occurred during the first half of the night.

From this selection, we excluded epochs representing potential outliers in terms of signal power within classical frequency bands. Specifically, the Power Spectral Density (Power-Spectral Density (PSD); Welch's method, Hamming windows, 8 sections, 50% overlap) of all N3 2s-epochs was calculated in delta (0.5-4Hz), theta (4-8Hz), alpha (8-12Hz), sigma (12-16Hz), beta (18-25Hz), gamma (30-45Hz) and broadband (0.5-45Hz) frequency ranges. Then, outlier segments for any of the seven considered frequency ranges (i.e., threshold = median PSD ± 2 median absolute deviations; MAD) were excluded from the random selection procedure (see Fig. 3).

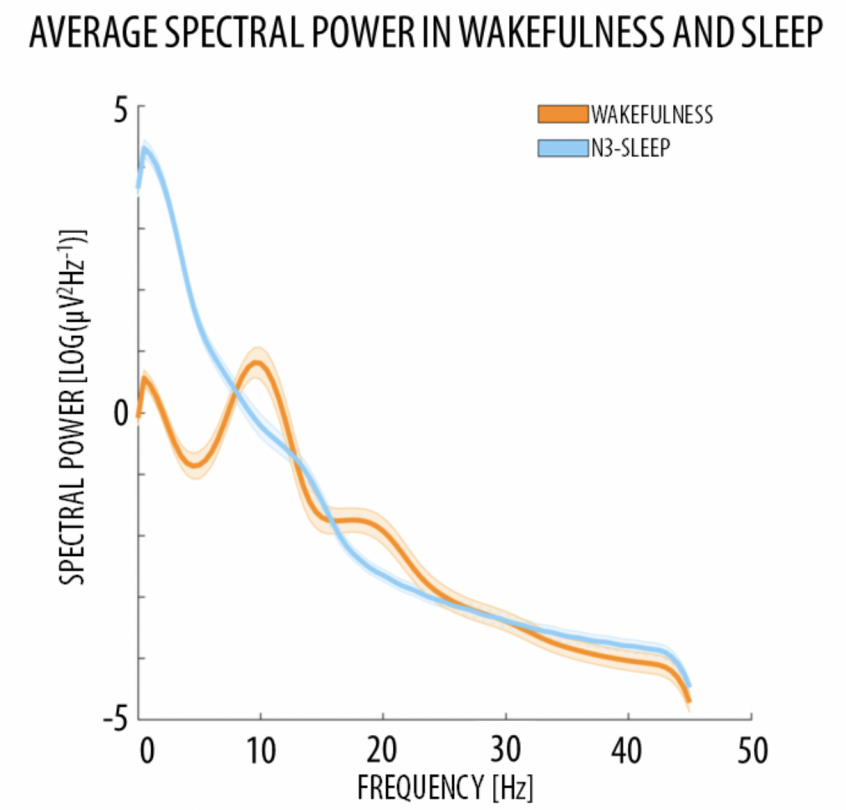

Figure 3: Group-level (N=12) average signal spectral power of data from wakefulness and N3-sleep. The shaded area reflects the standard error of the mean for each vigilance state.

For each condition and channel, the median wPLI and wSMI connectivity of each electrode to all other scalp electrodes was computed in all epochs for the 0.5-12 Hz frequency range (i.e., as in simulated data). The median one-to-all connectivity of each electrode was computed and compared to the average of the median one-to-all connectivity across surrogate datasets (1000 iterations) generated through time-point shuffling of the original recordings of each channel.

In this approach, the same permutation scheme was used for all subjects, and the global signal, corresponding to the average signal across all electrodes, was re-added to each shuffled dataset to ensure the preservation of the internal characteristics of the data and of the potential spurious (volume-conduction-dependent) interactions.

Paired comparisons were performed between i) wakefulness and surrogate data, and ii) wakefulness and N3-sleep (non-parametric permutation test; $p < 0.05$; see Explanation 2.2.1). Correction for multiple comparisons was ensured using a permutation-based supra-threshold cluster correction (Huber et al., 2004; Nichols and Holmes, 2002).

In brief, the same contrast was repeated (N=10000 iterations) after shuffling the labels of the two compared sets and the maximum size of significant electrode-clusters was saved in a frequency table. A cluster-size threshold corresponding to the 95th percentile of the obtained distribution ($\alpha = 0.05$) was applied to correct for multiple comparisons.

Whole-brain connectivity (median of one-to-all connectivity across all electrodes) was also evaluated and compared to surrogate data using a non-parametric permutation test (N=10000 iterations; $p < 0.05$).

Explanation 2.2.1: Permutation Testing

Given an EEG dataset with two conditions A and B, a potential hypothesis would be that a metric, derived from the EEG activity, is greater in condition A as compared to condition B. The null hypothesis would be that there is no difference in this metric between A and B. The procedure for testing for statistical significance would be structured in the following way (Maris and Oostenveld, 2007):

1. Randomly shuffle the labels across conditions A and B. [a]
2. Calculate the test statistic on this random partition.
3. Repeat steps 1) and 2) a large number of times N to obtain a more robust null distribution (histogram of the test statistics).
4. From the test statistic that was actually observed and the histogram in step 3), calculate the number of random partitions that resulted in a larger test statistic than the observed one and divide it by all tested partitions to obtain the p-value.
5. If the p-value is smaller than the critical alpha-level (conventionally 0.05), conclude that the data in the two experimental conditions are significantly different.

A correction for multiple comparisons is especially relevant, when performing topographic comparisons. One method is the Bonferroni-correction, that divides the critical alpha-level by the number of performed tests. It assumes that tests are independent, which is not the case for many EEG results (see section 1.3.1). Within nonparametric permutation testing, there are two intrinsic methods to correct for multiple comparisons: considering a) pixels and b) clusters (groups of suprathreshold pixels) to be the unit for determining a threshold (Cohen, 2014). [b]

[a] Across trials in within-subject analyses and across subjects in group-analyses.

[b] Cluster-based permutation tests are increasing in popularity despite a common overestimation of the temporal, spatial, and frequency precision of the associated statistical claims (Sassenhagen and Draschkow, 2019).

2.3 Results

The MATLAB-based (The MathWorks, Inc., Natick, Massachusetts, USA) 'Berlin Brain Connectivity Benchmark' (BBCB) framework (Haufe and Ewald, 2016) was used to simulate scalp-level hd-EEG recordings (108 channels, 500Hz, 120s) including bivariate relationships between two cortical sources. We modelled an intra-hemispheric interaction, between the right inferior parietal lobule (RIPL) and the right middle frontal gyrus (RMFG), and an inter-hemispheric interaction, between the left inferior parietal lobule (LIPL) and the right middle frontal gyrus (RMFG) (Fig. 6). The choice of these locations was motivated by previous neuroimaging studies showing that resting state activity of these areas is modulated by conscious perception and attention (Maksimow et al., 2005; Martuzzi et al., 2010; Vanhaudenhuyse et al., 2011, 2009).

2.3.1 Simulation of linear and nonlinear interdependencies in hd-EEG data

As detailed in the Methods section (see 2.2), nine different coupling relationships between the two sources were simulated, respectively based on: linear autoregressive (AR) model, Hénon map, Ikeda map, Rössler (x,y), Rössler (x,z), Rössler (y,z), Lorenz (x,y), Lorenz (x,z) and Lorenz (y,z) (see below for details).

For each pair of source locations (LIPL-RMFG and RIPL-RMFG) and each type of simulated source coupling dynamics we modelled 100 different signal-to-noise ratios (SNR; from 0.01 to 1 with steps of 0.01), which describe the weighting of simulated source signals with respect to simulated background activity.

In addition, 100 different background noise patterns were obtained for each considered SNR. As detailed below, the accuracy of wPLI and wSMI at detecting the different interaction dynamics was thus computed both across patterns of noise distribution (for accuracy at each SNR) and across SNRs (for an estimate of overall accuracy) (Fig. 2). First, we quantified the content of linear and nonlinear interdependencies in the nine examined interaction dynamics. In particular, to quantify the linear

content of the bivariate relationships between the original sources we used Cross-Correlation (CC), which offers a simple measure of similarity of two signals as a function of the displacement of one relative to the other (Quiroga et al., 2002).

In order to measure the nonlinear content, we took the average of the directional, nonlinear Independence Measure (N) in both directions of the source dynamics (Arnhold et al., 1999; Quiroga et al., 2002). For all cases, N was computed using the following parameters: embedding dimension (m=10), time lag (τ=5), theiler correction (theiler=50), number of nearest neighbours (nn=10). Similar results were obtained when optimal, individual parameters were selected for each time-series. Most of the interaction dynamics we modelled presented a mixture of linear and nonlinear dependencies, with the notable exception of Lorenz (x,z) and Lorenz (y,z), which showed a clear predominance of nonlinear interactions (Fig. 4).

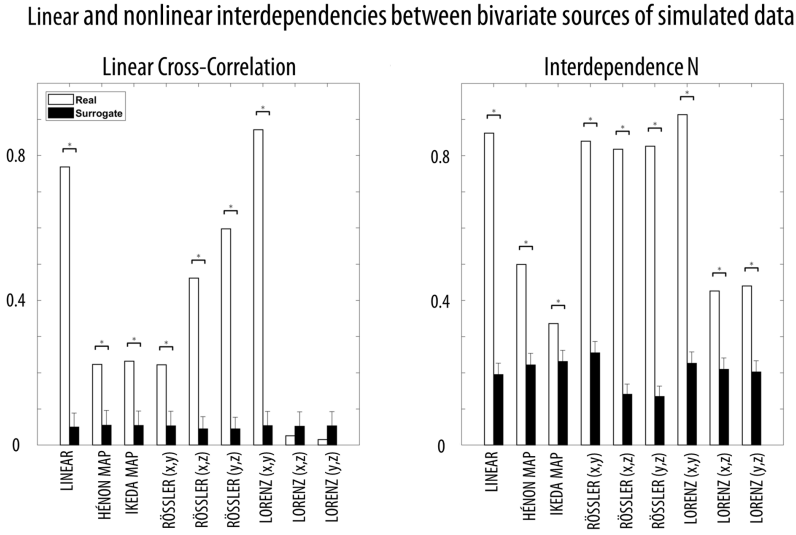

Figure 4: Linear and non-linear interdependencies between bivariate sources of simulated data. The absolute value of cross-correlation (CC; measure of similarity of two series as a function of the displacement of one relative to the other) and the interdependence measure N (measure of the non-linear relationship between two time series) were computed for simulated true source time-series (0.5-12 Hz) and the null distribution, obtained by shuffling the source time-series (N=1000, 0.5-12 Hz). For both CC and N, low values indicate total independence, while high values indicate strong dependence. The differences between the true simulated data and its null distribution, i.e. surrogate data, were computed (* for $p_{one-tail} < 0.05$, Bonferroni-corrected based on 18 comparisons). The error bars show the standard deviation for the null distribution.

2.3.2 Simulated data - whole-brain connectivity

The whole-brain detection accuracy was computed as the proportion of cases in which the whole-brain median connectivity value (across all channel-pairs) of each simulated EEG dataset passed the 95th percentile of the corresponding null distribution.

The null distribution consisted of whole-brain median connectivity values that were computed in matched simulated EEG datasets, where the time series between cortical sources of interest were subjected to one of two different surrogate procedures (time-point-shuffling or AAFT-randomization; see algorithm 2) to destroy their interaction relationship (see Figs 1 and 2).

Fig. 5A shows the mean accuracy of wPLI and wSMI (averaged over all SNRs) computed for each source pairing (intra/inter-hemispheric) and tested interaction dynamics. Fig. 5B shows the whole-brain accuracy at each SNR. Of note, the accuracy of the two connectivity measures was similar for intra- and inter-hemispheric connections.

The performance of both metrics was similar for the linear relationship in the broadband (0.5-12 Hz) signal. However, wPLI showed higher accuracy than wSMI in the intra-hemispheric case, when connectivity in the alpha-band (8-12 Hz; corresponding to the range in which the interaction was modelled) was specifically considered (Fig. 6).

While wSMI performed better at detecting the Hénon map dynamics for high SNRs (≥ 0.67), wPLI performed better at detecting the Ikeda dynamics, especially at intermediate SNRs (0.28-0-86).

Both wPLI and wSMI showed significant and comparable levels of accuracy for all Rössler (x,y; x,z; y,z) cases at all tested SNRs, with the exception of low SNRs (Rössler (y,z) SNRs 0.05-0.08), for which wSMI tended to achieve a better detection performance.

For the Lorenz (x,y) dynamics, wPLI achieved a better mean intra-hemispheric accuracy relative to wSMI, with the strongest differences observed for low SNRs (0.06-0.32). On the other hand, wSMI had higher accuracy for identifying Lorenz (y,z) dynamics for all SNRs ≥ 0.06. Finally, while no overall performance differences were observed at detect-

ing Lorenz (x,z)-based interaction dynamics, wPLI tended to achieve a higher accuracy for intermediate SNRs, between 0.41 and 0.51.

Of note, with the expected exception of the Rössler dynamics (see Methods), similar results were obtained when the null distributions were generated using phase-shuffling (AAFT) instead of time-point shuffling (Fig. 7).

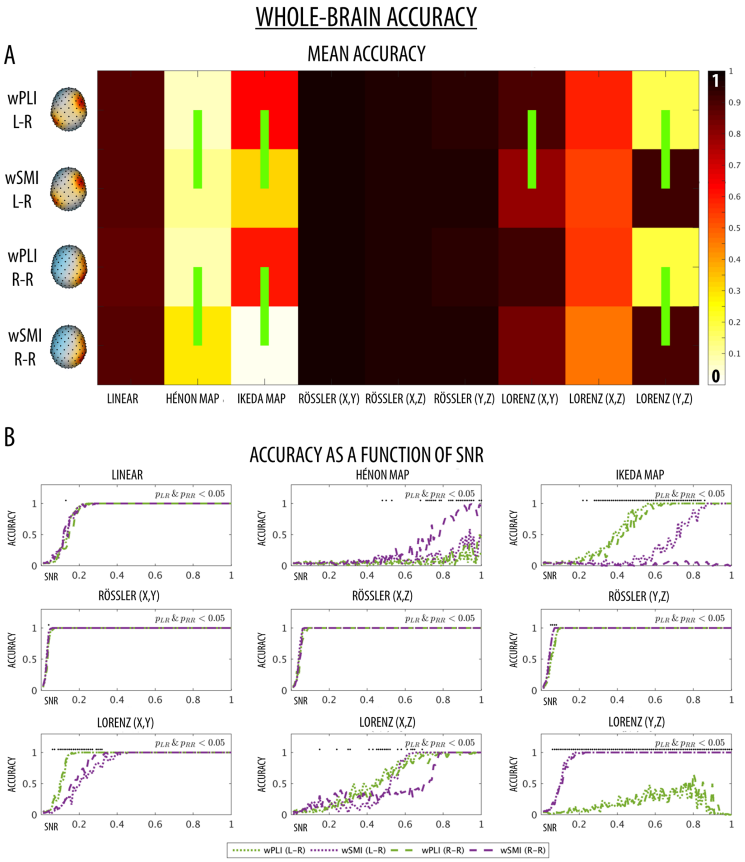

Figure 5: A) Mean whole-brain detection accuracy for all nine different relationships between the chosen source location pairings (L = left IPL to right MFG; R = right IPL to right MFG). The green vertical lines mark significant differences between wPLI and wSMI (permutation tests, $p < 0.05$) for each type of interaction, pairing of source locations and SNR. The brain images were plotted based on the Matlab scripts provided in the BBCB toolbox (Haufe and Ewald, 2016). B) Whole-brain detection accuracy for all nine different relationships between the chosen source location pairings as a function of SNRs (L = left IPL to right MFG; R = right IPL to right MFG). Black dots at the top of each graph mark significant accuracy differences between wPLI and wSMI for each specific SNR that were observed for both intra- and inter-hemispheric conditions

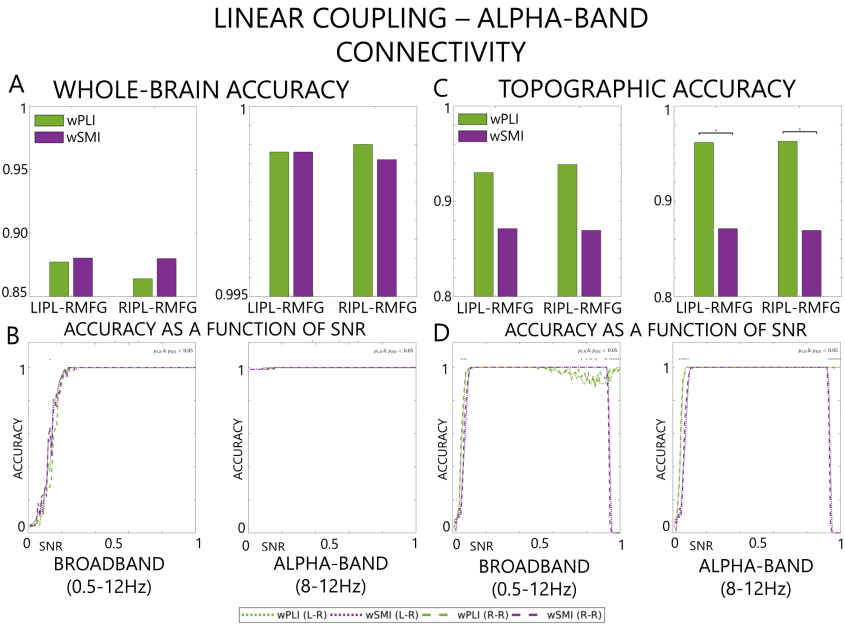

Figure 6: Whole-brain (A and B) and topographic (C and D) detection accuracy for linear dynamics analysed within the 0.5-12 Hz (broadband) or the 8-12 Hz (alpha-band) ranges (L = left IPL to right MFG; R = right IPL to right MFG). In bar plots (A, C), the * marks significant differences between wPLI and wSMI (permutation tests, $p < 0.05$). In B and D, accuracy is shown as a function of SNR. In these graphs, black dots mark significant accuracy differences between wPLI and wSMI (for a specific SNR) that were observed for both intra- and inter-hemispheric conditions

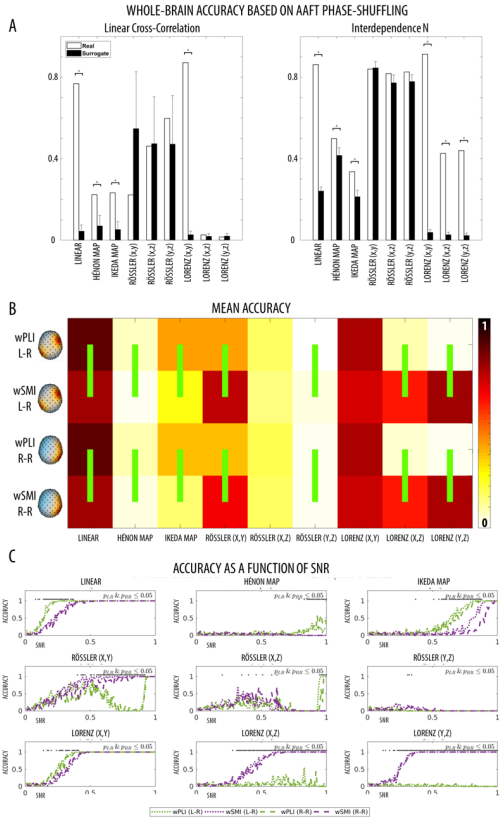

Figure 7: A) Absolute values of cross-correlation (CC; measure of similarity of two series as a function of the displacement of one relative to the other) and interdependence measure N (measure of the nonlinear relationship between two time series) for simulated source time-series (0.5-12 Hz) and for the corresponding time-series obtained after AAFT phase-shuffling (* for $p_{one-tail} < 0.05$, Bonferroni-corrected based on 18 comparisons). B) Mean whole-brain detection accuracy for the nine tested relationships between the chosen source location pairings (L = left IPL to right MFG; R = right IPL to right MFG). The green vertical lines mark significant differences between wPLI and wSMI (permutation tests, $p < 0.05$). C) Whole-brain detection accuracy for the nine tested relationships between the chosen source location pairings as a function of SNRs (L = left IPL to right MFG; R = right IPL to right MFG). Black dots at the top of each graph mark significant accuracy differences between wPLI and wSMI for each specific SNR that were observed for both intra- and inter-hemispheric conditions

2.3.3 Simulated data - topographic connectivity

The topographic accuracy was defined as the proportion of simulated EEG datasets (with true interactions between the cortical sources of interest), in which the connectivity between the two electrodes closest to the cortical sources passed the 95th percentile of all other electrode pairings. Results are similar to those described for whole brain accuracy (Fig. 8).

For the linear dynamics, wPLI and wSMI showed again similar mean accuracies, but wPLI tended to have higher accuracy for low SNRs (0.05-0.08) and high SNRs (> 0.94). Accuracy of wPLI (but not of wSMI) further improved for band-limited connectivity in the alpha-range (8-12 Hz; Fig. 6), especially for low SNRs (0.04-0.09) as well as high SNRs (≥ 0.93).

For both Hénon and Ikeda iterated maps, the mean topographic accuracy of wPLI was significantly higher than the mean topographic accuracy of wSMI. Specifically, in the Hénon case, wPLI had higher accuracy especially for SNRs ≥ 0.44, while in the Ikeda case, it had higher accuracy at low and intermediate SNRs (0.14-0.50).

Both wPLI and wSMI showed high levels of mean accuracy for the three Rössler (x,y; x,z; y,z) cases, although wPLI performed significantly better than wSMI in the intra-hemispheric case of Rössler (x,y), the inter-hemispheric case of Rössler (x,z) and both inter-and intra-hemispheric cases of Rössler (y,z). The evaluation of accuracy levels as a function of SNR showed that wSMI tended to perform better than wPLI for low SNRs (0.11-0.21) in the Rössler (y,z) case, while it showed a steep decrease in accuracy at high SNRs (R-R Rössler (x,y) ≥ 0.75; L-R Rössler (x,z) ≥ 0.86; L-R/R-R Rössler (y,z) ≥ 0.76/0.83).

Finally, while wPLI and wSMI showed similar mean accuracy in the Lorenz (x,y) case (with wPLI performing relatively better for SNRs in the range 0.03-0.06), only wSMI was able to detect interactions based on Lorenz (x,z) and Lorenz (y,z) dynamics (Lorenz (x,z) ≥ 0.07; Lorenz(y,z) ≥ 0.04).

Videos that show the mean connectivity matrices across all simulated hd-EEG recordings as a function of SNR can be found here.[3] A video showing frequency-resolved wPLI computed between the electrodes spatially closest to the sources can be found here.[4]

[3] Description: Connectivity matrices obtained in the presence of interacting sources and in surrogate data as a function of SNR. Different videos have been generated for each of the tested interaction dynamics. The connectivity matrices represent the mean across all possible brain noise instantiations at any particular SNR. The top two connectivity matrices represent the matrices obtained in the presence of LIPL-RMFG or RIPL-RMFG interacting sources, while the bottom two connectivity matrices show the result of shuffled source interaction dynamics for both source location pairings. The top right plot shows the values used to determine topographic accuracy, i.e. the value of connectivity between the electrodes spatially closest to the sources, described here as "LIPL-RMFG" and "RIPL-RMFG" and their corresponding threshold, described as "95% All". The bottom right plot shows the values used to determine whole-brain accuracy, i.e. the value of median connectivity across all channels in real ("L-R Real", "R-R Real") and surrogate data ("L-R Surr", "R-R Surr").

[4] Description: Connectivity matrices obtained in the presence of interacting sources and in surrogate data as a function of SNR. Different videos have been generated for each of the tested interaction dynamics. The connectivity matrices represent the mean across all possible brain noise instantiations at any particular SNR. The top two connectivity matrices represent the matrices obtained in the presence of LIPL-RMFG or RIPL-RMFG interacting sources, while the bottom two connectivity matrices show the result of shuffled source interaction dynamics for both source location pairings. The top right plot shows the values used to determine topographic accuracy, i.e. the value of connectivity between the electrodes spatially closest to the sources, described here as "LIPL-RMFG" and "RIPL-RMFG" and their corresponding threshold, described as "95% All". The bottom right plot shows the values used to determine whole-brain accuracy, i.e. the value of median connectivity across all channels in real ("L-R Real", "R-R Real") and surrogate data.

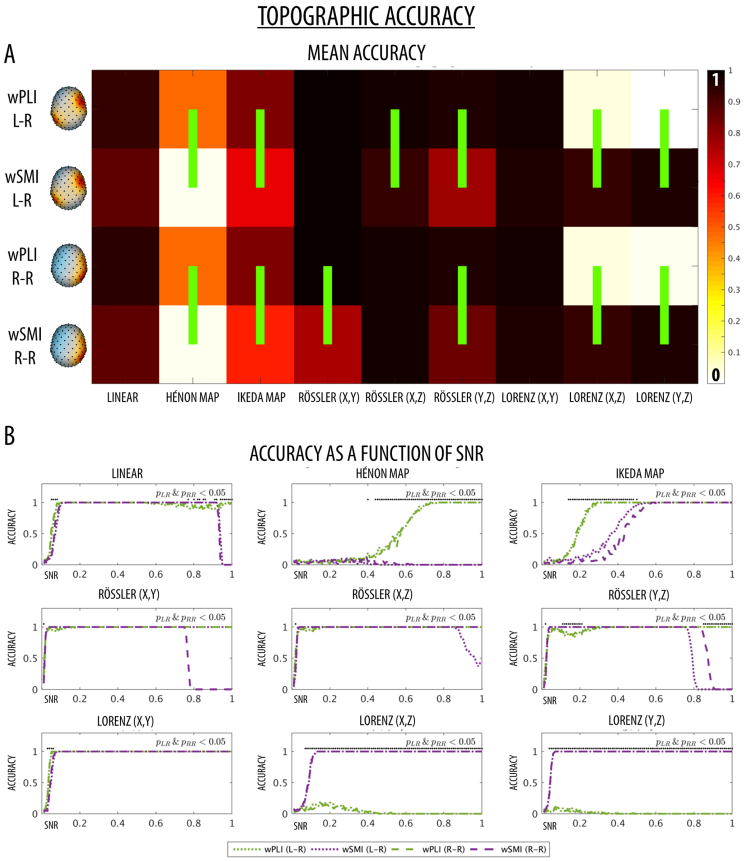

Figure 8: A) Mean topographic detection accuracy for all nine different relationships between the chosen source location pairings (L = left IPL to right MFG; R = right IPL to right MFG). The green vertical lines mark significant differences between wPLI and wSMI (permutation tests, $p < 0.05$) for each type of interaction, pairing of source locations and SNR. The brain images were plotted based on the Matlab scripts provided in the BBCB toolbox (Haufe and Ewald, 2016). B) Topographic detection accuracy for all nine different relationships between the chosen source location pairings as a function of SNRs (L = left IPL to right MFG; R = right IPL to right MFG). Black dots at the top of each graph mark significant accuracy differences between wPLI and wSMI for each specific SNR that were observed for both intra- and inter-hemispheric conditions

2.3.4 Experimental data in wakefulness and sleep

In wakefulness, both wPLI and wSMI revealed significant levels of connectivity in all tested electrodes ($p < 0.05$, cluster-corrected), relative to values observed in time-point shuffled data (Figs 9 and 10A; 0.5-12 Hz frequency range). In particular, for both measures the highest connectivity values were observed in posterior (occipital, parietal) areas.

However, in N3-sleep the two methods provided different results: wPLI revealed diffuse high connectivity values peaking in frontal areas, while wSMI showed reduced connectivity values (Figs 9 and 10B).

In line with these observations, the direct contrast between wakefulness and N3-sleep also revealed distinct changes based on wPLI and wSMI (Figs 9 and 10C). Specifically, while wSMI connectivity was significantly higher for wakefulness as compared to N3-sleep in all areas, there were no statistically significant differences in wPLI between these two states of vigilance.

Further analyses focusing on classical frequency bands (delta: 0.5-4Hz, theta: 4-8Hz, alpha: 8-12Hz), showed that both wPLI and wSMI were higher in wakefulness than in sleep within the alpha-band (figs. 12 and 13). However, wPLI was also lower in wakefulness relative to N3 in the delta-band. Frequency-resolved wPLI for wakefulness and sleep can be found in Fig 11.

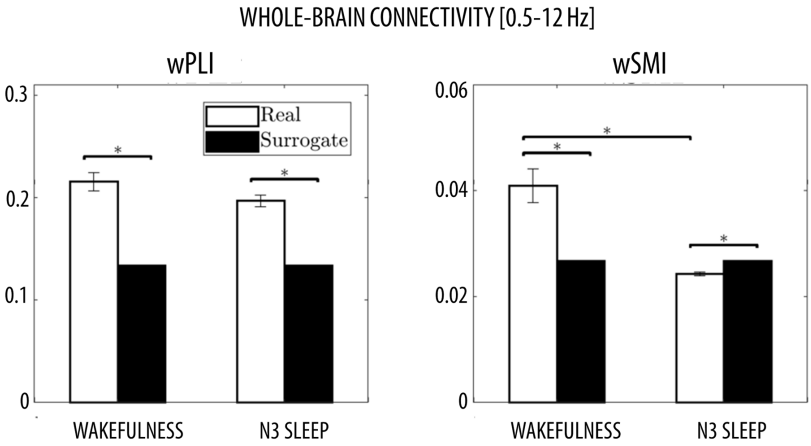

Figure 9: Whole-brain wPLI (left) and wSMI (right) connectivity in wakefulness and sleep (0.5-12 Hz). Paired comparisons were performed between median whole-brain connectivity in wakefulness and N3-sleep, as well as between experimental and surrogate data. * marks $p < 0.05$ (non-parametric permutation tests)

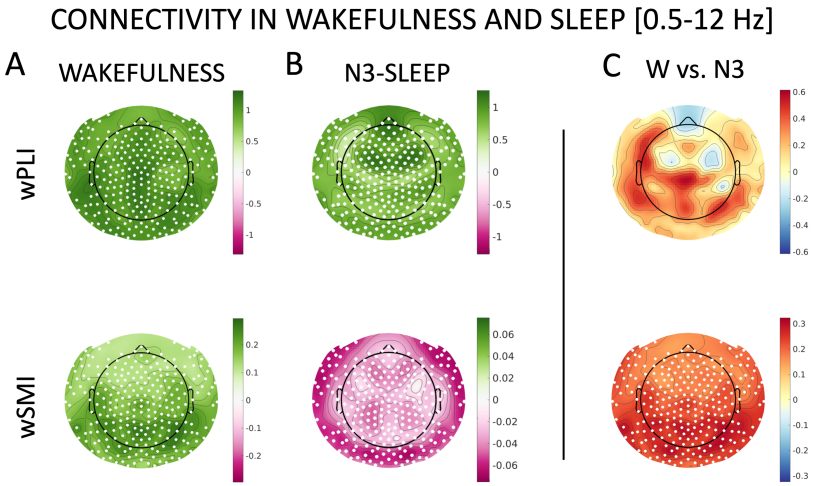

Figure 10: Topographic wPLI (left) and wSMI (right) connectivity in wakefulness and sleep (0.5-12 Hz). Paired comparisons were performed between A) wakefulness and shuffled surrogate data and B) N3-sleep and shuffled surrogate data and C) wakefulness and N3-sleep, for wPLI (top row) and wSMI (bottom row). White dots mark significant effects (cluster-based non-parametric permutation test, $p < 0.05$). Colorbars show the permutation test statistic for the difference between conditions, so that the green color marks higher values in real vs. surrogate data for panels A and B. In panel C, the red color indicates higher values in wakefulness, while the blue color indicates higher values in sleep. These images were generated using the 'topoplot' function in EEGLAB (Delorme and Makeig, 2004)

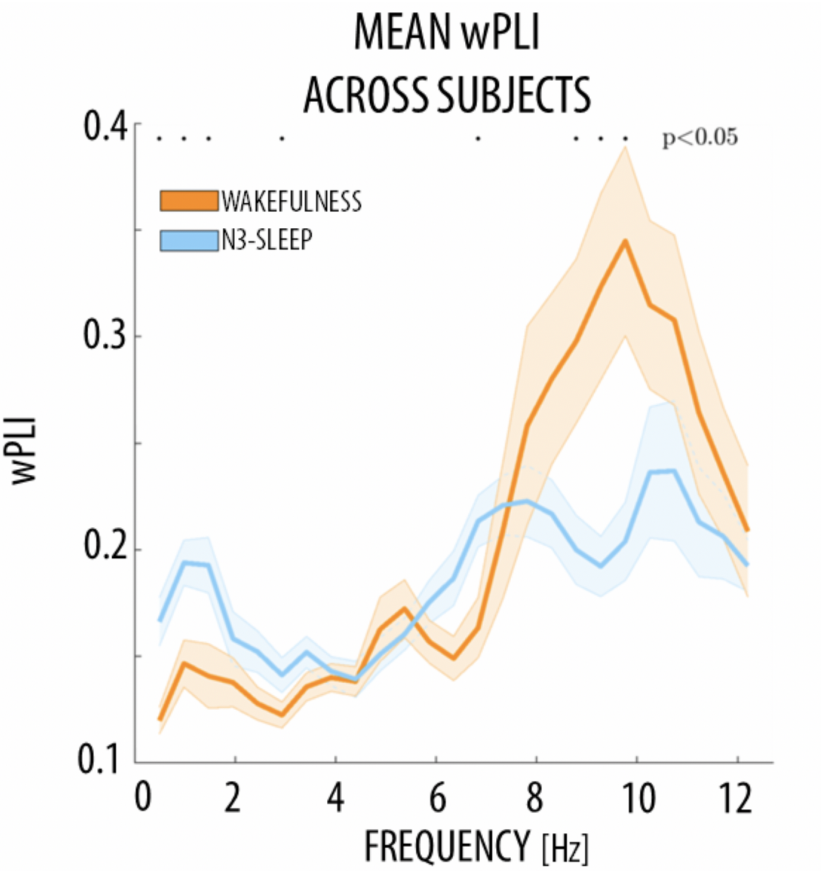

Figure 11: Group-level (N=12) average wPLI (median across channels) for each frequency-bin computed on data from wakefulness and N3-sleep. The shaded area reflects the standard error of the mean for each vigilance state. Black dots at the top mark significant differences between wakefulness and sleep for each specific frequency bin (non-parametric permutation tests, $p < 0.05$)

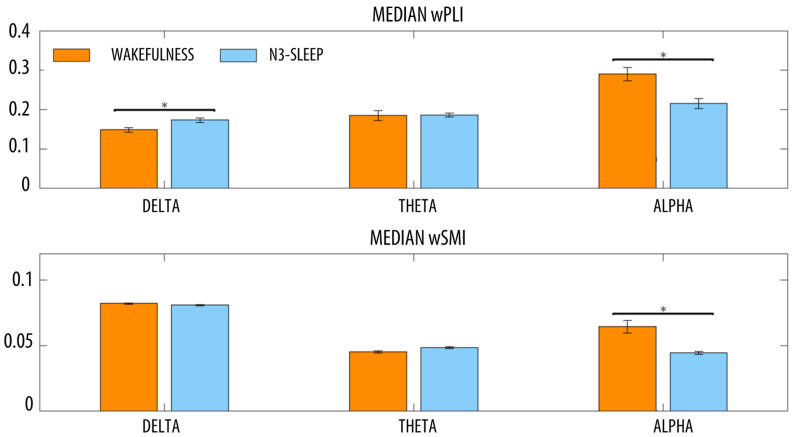

Figure 12: Whole-brain, median wPLI and wSMI in wakefulness (W) and N3-sleep in different frequency bands (delta: 0.5-4Hz, theta: 4-8Hz, alpha: 8-12Hz). Error bars show the standard error of the mean. Horizontal bars and * mark significant differences between conditions (non-parametric permutation tests, $p < 0.05$, Bonferroni-corrected for the number of tested frequency bands)

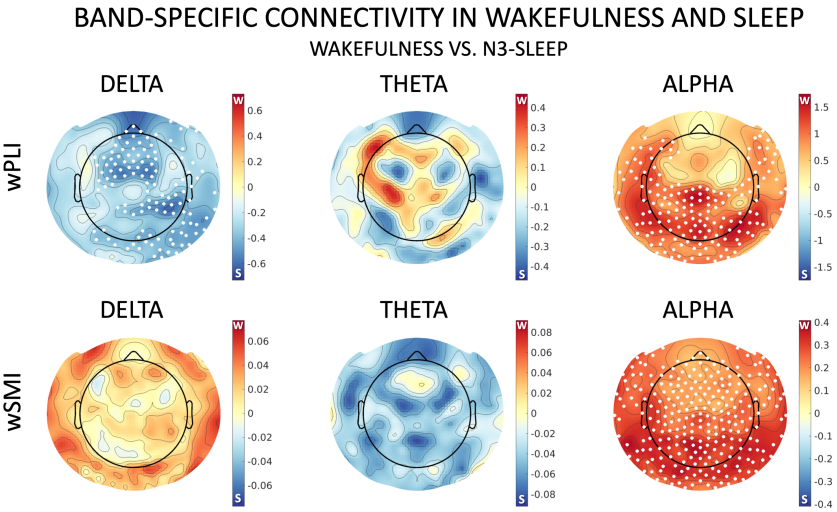

Figure 13: Topographic wPLI and wSMI connectivity in wakefulness (W) and N3-sleep in different frequency bands (delta: 0.5-4Hz, theta: 4-8Hz, alpha: 8-12Hz). Colorbars show the permutation test statistic for the differences between wakefulness and N3-sleep. The red color marks higher values in wakefulness, while the blue color indicates higher values in sleep. White dots mark significant differences between conditions (cluster-based non-parametric permutation test, $p < 0.05$). These images were generated using the 'topoplot' function in EEGLAB (Delorme et al., 2011)

2.4 Discussion

The weighted Phase Lag Index (Vinck et al., 2011) and the weighted Symbolic Mutual Information (King et al., 2013) are two robust functional connectivity approaches increasingly applied to M/EEG data, because of their relative immunity to volume conduction effects (Canales-Johnson et al., 2017; Chennu et al., 2017, 2014, 2016; Cohen, 2015; Comsa et al., 2019; Lau et al., 2012; Lee et al., 2017a,b; Ortiz et al., 2012; Parra et al., 2017; Robinson and Mandell, 2015; Simor et al., 2018; Sitt et al., 2014; Tramonti et al., 2018; Xing et al., 2017).

Here we set out to investigate whether the two methods are able to capture overlapping or complementary information regarding variations in brain inter-regional interactions.

By combining analyses on simulated hd-EEG data and real hd-EEG recordings collected in different states of vigilance, we demonstrated that wPLI has an optimal sensitivity for interaction dynamics presenting a mixture of linear and nonlinear components, whereas wSMI has higher sensitivity to predominantly nonlinear dynamics. Given that the brain is a highly complex system typically characterised by both linear and nonlinear interaction dynamics (Stam, 2005), it may be better described through the combined use of different measures (David et al., 2004).

Consistent with this view, our results suggest that the conjoint use of wPLI and wSMI may allow researchers to measure complementary information about FC interactions, and thus to better describe relative changes associated with distinct behavioural states.

2.4.1 Performance of wPLI and wSMI in simulated data

The 'Berlin Brain Connectivity Benchmark' (BBCB) framework (Haufe and Ewald, 2016) was adapted and employed to generate hd-EEG recordings in sensor-space. This framework allowed us to model different interaction dynamics between two cortical sources, noise with temporal and spatial structure as well as source mixing due to volume conduction, in a highly realistic electromagnetic volume conductor (head) model.

In particular, we generated interaction dynamics with different degrees and types of nonlinearity, from linear to exclusively nonlinear, and specifically tested the sensitivity of wPLI and wSMI at detecting these inter-regional dependencies. Of note, for each of the tested dynamics, we also tested two different source locations (intra- and inter-hemispheric interactions) and different signal-to-noise ratios (SNR).

Our results showed that the phase-based measure wPLI performs generally better at detecting inter-regional couplings presenting both linear and nonlinear components. Only in two of the more complex nonlinear coupling cases (Lorenz (x,z) and Lorenz (y,z)), characterised by non-significant cross-correlation values (see Figs 5 and 8), wPLI had a very low accuracy.

Contrarily, the information-theoretic measure wSMI had a significantly higher accuracy for these two interaction dynamics, but performed significantly worse for the Ikeda-based couplings and also had lower topographic accuracy for Hénon- and Rössler-based couplings.

With few exceptions, the accuracies of wPLI and wSMI were very similar for intra- and inter-hemispheric interactions, and the detection accuracy of both methods tended to increase with an increase in SNR. Of note, however, the spatial (topographic) accuracy of wSMI (but not the whole-brain accuracy based on median global connectivity) showed instead a decrease at high SNRs for linear and Rössler interactions. This accuracy reduction may be related to an increase in the spatial spreading of the source signals to more distant scalp electrodes with increasing SNRs, which may have led a greater proportion of electrodes to detect the underlying functional coupling (loss of spatial resolution).

Moreover, at high SNRs a relative 'cross-contamination' may be expected to occur between the two electrodes spatially closest to the interacting sources. In particular, the activity of one source may be 'volume-conducted' to the electrode closest to the other source (and vice-versa). Due to the particular weighting approach used for wSMI, the increased similarity between the signals of these particular channels may limit the maximum attainable connectivity strength, thus reducing the relative difference with respect to all other electrode pairings.

On the other hand, such effects of volume conduction at high SNRs can be expected to have had only a marginal impact on (or even to improve) the estimation of whole-brain accuracy with respect to null-datasets generated from point- or phase-shuffled time-series.

In the linear case, where interacting dynamics were fixed in the alpha-range, we noted that both wPLI and wSMI had a lower accuracy at detecting the presence of interacting sources when evaluating the broad-band signal instead of the band-limited one (Fig. 6). As described below, this was confirmed by the analysis on experimental data, which revealed a higher sensitivity of the band-limited analysis to potential differences across vigilance states (Fig. 13).

These observations indicate that wPLI and wSMI may have a lower sensitivity when computed on a frequency range larger than the one in which the interaction actually occurs. For this reason, a-priori knowledge regarding the potential frequency ranges of interest should be used to guide the analyses whenever possible. In this respect, however, wPLI has the important advantage of also allowing more exploratory, frequency-resolved analyses; however, such analyses may raise statistical issues when many distinct interactions have to be tested.

Overall, our results demonstrated that wPLI, as a measure of phase synchronization, performs generally better at detecting functional couplings presenting a mixture of linear and nonlinear dynamics, whereas wSMI, fundamentally rooted in mutual information, has higher sensitivity for exclusively nonlinear dynamics, such as Lorenz (x,z) and Lorenz (y,z) dynamics. Importantly, present results also demonstrated that both wPLI and wSMI are characterised by a high spatial (topographic) accuracy, thus supporting their use in graph theoretical analysis at sensor-level.

2.4.2 Performance of wPLI and wSMI in distinct states of vigilance

To evaluate whether the results we obtained from simulated EEG data are relevant to the analysis of real experimental data, we tested and com-

pared the performance of the two connectivity measures in hd-EEG recordings collected in humans in different states of vigilance. In fact, both wPLI and wSMI have been previously shown to successfully identify relative variations in brain FC associated with different degrees of consciousness under anaesthesia or following severe brain injury (Chennu et al., 2014, 2016; King et al., 2013; Lee et al., 2017a,b; Sitt et al., 2014).

Based on these premises, here we asked whether the two methods may identify similar or distinct changes associated with variations in the level of consciousness of healthy subjects from wakefulness to deep NREM-sleep (N3). In humans, N3-sleep is characterised by the occurrence of large and diffuse EEG slow waves (0.5-4 Hz), by relative sensory disconnection (Rechtschaffen et al., 1966) and by a low probability of having any conscious experiences (dreams) (Siclari et al., 2017). It has been suggested that slow waves, representing the alternation of neuronal silence (off-period) and firing (on-period), and occurring out-of-phase in different cortical areas, may contribute to the fading of consciousness through the interruption of causal interactions between distant brain regions (Jobst et al., 2017; Massimini et al., 2005; Pigorini et al., 2015; Vecchio et al., 2017). Here we showed that N3-sleep is associated with a significant and diffuse decrease in wSMI connectivity within the 0.5-12 Hz frequency range. This difference appeared particularly prominent in posterior brain areas. In contrast, we observed no significant differences between wakefulness and N3-sleep in broadband wPLI-connectivity.

A band-limited analysis revealed that changes in wSMI were mainly driven by an overall decrease in alpha (8-12 Hz) connectivity in N3 relative to wakefulness. Of note, alpha-band wPLI connectivity also showed a similar, but more localized, decrease during N3-sleep, especially in posterior areas. These results are in line with previous work showing that the transition into unconsciousness due to sedation or physiological sleep (stage N1/N2) is associated with a decrease in alpha wPLI-connectivity (Blain-Moraes et al., 2014; Chennu et al., 2016; Comsa et al., 2019; Lee et al., 2017a,b), especially in posterior regions (Lee et al., 2017a,b) and for posterior-anterior interactions (Blain-Moraes et al., 2014; Chennu et al., 2016; Comsa et al., 2019).

Moreover, they are consistent with evidence indicating that relative to healthy individuals, patients with unresponsive wakefulness syndrome (UWS) or in a minimally conscious state (MCS) display a connectivity decrease that mainly affects posterior areas or posterior-anterior interactions (Chennu et al., 2017, 2014; King et al., 2013; Lehembre et al., 2012; Sitt et al., 2014).

Similarly, alpha-band wSMI has been found to be lower in UWS as compared to MCS patients (Sitt et al., 2014). Therefore, our findings indicate that both wPLI and wSMI may be suited to capture variations in alpha-connectivity associated with relative changes in vigilance and/or responsiveness to the environment.

However, wPLI also revealed a relative increase in delta (0.5-4 Hz) connectivity. Importantly, the change in delta-wPLI is consistent with the presence of traveling slow waves during sleep (Massimini et al., 2004) as well as with a recent similar observation of increased parietal and parieto-frontal delta-wPLI connectivity during propofol sedation (Lee et al., 2017b) and midazolam-based anaesthesia (Lee et al., 2017a). Moreover, wPLI in the delta/theta-band has been shown to be increased in patients with disorders of consciousness (UWS, MCS), relative to healthy awake subjects (Chennu et al., 2014).

In summary, the analysis of wPLI- and wSMI-based connectivity in different states of vigilance confirmed our findings in simulated data, indicating that the two methods are sensitive to distinct brain dynamics. While an in-depth characterization of the differences in FC between wakefulness and sleep was beyond the scope of the present work, our results also suggest that wakefulness may be characterised by a mixture of 'simple' (i.e., mainly linear; better described by wPLI) and more complex (i.e., mainly nonlinear) interactions (better described by wSMI) in the alpha range, while sleep may be dominated by 'simpler' delta-band connectivity (better captured by wPLI), likely reflecting the occurrence of traveling slow waves. This interpretation is in line with previous observation indicating that N3 is associated with lower complexity or entropy (Ma et al., 2018; Stam, 2005) as compared to wakefulness.

2.5 Conclusions

Our study demonstrates that wPLI and wSMI connectivity metrics provide distinct but complementary information about inter-regional interactions and indicate that the combined use of these two methods may provide a better and more complete characterization of brain functional dynamics within and across distinct behavioural states. In particular, we showed that while wPLI displays an optimal sensitivity for interaction dynamics with linear and nonlinear components, wSMI has a higher sensitivity for predominantly nonlinear dynamics.

We also showed that this finding may have significant implications for the analysis of functional connectivity in states of vigilance associated with different levels of consciousness.

In light of recent evidence indicating that the independent application of wPLI and wSMI connectivity metrics may allow to identify changes in brain connectivity associated with variations in the level of consciousness, our results point to their possible combined use as a powerful tool to increase their accuracy and predictive value. Nonetheless, our findings may also have more general implications for the study of functional connectivity in a wide variety of behavioural conditions characterised by distinct underlying brain dynamics.

Chapter 3

Cross-Participant Prediction of Vigilance Stages through the combined use of wPLI and wSMI EEG Functional Connectivity Metrics

3.1 Introduction

All the results shown in this chapter refer to the same-titled abstract, presented at the World Sleep Congress 2019 in Vancouver.

Classically, the transition from wakefulness to sleep and the alternation of the different sleep stages are described in terms of variations in electrophysiological brain activity. The falling asleep process is characterized by a shift from fast-frequency, low-amplitude oscillations, to low-frequency, high amplitude activity, with typical slow waves (0.5-4Hz) and spindles (12-16Hz) (Marzano et al., 2013; Ogilvie, 2001; Siclari et al.,

2014). An increase in the incidence and amplitude of regional slow waves then marks the deepening of Non-REM sleep. The occurrence of REM sleep, every 60-150min, is instead identified by a relative EEG desynchronization, with an increase in theta activity (4-8Hz), and by bursts of sawtooth-waves (2-5Hz) that commonly precede the occurrence of rapid eye movements (Aserinsky et al., 1953; Bernardi et al., 2019b; Dement and Kleitman, 1957).

All these changes may be efficiently captured through the analysis of signal power in classical frequency bands, although evidence indicates that the different stages of vigilance are also characterized by relative variations in the way distinct areas of the brain interact with each other (e.g., Imperatori et al. (2019); Langheim et al. (2011); Migliorelli et al. (2019); Rusterholz et al. (2017); Vecchio et al. (2017)). These differences can be explored using functional connectivity (FC) metrics, which identify statistical (undirected) associations among the EEG time-series of spatially distinct brain regions. Interestingly, distinct FC indices may allow the detection of partially different interaction dynamics, with distinct weights of linear and nonlinear components, and may thus produce partially different results (Imperatori et al., 2019; Migliorelli et al., 2019). However, it is still unclear whether connectivity metrics, either analysed individually or in combination, can actually provide relevant or rather overlapping (i.e., redundant) information about the current stage of vigilance of an individual with respect to classical (power-based) measures of EEG brain activity.

The weighted Phase Lag Index (wPLI (Vinck et al., 2011)) and the weighted Symbolic Mutual Information (wSMI (King et al., 2013)) are two robust FC approaches increasingly applied to MEG and EEG data because of their relative immunity to volume conduction. Thanks to this property, wPLI and wSMI are less likely to detect spurious functional interactions determined by the quasi-simultaneous conduction of real brain signals and of physiological or non-physiological noise to EEG-sensors distant from the actual source. Interestingly, both these methods have been suggested to track the level of consciousness based on promising findings in patients with severe brain injury (minimally con-

scious state, unresponsive wakefulness syndrome) or in participants under anaesthesia (Chennu et al., 2014, 2016; King et al., 2013; Lee et al., 2017a,b; Nir and Tononi, 2010). Of note, we recently demonstrated that wPLI and wSMI present a different sensitivity to distinct FC dynamics and may thus provide complementary information regarding brain inter-regional interactions (Imperatori et al., 2019). Specifically, while wPLI has an optimal sensitivity for dynamics presenting a mixture of linear and nonlinear components, wSMI has higher sensitivity to predominantly nonlinear dynamics.

In light of the above premises, here we set out to investigate whether wPLI and wSMI may allow the detection of FC differences across distinct stages of vigilance including wakefulness, light NREM sleep (N2), deep NREM sleep (N3) and REM sleep, and whether the provided information is redundant or complementary with respect to that granted by power-based indices of brain activity. To this aim, a supervised classification approach was used to identify the optimal combination of power- and FC-based features allowing to distinguish among vigilance stages across different sets of subjects. Crucially, this classification was cross-validated across different sets of participants, thus allowing to determine the ability of the predictive model to generalise across independent groups of subjects. For each individual feature, we also investigated its relevance, information content and degree of redundancy with other examined features.

In addition, the present study offered us the opportunity to investigate the potential value of FC-derived indices as markers of the levels of consciousness and of sensory disconnection during sleep. Indeed, the probability of having a conscious experience varies greatly between wakefulness and sleep as well as across the different sleep stages: subjects may report a conscious experience (a dream) in less than 30% of the awakenings from deep (N3) NREM sleep, while this percentage may get close to 100% in REM sleep (Nir and Tononi, 2010; Siclari et al., 2017, 2018, 2013). Yet, while REM sleep is populated by rich and vivid conscious experiences that often resemble in many aspects those of wakefulness, it is also characterized by a relative disengagement (or 'disconnection') of

the individual from the external environment (Bonnet and Moore, 1982; Darracq et al., 2018; Nir and Tononi, 2010). Therefore, we specifically investigated whether FC-based indices could significantly contribute to the classification of states characterized by high (wakefulness, REM) vs. low (NREM) levels of consciousness, as well as by 'connected' (wakefulness) and 'disconnected' (REM) consciousness (Darracq et al., 2018).

3.2 Methods

3.2.1 Participants

Twenty-four healthy adult participants (26.7 ± 5.7yrs, 13F) underwent hd-EEG recordings (256 channels, 500Hz) during the night and while awake in bed after sleep (8am; 6min, eyes-closed). The overnight recordings were started at the usual bed-time of each subject and interrupted at 7am. Twelve subjects (25.5 ± 3.7yrs, 6F; dataset-1) were studied in the context of a project aimed at exploring the effects of short-term visual deprivation on brain activity during sleep (Bernardi et al., 2019a). Here we only included data from the control condition, in which subjects remained in the sleep laboratory and watched movies of their choice (selected from a pre-defined list) from 3 to 8pm.

The other twelve subjects (27.9 ± 7.1 yrs, 7F; dataset-2) only arrived at the laboratory 2h prior to the beginning of the overnight recording. All volunteers had a good sleep quality as assessed by the Pittsburgh Sleep Quality Index (PSQI score ≤ 5;(Buysse et al., 1989)) and scored ≤ 10 points on the Epworth Sleepiness Scale (ESS; Johns (1991)). Volunteers were asked to maintain a regular sleep-wake schedule in the week preceding the overnight recording. Compliance was verified using wrist-worn actigraphy devices (MotionWatch 8, CamNtech). The study was approved by the ethical committee of the Lausanne University Hospital. Written informed consent was obtained from each subject.

3.2.2 EEG Recordings

Wake EEG recordings

Resting-state eyes-closed recordings collected in the morning, during wakefulness (W), were bandpass-filtered between 0.5 and 45 Hz. Each recording was divided into nonoverlapping 5s epochs and visually inspected to identify and reject bad channels and epochs containing large artefacts (NetStation 5; Electrical Geodesic). An independent component analysis (ICA) was then performed to remove residual ocular, muscular, and electrocardiograph artefacts using EEGLAB (Delorme and Makeig, 2004). [1] Rejected channels were eventually interpolated using spherical splines. Finally, the first 0.5s and the last 0.5s of each 5s epoch were discarded and excluded from further analyses.

Sleep EEG recordings

Sleep EEG recordings were scored according to standard criteria using 30-s epochs (Iber, 2007). [2] Recordings were bandpass-filtered between 0.5 and 45 Hz. All epochs scored as N2, N3 (NREM) or REM were then extracted and visually inspected to remove bad channels (later replaced by spherical spline interpolation). [3] An ICA-based procedure was used to remove potential artefacts. Given that NREM and REM sleep are affected by homeostatic and circadian factors, and that REM sleep is especially represented toward the morning hours, further analyses were focused on NREM epochs extracted from the first half of the night and on REM epochs identified in the second half of the night. [4]

[1] This procedure has been shown to reduce the impact of EEG artefacts on power computation and on the identification of individual grapho-elements while producing negligible changes in physiological signals of interest (Iriarte et al., 2003; Romero et al., 2003).

[2] For scoring purposes, electrodes located in the chin-cheek region were used to evaluate muscular activity, whereas four electrodes placed near the eyes were used to monitor horizontal and vertical eye movements (Siclari et al., 2014).

[3] N1 was not considered in the analysis, as it is a transitional state and therefore generally very short, accounting for only about 5% of total sleep time.

[4] This approach also allowed us to minimize the impact of inter-subject differences in the relative distribution of NREM and REM epochs across the night (e.g., due to the lack of consistent REM sleep during the first sleep cycle in some participants).

3.2.3 Data bootstrapping

A bootstrapping procedure with replacement (see explanation 3.2.1) was applied to account for differences in the amount of data available for each stage of vigilance. Specifically, at each iteration of the bootstrapping procedure (N=2000) and for each considered stage (W, N2, N3 and REM), fifteen 2s segments were randomly chosen, obtaining 30s-long data epochs.

A current-source-density transform was applied to all extracted EEG data epochs using the CSD toolbox (Kayser and Tenke, 2006), as described in previous works (Imperatori et al., 2019; King et al., 2013; Vinck et al., 2011). This method provides a reference-independent signal and acts as a spatial filter, leading to a relatively improved spatial resolution (Nunez et al., 2006).

Explanation 3.2.1: Bootstrapping

Bootstrapping relies on the idea that the repetition of experiments provides us with estimates on the uncertainty of the sampling distribution such as the standard error of the mean or the confidence intervals. The key idea is that rather than physically having to repeat the experiments, we can simulate the replications.
In the non-parametric bootstrapping procedure (Efron, 1992), the original data set is essentially treated as a complete population and – at every bootstrapping iteration – a new, simulated sample is drawn from it, picking each observation with equal probability (allowing repeated values). The parameters of interest are then calculated either directly from the empirical distribution, or by applying a model to this surrogate data, leading to the uncertainty estimation of the distribution.
In contrast to permutation testing, another statistical resampling procedure, in bootstrapping, the goal is often to define confidence intervals on data characteristics (such as mean or variance) based on subsampling the data (Cohen, 2014). Conversely, the goal in permutation testing is to determine the probability that the observed test statistic could have been obtained if the null hypothesis were true (i.e. whether a finding is statistically significant).

3.2.4 Feature Extraction

Relative Power

The PSD (Welch's method, Hamming windows, 8 sections, 50% overlap) was calculated for each electrode in 2s data segments. Then, the signal power (POW) was computed for delta (0.5-4Hz), theta (4-8Hz), alpha (8-12Hz), sigma (12-16Hz), beta (18-25Hz), gamma (30-45Hz) and broad-band (0.5-45Hz) frequency ranges by integrating the PSD values in the frequency ranges of interest.

Relative power (relPOW) was computed by expressing the value of each frequency band as a percentage with respect to the total broad-band power. Finally, the mean was computed across the 15 segments of each 30s epoch (N=1000) and the median power was computed across all electrodes.

wPLI

wPLI was computed using the Fieldtrip toolbox (Oostenveld et al., 2011) (multi-taper method fast Fourier transform, single Hanning taper, 0.5 Hz frequency resolution, Vinck et al. (2011)). The mean value across the frequency-bins in the frequency range of interest was computed to obtain a single wPLI coupling value.

wSMI

The kernel k was chosen to be 3, implying that the symbols are constituted of three elements, leading to 3!=6 different potential symbols in total (King et al., 2013; Sitt et al., 2014). The temporal separation of elements that constitute a symbol was set to be $\tau = [41, 21, 14, 10, 6, 3]$ frames, such that the maximum resolved frequency was $f_{\max} = \frac{f_s}{k\tau}$, and therefore $[4.1, 7.94, 11.90, 16.67, 27.78, 55.56]$Hz depending on the chosen τ, whereby - due to the band-pass-filtering of the signal up to 45Hz - the maximum resolved frequency for $\tau = 3$ was 45Hz.

Prior to wSMI computation, the signal was either low-pass-filtered using a 6^{th} order Butterworth IIR filter - with an additional mirror padding

(`ft_preproc_padding`) of 1s before and after each individual segment to avoid potential filter edge-artifacts - or bandpass-filtered (4^{th} order Butterworth IIR filter) with the same padding scheme, depending on the chosen frequency-range.

3.2.5 Statistical comparisons

As described above, for each bootstrapping iteration, we computed the median power across electrodes and the median (wPLI/wSMI) connectivity across all pairs of channels in delta, theta, alpha, sigma, beta, and gamma frequency bands, thus obtaining 6 features per metric and 18 features in total. For each individual feature, non-parametric paired permutation tests (N=10000) were performed between all vigilance stages. A Bonferroni-correction was applied for the number of tested comparisons, separately for power-, wPLI- and wSMI-based features (N=36; corrected $p < 0.05$).

3.2.6 Classification Procedure

The subjects were divided into two equal-sized groups (N=12) corresponding to dataset-1 and dataset-2. A two-fold (i.e. training on dataset-1(2) and testing on dataset-2(1)) Linear Discriminant Analysis (LDA) was applied to investigate the ability of power- and connectivity-based features obtained from one dataset to discriminate vigilance stages in the other dataset (Duda et al., 2012; Li et al., 2006) (see algorithm 4). [5]

Specifically, the classifier was trained on a single 30s sampled epoch per stage of interest from each one of the 12 subjects in dataset-1 (2) (one bootstrapping iteration) and tested on a single 30s epoch per stage of interest from each one of the 12 subjects in dataset-2 (1). This procedure was repeated for all bootstrapping iterations (i.e. Nboot=2000 times) to estimate the corresponding classification accuracy.

[5] Of note, the obtained features and accuracies were very similar irrespective of which classifier (e.g., linear, quadratic LDA, support-vector machine (SVM) or Naive Bayes classifier) or accuracy metrics (e.g., accuracy or micro-averaged F1-score) were chosen.

Algorithm 4: Linear Discriminant Analysis

Result: Reduce f features to k linear discriminants (essential linear combinations of the original features) that separate the classes.

1 Compute the f-dimensional mean vectors for the c different classes from the dataset;

2 Compute the fxf scatter matrices (in-between-class S_B and within-class S_W scatter matrix);

3 Compute the eigenvectors ($\mathbf{e_1}, \mathbf{e_2}, ..., \mathbf{e_f}$) and corresponding eigenvalues ($\lambda_\mathbf{1}, \lambda_\mathbf{2}, ..., \lambda_\mathbf{f}$) for the matrix product of the scatter matrices $S_W^{-1} S_B$ to obtain the linear discriminants;

4 Sort the eigenvectors by decreasing eigenvalues and choose k eigenvectors ($k < f$) with the largest eigenvalues to form a fxk dimensional matrix $\mathbf{W}$;

5 Use this fxk eigenvector matrix to transform the samples onto the new subspace. This can be summarized by the matrix multiplication: $\mathbf{Y} = \mathbf{XxW}$, where $\mathbf{X}$ is a nxf-dimensional matrix, representing the n-samples and $\mathbf{Y}$ are the transformed nxk-dimensional samples;

6 → Obtain a feature subspace that maximises the between-class variance as compared to the within-class variance.

A forward selection procedure was performed to identify the optimal feature set (see Algorithm 5). The procedure started with an empty feature set. At each step of the forward selection procedure, the accuracies of classification models based on each available additional feature were computed. The feature giving rise to the highest classification accuracy was then added to the existing feature set. The selection was stopped when the added feature provided no further increase in mean accuracy (i.e. accuracy increase ≤ 0). Finally, a permutation-based null-hypothesis significance test was performed on the bootstrap mean estimate for the optimal feature set obtained from the forward selection procedure. For each permutation (Nperm=2000), the labels were shuffled in the training set of the classifier and the mean accuracy estimate per permutation was obtained using the same bootstrapping procedure as for the original labels. The true mean accuracy across bootstrapping iterations was compared to the 99%ile of the null distribution ($P < 0.01$).

Algorithm 5: Applied Forward Selection Procedure

Result: Features Relevant for the Classification

Start with empty feature set;
for *Step=1:NFeat* **do**
  for *Feat=1:NFeat* **do**
    Add Feat to existing set of features (temporarily);
    for *Boot=1:NBoot* **do**
      Perform classification (LDA);
    end
    Obtain mean estimate of accuracy per additional feature;
  end
  Select "additional" feature giving rise to highest accuracy;
  Add this feature to the existing set of features;
  if $Acc_{Step} < Acc_{Step-1}$ **then**
    Stop;
    Test the final model for all features included up to 'Step-1' by permuting the classification labels in the training set;
    for *Perm=1:NPerm* **do**
      Permute Labels in the training set;
      for *Boot=1:NBoot* **do**
        Perform classification (LDA) with permuted labels;
      end
      Obtain mean estimate of accuracy per permutation;
    end
    Obtain the 99% threshold of the null distribution (Acc_{perm})) and compare it to the mean estimate of accuracy (Acc_{Step-1}));
  else
    Continue with the Forward Selection Procedure;
  end
end

3.2.7 Mutual information analysis

To complement the findings regarding the best combination of features from the LDA-classification procedure described above, here we investigated the relevance of each individual feature in more detail. Specifically, the single-feature mutual information (MI) value was contrasted with the single-feature classification accuracy. MI was quantifies how much information each individual feature contains about the three different comparisons of vigilance stages: W vs. N2 vs. N3 vs. REM, W+REM vs. N2+N3 and W vs. REM. The continuous feature values were binned based on ranks into 4 equal-population bins, and the standard discrete formulation of MI was used (Cover et al., 2006; Ince et al., 2017). A Miller-Madow bias correction was applied (Miller, 1955).

A data augmentation procedure was used to ensure that a minimum of 100 values was available in each subject for enabling MI computation. Specifically, 50 data epochs were repeatedly sampled with replacement (2000 iterations) from the previously generated data distribution (see section 3.2.3). Of note, this procedure was especially necessary for wakefulness data, since only few minutes were recorded in all subjects, whereas more than 25 min of data were available for all other stages in 23 of the 24 studied volunteers.

In order to compare MI values with LDA accuracies for each feature, the single-feature LDA classification procedure (regarding the predictability across subjects) was repeated by performing the training on the same augmented datasets obtained for MI computation and tested on one 30s epoch per subject. The aim of this analysis is to qualitatively display the information content of all examined power- and FC-based features, by contrasting the within-subjects MI analysis with the across-subjects LDA classification analysis.

3.2.8 Partial information decomposition

Partial Information Decomposition (PID) (Ince, 2017; Williams and Beer, 2010) was used to determine the level of information about the stage of vigilance that is shared by all pairs of examined features (see detailed explanation C.2.2 in appendix C).

In fact, two features could convey the same, shared information, which is quantified as redundancy. Each feature could convey unique information that is not available from the other feature. Moreover, two features could also convey more information together than they do separately, i.e. if the relationship between the feature values is itself informative about the vigilance stage. This is quantified as synergy. PID was computed on for each subject using the same augmented dataset described above.

An additional analysis that compares the performance of two methods that are used to quantify redundancy or synergy, PID and Interaction Information (II), can be found in appendix C. This analysis of Electrocorticography (ECoG)-data recorded in marmosets (using a roving oddball paradigm) shows that co-information (see explanation C.2.1 in appendix C) only gives a "net-effect", as compared to PID, which shows that redundancy and synergy cancelling is not only a theoretical concern, but can occur in real experimental data. Please refer to appendix C for more detailed explanations regarding the differences between the two frameworks.

3.3 Results

3.3.1 Classification of vigilance stages

For the classification across all considered vigilance stages (W, N2, N3, REM) the accuracy estimate obtained with each single metric was 66.84% for relPOW, 58.24% for wPLI and 60.38% for wSMI (Figure 14A).

The combination of two feature sets increased accuracy to 76.68% for relPOW+wPLI, 74.94% for relPOW+wSMI, and 70.22% for wPLI+wSMI. The highest accuracy (80.53%) was obtained, when all sets of features were considered together (relPOW+wPLI+wSMI). This model was found to be statistically different from the null distribution ($P < 0.0005$). The three most relevant features for this model included elements from each of the considered metrics, namely delta-POW, sigma-wPLI and sigma-wSMI (Figure 14C).

Statistical comparisons based on paired non-parametric permutation tests ($p < 0.05$, Bonferroni correction) showed that both NREM (N2/N3) and REM sleep were characterised by increased delta-POW ($N3 > N2 > REM > W$), with respect to W, while sigma-wPLI ($N2 > N3 > REM = W$) and sigma-wSMI ($N2 = N3 > REM = W$) were higher in NREM relative to both wakefulness and REM sleep (Figure figs. 15 to 17). Additional relevant features included alpha-wSMI ($W > N3 > N2 > REM$), delta-wPLI ($N2 > N3 = REM > W$), theta-wSMI ($N3 > N2 = W = REM$) and alpha-wPLI ($W = N2 > N3 > REM$).

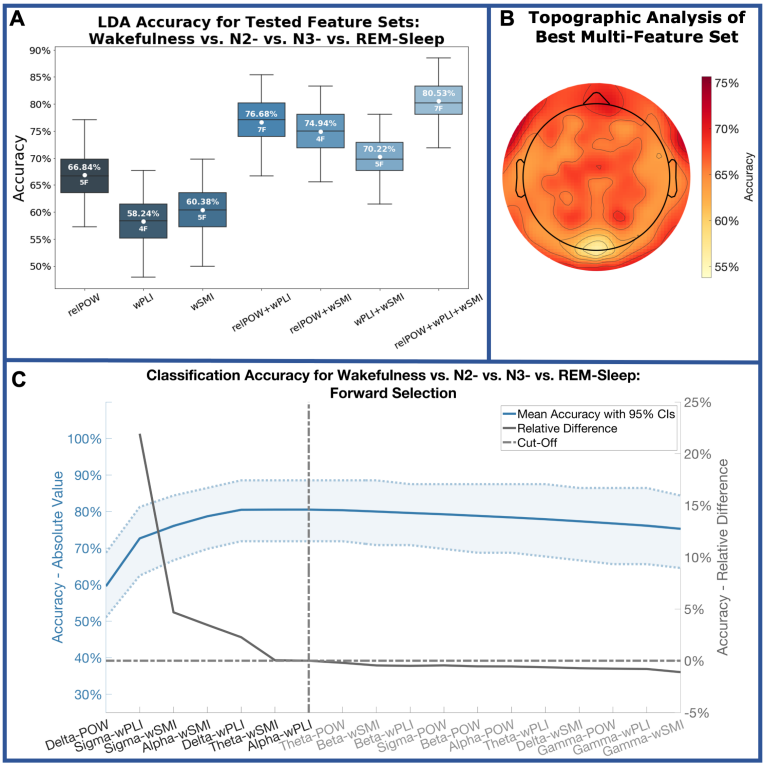

Figure 14: Four-way classification of W, N2, N3 and REM vigilance stages. A) LDA accuracy for tested feature sets in the classification of W vs. N2 vs. N3 vs. REM sleep. The top values reported in each box indicate the mean accuracy across bootstrapping iterations (marked by a white dot), while the bottom values indicate the number of included features F based on the forward selection procedure. B) Topographic analysis for the best-performing multi-feature-set chosen based on whole-brain results. The same selection of features was extracted from individual channels (instead of whole-brain median power or connectivity) by considering the single-channel power value and median connectivity between each electrode and all the other electrodes respectively. C) Forward feature selection for the classification of W vs. N2 vs. N3 vs. REM sleep. The blue continuous line represents the mean classification accuracy across bootstrapping iterations, while the dashed lines represent the 2.5% and 97.5% confidence interval boundaries on the accuracy estimate. The grey line indicates the percent change in accuracy granted by each individual feature added to the model. The dashed grey vertical line indicates the threshold for which inclusion of additional features did not improve classification accuracy.

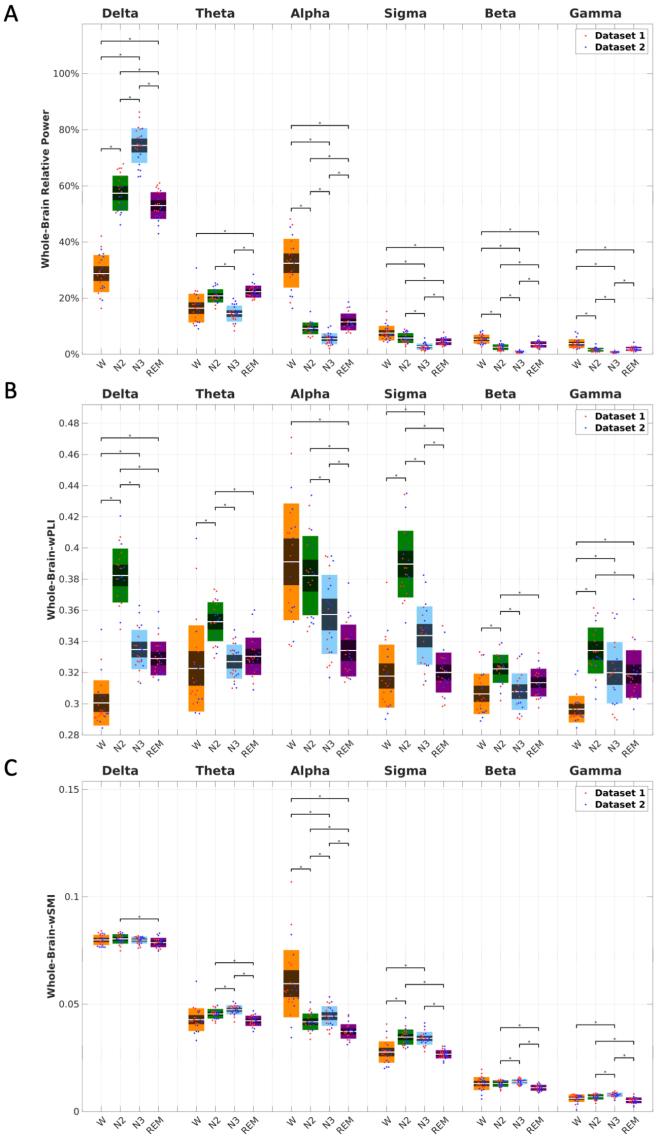

Figure 15: Statistical comparisons between stages of vigilance in delta, theta, alpha, sigma, beta and gamma frequency bands for whole-brain A) relative power, B) wPLI and C) wSMI. Red dots indicate subjects of dataset-1, while blue dots indicate subjects of dataset-2. $*p < 0.05$, Bonferroni correction across all performed comparisons for each considered metric.

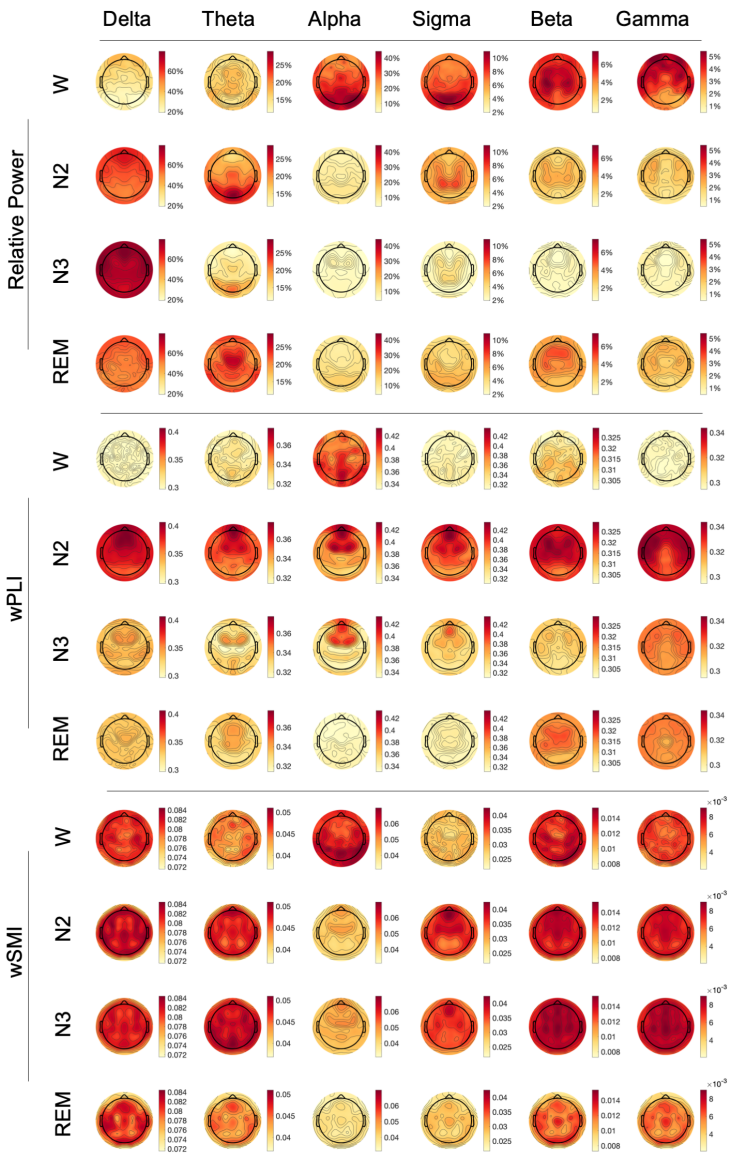

Figure 16: Topographic distribution of power (top panel), wPLI (mid panel) and wSMI (bottom panel) values in wakefulness, N2, N3 and REM sleep, for delta, theta, alpha, sigma, beta and gamma frequency ranges. For each metric and frequency band the colour-scale minimum and maximum were kept fixed in order to facilitate qualitative comparison across vigilance stages.

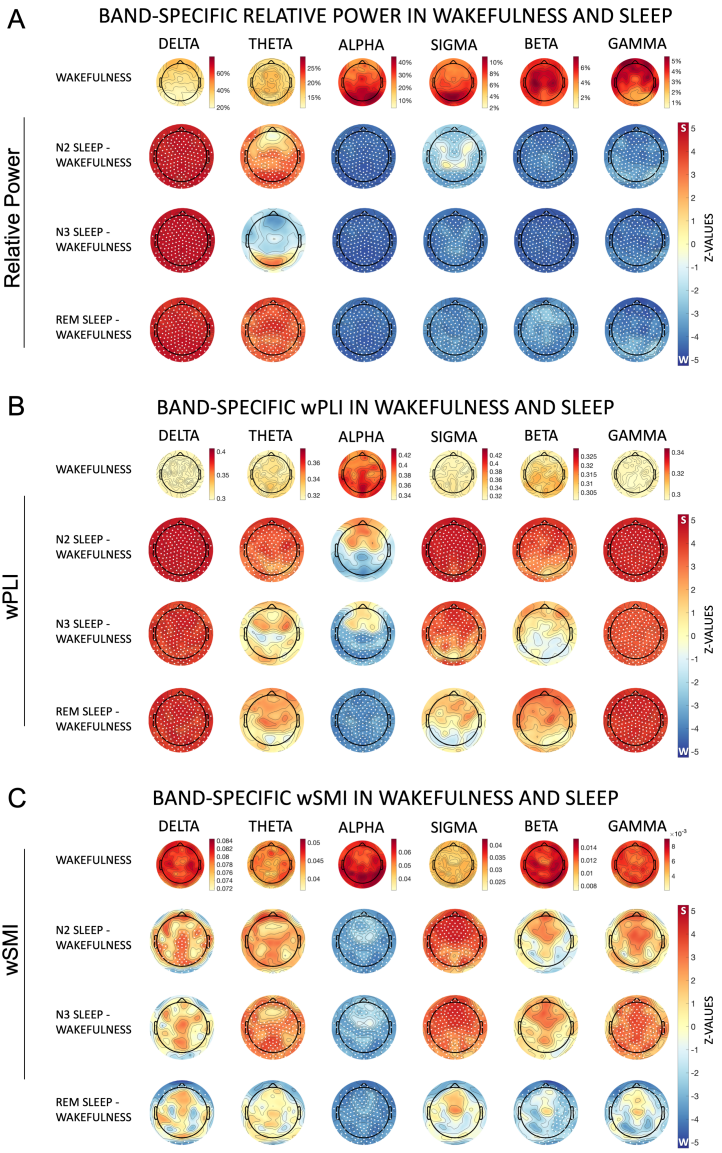

Figure 17: Topographic comparisons of power (A), wPLI (B) and wSMI (C) values in N2, N3 and REM sleep expressed as the difference (permutation test) with respect to wakefulness, in the classical frequency bands (delta, theta, alpha, sigma, beta, gamma). White dots mark $p < 0.05$, cluster-based correction.

Investigation of Relationships between Delta-Connectivity and Slow Waves in NREM-Sleep

As delta-wPLI was found to be higher in all sleep stages, especially in N2 and N3 sleep, relative to wakefulness (see figs. 15 and 18), we investigated whether there is an association between the properties of slow waves (Massimini et al., 2004) and the strength of wPLI connectivity. [6]

This analysis was not based on the bootstrapping procedure outlined above. Instead, all recorded, artifact-free 30s-epochs of N2/N3 sleep, were included. Slow wave amplitude and number were computed for each 30s epoch using validated algorithms (Riedner et al., 2007). Moreover, the median delta-wPLI (across channels) was obtained for each corresponding 30s epoch, by segmenting it in fifteen 2s trials before computing wPLI ($15 \times 2s$).

For each subject, Spearman's correlations between wPLI and either the number of slow waves or the maximum negative amplitudes were computed. Prevalence tests (see 3.3.1) were used to account effectively for the variability of the tested effect in the group (Allefeld et al., 2016; Donhauser et al., 2018). They were specifically employed to infer whether the effect of the correlation between delta-connectivity and slow-wave peak amplitude was present or absent in the population.

The majority null hypothesis ($\gamma_0 \leq 0.5$) can only be rejected for the correlations between delta-wPLI and the mean maximum negative peak amplitude of the slow waves in N2-Sleep. The highest γ_0 that can be rejected at the given significance level can be interpreted as a lower-bound estimate on the population prevalence.

The correlation between delta-wPLI and the mean maximum negative-peak-amplitude led to $\gamma_0 = 0.876$ in N2-Sleep (Figure 19), while the correlation between delta-wPLI and the mean maximum negative-peak amplitude led to $\gamma_0 = 0.13$ in N3-Sleep (Figure 20).

[6] Our previous preliminary investigation (Imperatori et al., 2019) also highlighted significant differences in delta-connectivity between N3 and Wakefulness for wPLI, but not for wSMI.

Explanation 3.3.1: Prevalence Test

The population prevalence γ represents the proportion of the population, from which our sample was drawn that we would expect to show the tested relationship (Allefeld et al., 2016; Donhauser et al., 2018). We make inferences on the population prevalence based on the results of within-participant statistical testing in our sample.
A prevalence null hypothesis, H0: $\gamma \leq \gamma_0$, can be tested using a modified binomial distribution (Allefeld et al., 2016; Donhauser et al., 2018; Friston et al., 1999). The null hypothesis can be e.g., that the effect is absent from the population (γ_0= 0, global null hypothesis) or that it is present in less than half of the population ($\gamma \leq \gamma_0$), majority null hypothesis).
The null hypothesis is rejected if the probability, under the null, of observing the number of significant subjects we do in our sample, or greater, is less than a critical value (here $p_{crit} = .05$)

Interestingly, when only considering large-amplitude slow waves (> 100μV), all 24 subjects showed a significant correlation between delta-wPLI and number of slow waves, while only half of the subjects showed a correlation between delta-wPLI and the total number of slow waves (of all sizes). The same was observed for the correlation between delta-wPLI and number of slow waves in N3-Sleep (from 5 of 24 subjects for slow waves of all sizes to 12 of 24 subjects for the inclusion of large slow waves only (> 100μV)).

The high correlation between delta-wPLI and slow wave amplitude in all subjects in N2, but not N3, and the greater sensitivity to larger slow waves suggest that wPLI may be strongly affected by the occurrence of K-complexes that are known to represent large-amplitude, temporally isolated slow-wave-like events. While K-complexes are global slow waves, most cortical slow waves (more common during N3 sleep) are relatively local events, that may occur out of phase across different brain regions. These local events may thus be expected to present a less efficient and widespread cortical propagation compared to K-complexes.

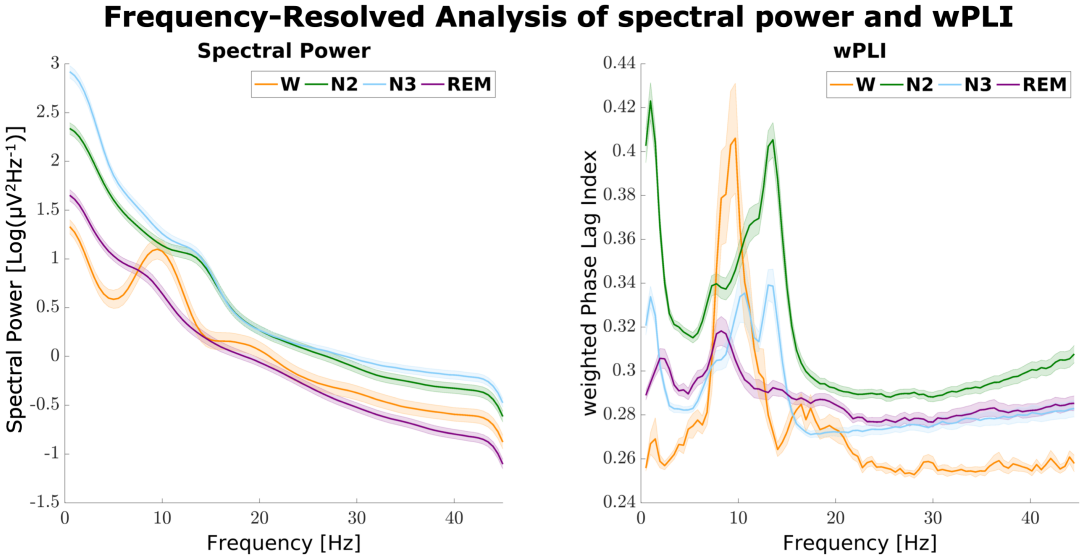

Figure 18: Frequency-Resolved Whole-Brain Power-Spectral-Density in Wakefulness, NREM- andREM-Sleep. The shaded area reflects the standard error of the mean across subjects for each vigilance stage.

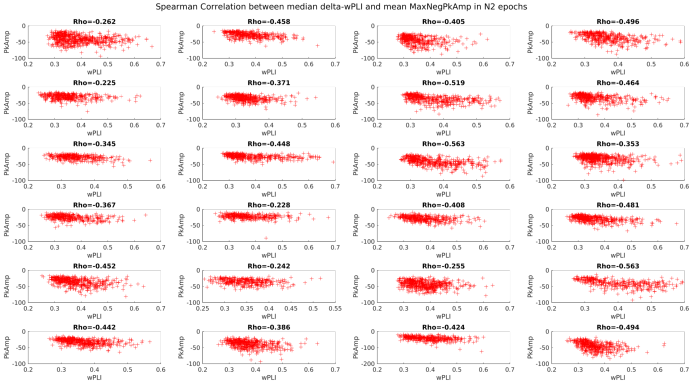

Figure 19: Spearman-Correlations between median delta-wPLI (across channels) and mean maximum negative amplitudes (of the slow wave envelope) in N2-Sleep were performed for all 24 subjects. Each subplot represents one subject and each point represents one epoch. Points were marked in red for $p < 0.05$ and in blue otherwise.

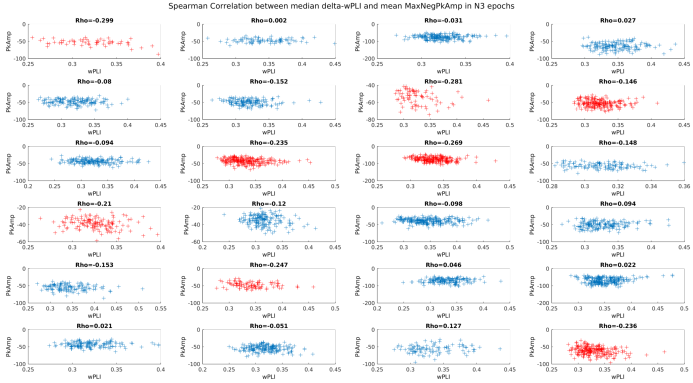

Figure 20: Spearman-Correlations between median delta-wPLI (across channels) and mean maximum negative amplitudes (of the slow wave envelope) in N3-Sleep were performed for all 24 subjects. Each subplot represents one subject and each point represents one epoch. Points were marked in red for $p < 0.05$ and in blue otherwise.

3.3.2 Classification of high vs. low level of consciousness

For the classification between stages associated with higher (W+REM) and lower (N2+N3) probability of conscious experiences, the classification accuracy estimate obtained with each single metric was 81.58% for relPOW, 75.53% for wPLI and 81.84% for wSMI (Figure 21). The combination of two feature sets increased accuracy to 89.44% for relPOW+wPLI, 89.24% for relPOW+wSMI, and 84.95% for wPLI+wSMI (Figure 21).

The highest accuracy (92.66%) was obtained, when all feature sets were included (relPOW+wPLI+wSMI). This model was found to be statistically different from the null distribution ($P < 0.0005$). The most relevant features in this model resulted to be sigma-wSMI, delta-POW and sigma-wPLI.

Statistical comparisons based on paired non-parametric permutation tests ($p < 0.05$, Bonferroni correction) showed that both NREM (N2/N3) and REM-sleep were characterised by increased delta-POW ($N3 > N2 > REM > W$) and higher sigma connectivity (wPLI/wSMI) in N2/N3-sleep with respect to both W and REM-sleep (no differences between W and REM). Additional relevant features included delta-wPLI, gamma-wSMI and beta-POW.

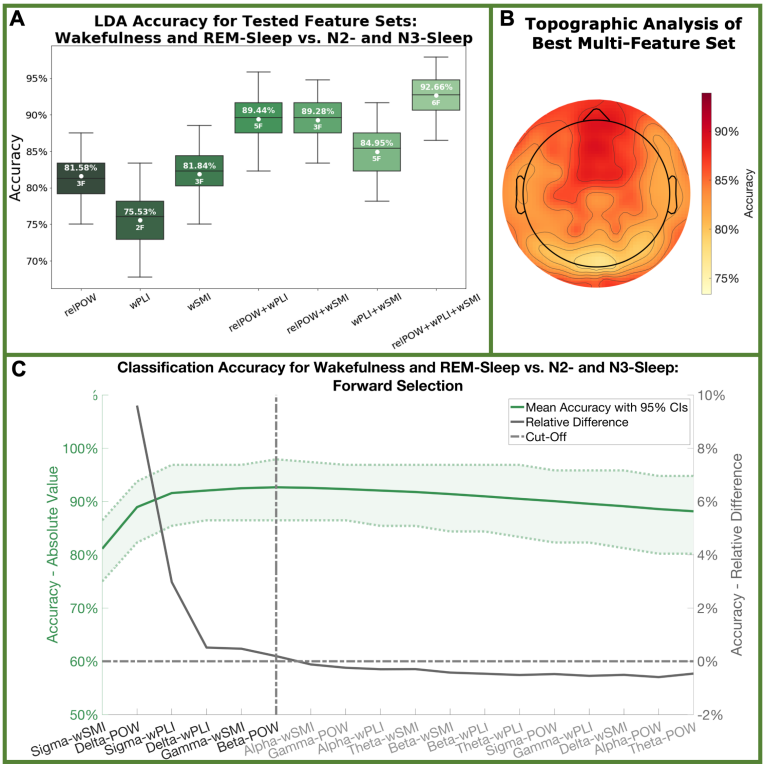

Figure 21: Two-way classification of W+REM vs N2+N3 vigilance stages. A) LDA accuracy for tested feature sets in the classification of W+REM vs N2+N3 vigilance stages. The top values reported in each box indicate the mean accuracy across bootstrapping iterations (marked by a white dot), while the bottom values indicate the number of included features F based on the forward selection procedure. B) Topographic analysis for the best-performing multi-feature-set chosen based on whole-brain results. The same selection of features was extracted from individual channels (instead of whole-brain median power or connectivity) by considering the single-channel power value and median connectivity between each electrode and all the other electrodes respectively. C) Forward feature selection for the classification of W+REM vs N2+N3 vigilance stages. The green continuous line represents mean classification accuracy across bootstrapping iterations, while the dashed lines represent the 2.5% and 97.5% confidence interval boundaries on the accuracy estimate. The grey line indicate the percent change in accuracy granted by each individual feature added to the model. The dashed grey vertical line indicates the threshold for which inclusion of additional features did not improve classification accuracy.

3.3.3 Classification of 'conscious' stages with and without sensory disconnection

For the comparison between wakefulness ('connected' consciousness) and REM sleep ('disconnected' consciousness), the maximum classification accuracy obtained with each single metric was 92.91% for relative POW (relPOW), 77.29% for wPLI and 86.07% for wSMI (Figure 22). The combination of two feature sets increased accuracy to 93.08% for relPOW+wPLI, 94.04% for relPOW+wSMI, and 85.72% for wPLI+wSMI (Figure 22).

The highest accuracy (94.09%) was obtained, when all feature sets were included (POW+wPLI+wSMI). This model was found to be statistically different from the null distribution ($P < 0.0005$). The most relevant features in this model resulted to be delta-POW, theta-POW and alpha-wSMI.

Statistical comparisons based on paired non-parametric permutation tests ($p < 0.05$, Bonferroni correction) showed increased delta-power and theta-power and decreased alpha-wSMI in REM sleep with respect to wakefulness. Additional relevant features included gamma-POW and beta-wPLI.

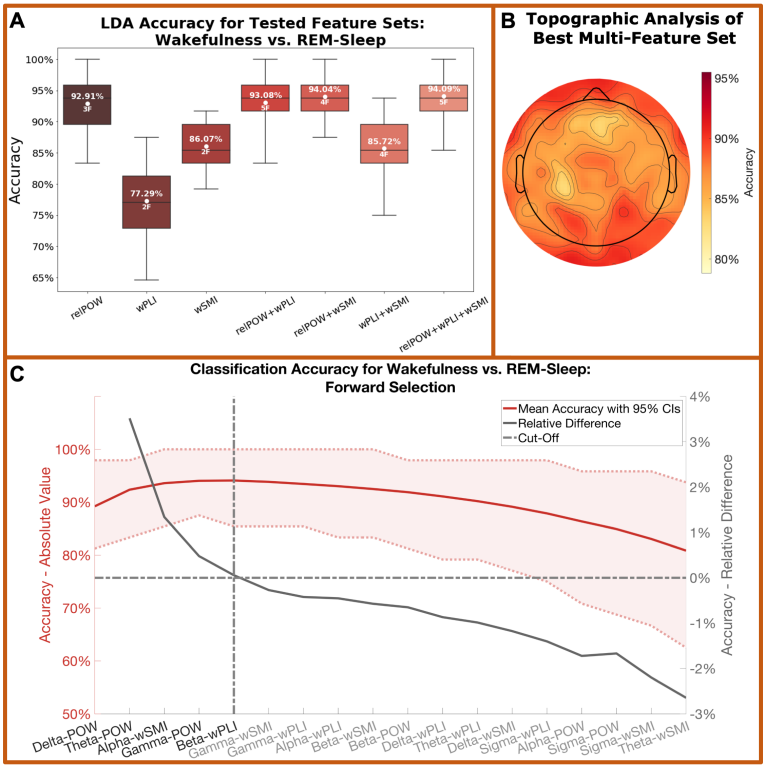

Figure 22: Two-way classification of W and REM vigilance stages. A) LDA accuracy for tested feature sets in the classification of W vs. REM-sleep. The top values reported in each box indicate the mean accuracy across bootstrapping iterations (marked by a white dot), while the bottom values indicate the number of included features F based on the forward selection procedure. B) Topographic analysis for the best-performing multi-feature-set chosen based on whole-brain results. The same selection of features was extracted from individual channels (instead of whole-brain median power or connectivity) by considering the single-channel power value and median connectivity between each electrode and all the other electrodes respectively. C) Forward feature selection for the classification of W vs. REM-sleep. The red continuous line represents mean classification accuracy across bootstrapping iterations, while the dashed lines represent the 2.5% and 97.5% confidence interval boundaries on the accuracy estimate. The grey line indicate the percent change in accuracy granted by each individual feature added to the model. The dashed grey vertical line indicates the threshold for which inclusion of additional features did not improve classification accuracy.

3.3.4 Best individual features

In order to further evaluate which individual features carry more relevant information for distinguishing between considered classes (i.e., vigilance stages), we contrasted the single-feature LDA performance (regarding the predictability across subjects) with the mutual information each feature contains about the classes (within subjects' analysis).

On the one hand, LDA tests the generalisation of predictive accuracy of a specific feature to a new set of subjects. On the other hand, MI is a within-subject analysis, determining the predictive power of the feature within each individual. In this light, the two approaches provide related but complementary information. Results obtained from this analysis are shown in Figure 23.

For the differentiation between all stages of vigilance (W, N2, N3, REM), delta-POW resulted as the best feature based on both its individual classification performance and mutual information value (59.83%, MI=0.93bits; Figure 23A). For the comparison between NREM (N2, N3) sleep and W+REM, sigma-wSMI resulted as the best feature (81.30%, MI=0.53bits); Figure 23B.

Finally, for the comparison of W and REM sleep, alpha-wSMI alone achieved 87.17% accuracy (with an MI value of 0.73bits), although a higher LDA accuracy was obtained by delta-POW.

3.3.5 Redundancy Analysis

In order to determine to what extent the statistical relationship in two features is common or overlapping, we used an information theoretic framework called partial information decomposition (PID; (Allen et al., 2017; James et al., 2018); see explanation C.2.2 in appendix C).

Here, we assessed whether the information that any particular feature contains regarding the label (W vs. N2 vs. N3 vs. REM in Figure 24A, W+REM vs. N2+N3 in Figure 24B, W vs. REM in Figure 24C) is shared among two features or is unique to that feature. Results shown in Figure 24 indicate that especially power-based features are highly redundant with each other.

Indeed, non-parametric permutation tests (N=10000) showed that redundancy among power-features is higher than that among wPLI and wSMI features respectively ($42.98 \pm 7.51\%$ vs. $16.77 \pm 3.41\%$ vs. $28.28 \pm 7.62\%$; $p = 0.0001$) for the comparison among all the four vigilance stages (W, N2, N3, REM). Power with respect to wSMI features are more redundant with each other ($27.43 \pm 5.10\%$) as compared to power with respect to wPLI ($19.56 \pm 3.30\%$) and wPLI with respect to wSMI features ($18.54 \pm 3.30\%$). Similar differences were observed for the W+REM vs. N2+N3 and W vs. REM comparisons.

Interestingly, in the W vs. REM case, both alpha-POW and alpha-wSMI appeared to be highly redundant with respect to delta-POW (83.44% and 72.27%, respectively) and with each other (72.42%). This may explain both why alpha-POW was not included in the forward selection procedure and the fact that the inclusion of alpha-wSMI determines only a marginal increase in classification accuracy (Figure 22).

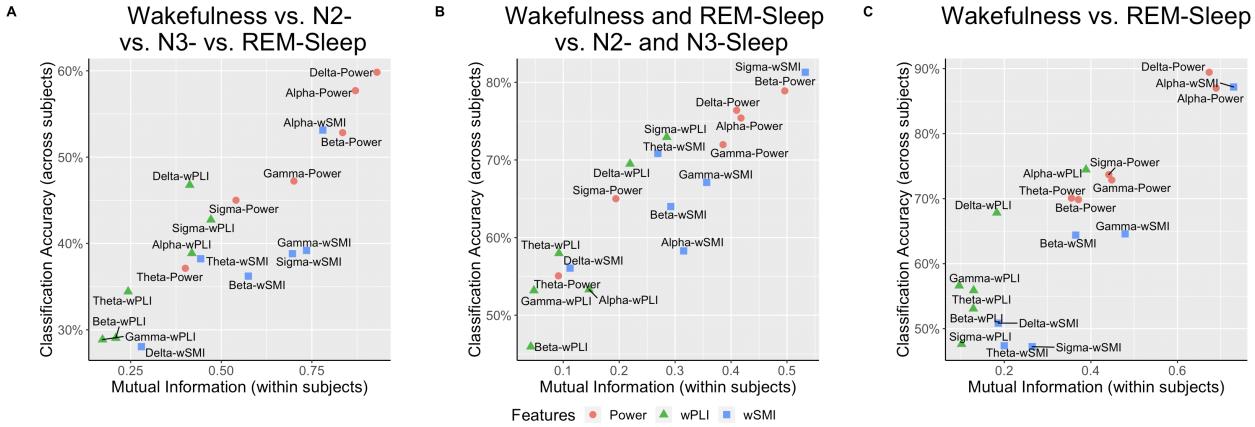

Figure 23: Mutual Information vs. LDA Classifier Accuracy. Each plot represents the single-feature LDA performance (y-axis) with respect to the mean within-participant MI conveyed by the feature about the vigilance classes (x-axis) for all three tested comparisons: A) W vs. N2 vs. N3 vs. REM, B) W+REM vs. N2+N3, C) W vs. REM.

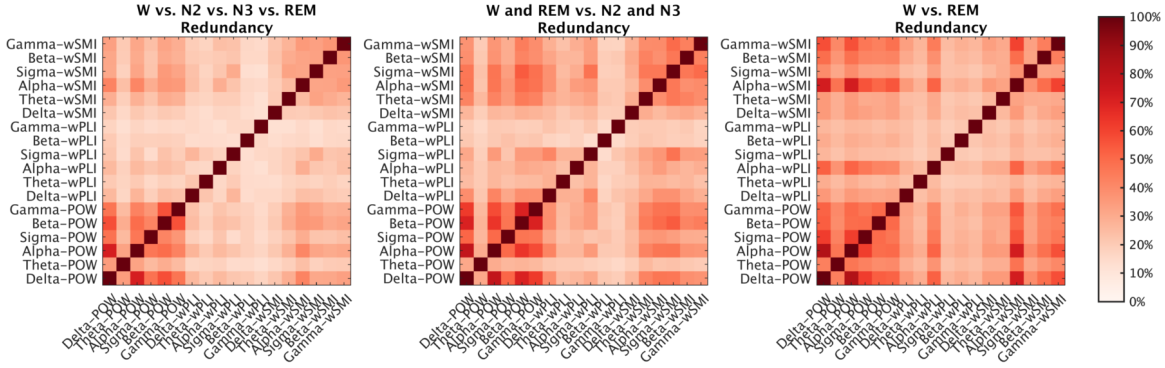

Figure 24: Relative Redundancy among features (redundancy as computed by PID divided by the sum of redundancy, synergy, unique X and unique Y information values). The three matrices display the results based on partial information decomposition (PID) for the three tested comparisons: A) W vs. N2 vs. N3 vs. REM, B) W+REM vs. N2+N3, C) W vs. REM. A higher value (darker colour) indicates higher redundancy between two features.

3.4 Discussion

Power-based features are known to significantly differ across vigilance stages and may be used for the development of automated sleep scoring algorithms with a satisfactory level of accuracy (Berthomier et al., 2007; Koley and Dey, 2012; Zoubek et al., 2007). However, previous work also showed that vigilance stages may differ in terms of functional connectivity (FC), and that distinct FC-metrics may also reveal distinct variations in inter-regional neural communication as a function of their specific sensitivity for linear and nonlinear interaction dynamics (Imperatori et al., 2019; Migliorelli et al., 2019). Yet it was still unclear whether FC metrics actually provide relevant or rather redundant information with respect to classical measures of brain EEG activity.

By using a linear discriminant analysis (LDA) with feature sets including signal power and two connectivity metrics with known distinct sensitivity for linear and nonlinear interactions (i.e., wPLI and wSMI), here we showed that the inclusion of connectivity-based features increases the classification accuracy of vigilance stages. Moreover, we determined which specific individual features provide the best accuracy not only for distinguishing among all vigilance stages, but also for comparisons contrasting states associated with lower or higher probabilities of having a conscious experience (typically in the form of dreams during sleep), and states associated with more or less 'disconnection' from the external environment.

In line with previous evidence (Chennu et al., 2014; Lee et al., 2017a,b; Massimini et al., 2004), obtained results showed that delta-power carries relevant information for all of these comparisons. Moreover, our results indicate that sigma-FC may be especially relevant for distinguishing among vigilance stages respectively characterized by higher and lower probability of conscious experiences during sleep, while changes in alpha-FC may mainly mark the degree of sensory disconnection rather than the level of consciousness per se.

3.4.1 Contribution of connectivity metrics to the classification of vigilance stages

Relative variations in brain activity that characterize distinct vigilance stages may be efficiently captured through the analysis of signal power in classical frequency bands. Of note, however, evidence indicates that the different stages of vigilance are also accompanied by relative variations in the way distinct areas of the brain interact with each other (Migliorelli et al., 2019).

Here we showed that information granted by FC analysis, as determined using wPLI and wSMI metrics, is not redundant with respect to power-based features. In fact, while individual FC metrics showed a lower accuracy ($58 - 60\%$) at discriminating the four examined stages of vigilance (W, N2, N3, REM) with respect to power-based features (67%), their inclusion in the model considerably increased the overall accuracy, which reached 81%. Importantly, the adopted LDA classifier was trained on one group of subjects and tested on a separate group of individuals, thus supporting the generalisability of our findings.

The evaluation of the individual features for this classification showed that delta-power is the most relevant feature for the cross-participant classification for all vigilance stages and carries the most information at the within-subject level. Other relevant features included several FC features based on both wPLI (sigma-wPLI, delta-wPLI, alpha-wPLI) and wSMI (sigma-wSMI, alpha-wSMI, theta-wSMI).

Overall, these results indicate that the inclusion of FC-based features in the classification of vigilance stages can lead to a higher accuracy with respect to using power-based features alone, and that the inclusion of multiple FC-metrics with sensitivity to inter-regional interactions having distinct linear and nonlinear weights could lead to a further gain in accuracy.

3.4.2 Classification of states with high or low levels of consciousness or disconnection

Previous works reported differences in delta (Chennu et al., 2014; Lee et al., 2017a,b) and alpha (Blain-Moraes et al., 2014; Chennu et al., 2016; Comsa et al., 2019; Lee et al., 2017a) connectivity between states characterized by high or low levels of consciousness. These studies compared healthy adult individuals and patients in unresponsive wakefulness syndrome (UWS) or minimally conscious state (MCS), or the same subjects before, after and during anaesthesia. However, any valid metric of consciousness should be able to identify differences between wakefulness with awareness and all states associated with a reduced level of consciousness, including dreamless sleep (Demertzi et al., 2019; Sarasso et al., 2014). Thus, here we investigated whether, in line with previous studies, FC-based indices could be used to distinguish between states characterized by a higher level of consciousness, that are wakefulness and REM sleep, and states associated with a relatively reduced probability of having a conscious experience, corresponding to N2 and N3 sleep. [7]

The obtained classification model led to a high accuracy (93%), which was mainly driven by a subset of FC- and power-based features. In particular, the strongest contribution to accuracy was provided by sigma-wSMI, delta-power and sigma-wPLI. Delta-wPLI, gamma-wSMI and beta-power provided a smaller contribution.

Of note, the contribution of delta power and connectivity is especially consistent with previous findings indicating a relationship between these parameters and changes in the level of consciousness during sleep and in pathological states or anesthesia (Chennu et al., 2014; Lee et al., 2017a,b; Massimini et al., 2005). Variations in sigma-connectivity have been less often reported, but may reflect here the occurrence and cortical 'propagation' of sleep spindles (Andrillon et al., 2011; Muller et al., 2016). In fact, previous work indicate that changes in spindle parameters may be re-

[7] Notably, as previous studies have shown (Siclari et al., 2013), conscious experiences are also common to N2 and N3 sleep; however, the probability of their occurrence is significantly lower as compared to REM-sleep and wakefulness.

lated to the presence of conscious experiences during NREM sleep (Siclari et al., 2018). It should be noted, though, that sigma-power did not significantly contribute to classification accuracy.

The additional classification between wakefulness and REM-sleep, respectively representing states of connected and disconnected consciousness, revealed alpha-FC as one of the strongest contributors to classification accuracy (other features included delta-power, theta-power, gamma-power and beta-wPLI). As mentioned above, this feature did not contribute instead to the distinction between states characterized by high or low levels of consciousness. Based on this finding, we suggest that alpha connectivity may mainly mark disconnection or disengagement from the external environment rather than the current level of consciousness, in line with recent findings describing a suppression in TMS-evoked alpha activity during disconnected consciousness in REM sleep (Darracq et al., 2018).

Interestingly, delta-power appeared among the most relevant features for all tested classifications. Stage-related variations in this parameter may depend on the occurrence and cortical spreading of sleep slow waves (0.5-4Hz). Indeed, the sleep slow wave, which marks temporary neuronal off-periods at cortical level, has been suggested to interrupt the causal flow of information among brain areas, thus impairing the possible emergence of conscious experiences in both NREM and REM sleep (Pigorini et al., 2015; Siclari et al., 2017; Tononi and Massimini, 2008). Moreover, slow-wave-like events (i.e., K-complexes) have been suggested to also have a direct role in the relative disconnection that characterize sleep through the quenching of incoming sensory information (Cash et al., 2009; Halász, 2016; Laurino et al., 2014, 2019).

3.4.3 Limitations of the study

While it has been shown that the probability of dreaming in NREM sleep is around 50% (across N2 and N3) as compared to $80-100\%$ in REM sleep and wakefulness (Siclari et al., 2018), we did not directly assess the presence of conscious experiences and the level of consciousness in

the present data. Similarly, we did not directly assess the level of relative sensory disconnection. Therefore, analyses investigating the power- and connectivity-based correlates of consciousness and disconnection should be considered as preliminary. Future studies should include within-stage analyses comparing conditions with or without conscious experiences and with low or high responsiveness to external stimuli (high/low arousal threshold).

Moreover, here only the whole-brain, median connectivity and power were used, and topographic differences in the distribution of evaluated features were not included in the LDA classifiers. However, recent studies clarified that local variations in brain activity may determine significant variations in the level of consciousness within and across sleep stages (Siclari et al., 2017, 2018). Thus, the inclusion of topographic information could be expected to increase classification accuracy. It would also be important for future studies to investigate whether considering a smaller sensor layout would lead to similar results with respect to those obtained here using hd-EEG with 257 electrodes (Engemann et al., 2018).

3.5 Conclusions

Our results demonstrate that changes in brain activity across sleep stages are better characterised by the combined use of the signal power and the two connectivity metrics wPLI and wSMI, relative to both individual connectivity approaches and power-based indices alone. In line with previous studies regarding the neural correlates of consciousness, present results also showed that variations in delta power and connectivity are among the most relevant classification features. On the other hand, in contrast to previous works, alpha-connectivity did not contribute to the classification of states with high and low levels of consciousness, and was instead found to represent one of the best features for distinguishing between wakefulness and REM sleep, a state typically characterized by vivid conscious experiences. In this light, present results suggest that connectivity changes in the alpha range could mark disconnection from the external environment rather than the level of consciousness per se.

Overall, our results indicate that connectivity metrics provide relevant, complementary information with respect to metrics based on signal power, and also showed that the application of connectivity approaches with different sensitivity to linear and nonlinear dynamics may allow to achieve a more complete description of brain activity across different behavioural and vigilance states.

Chapter 4

Predictive value of EEG connectivity metrics for motor training outcome in multiple sclerosis: an observational longitudinal study

4.1 Introduction

All the results shown in this chapter refer to the same-titled article, published in the European Journal of Physical and Rehabilitation Medicine (Tramonti et al., 2018).

Functional connectivity (FC) metrics identify statistical (undirected) associations among spatially distinct brain areas. EEG- and MEG-based metrics have previously been employed to characterise the functional interactions between different brain regions in multiple sclerosis (MS) patients as compared to healthy subjects (Cover et al., 2006; Leocani et al.,

2000; Van der Meer et al., 2013; Zhong et al., 2016). These studies mainly described relative reductions in brain connectivity, especially within the alpha range, in Multiple Sclerosis (MS) patients (Cover et al., 2006; Leocani et al., 2000).

However, here, we were mainly interested in the functional correlates of training-induced plasticity in MS patients (Tomassini et al., 2012b). Previous studies showed that adaptive brain plasticity can occur in MS patients, despite a high occurrence of cerebral pathology and disability (Reddy et al., 2000; Rocca et al., 2005; Tomassini et al., 2012a), providing that appropriate interventions facilitate enhanced neural reorganization and motor recovery (Tomassini et al., 2012b).

Here we aimed at testing whether wPLI and wSMI can predict and track behavioural changes induced by a Task-Oriented Circuit Training (TOCT) paradigm for gait rehabilitation in MS patients, previously validated in Chisari et al. (2014). We hypothesized that EEG-based connectivity could represent an adequate technique to predict and track motor performance changes induced by TOCT.

Firstly, we anticipated that brain connectivity metrics prior to the training may predict the success of the intervention. Specifically, we hypothesized patients with stronger connectivity to have more residual functional resources, favouring a greater post-treatment behavioural performance.

Secondly, we expected clinical improvement induced by the intervention to be associated with brain functional reorganization. Specifically, we predicted an increase in connectivity to be correlated to an increase in motor performance after rehabilitation.

We tested these hypotheses using wPLI and wSMI, as we exptected their different sensitivities for linear and non-linear brain dynamics (Imperatori et al., 2019) to be reflected in their corresponding predictive value for the outcome of the undergone rehabilitative treatment in MS patients.

4.2 Methods

4.2.1 Patients

Sixteen MS patients (10 females; mean age = 51.44 years; range: 27 - 67 years were included based on the following criteria:

- age > 18 years;
- diagnosis of MS according to McDonald Revised Criteria (Polman et al., 2005) (relapsing - remitting, primary progressive) [1];
- clinical stability for at least three months (no relapses, no disability worsening and no other medical complications);
- motor impairment score between 3.5 and 5.5 as assessed with the Expanded Disability Status Scale (EDSS) (Kurtzke, 1983).

4.2.2 Rehabilitative Intervention

Subjects performed TOCT, including six different workstations of physical exercise. The rehabilitative treatment lasted 2 weeks, with a frequency of 5 days/week and each session lasting around 120 minutes overall. Each session comprehended gait training with treadmill, stretching exercises and task oriented circuit training.

The task-oriented circuit was organized in several stations in which patients were asked to: overcome an obstacles course; achieve various targets placed at different heights sights on a mirror with the feet, walk along a 10 meter long line drawn on the ground, climb and descent stairs. For further details on methodology, please refer to (Chisari et al., 2014).

4.2.3 Motor Performance Assessment

All patients underwent a comprehensive examination including five different clinical tests to assess mobility, walking endurance, speed, gait performance and energy expenditure during exercise.

[1] Notably, two subjects had primary progressive (MS-PP), while the other fourteen subjects had relapsing-remitting MS (MS-RR).

Here, we were especially interested in their performance in the Timed Up & Go (TUG) task (Learmonth et al., 2012). Their performance was evaluated before (T0) and after (T1) treatment.

4.2.4 Data Collection, Preprocessing and Analysis

EEG recordings were performed at T0 and T1 with a 64 - electrodes high-density (hd-)EEG system (Micromed), using a sampling frequency of 256 Hz. Of note, data from one subject was not available at T1, and analyses including this time-point were thus performed on a subset of fifteen subjects. Each data acquisition session included ten minutes of eyes - closed resting condition.

Preprocessing and analysis of EEG recordings was performed using MATLAB R2017a (The Mathworks, Inc.) and the EEGLAB toolbox (Delorme and Makeig, 2004), similarly to previous work (Bernardi et al., 2015). Specifically, all EEG recordings obtained at T0 and T1 were band-pass-filtered between 1 and 45 Hz and segmented in non-overlapping 4 s epochs.

A visual inspection was performed to identify and reject bad channels and data epochs containing clear artifacts. An Independent Component Analysis (ICA) was applied on retained data to remove residual ocular, muscular and cardiac artifacts using EEGLAB routines (Delorme and Makeig, 2004; Delorme et al., 2011). Then, the signal of rejected electrodes was replaced with data interpolated from nearby channels using spherical splines. Finally, the signal of each channel was re-referenced to average reference.

The Welch's method (4 s Hamming windows, 8 segments, 50% overlap; 0.25Hz bin resolution) was used to compute power estimates for the following frequency bands: delta (1 - 4.5 Hz), theta (5 - 8 Hz), alpha (8 - 12 Hz) and beta (18 - 25 Hz). For each frequency range, (global) mean power values were calculated across all scalp electrodes.

Functional connectivity metrics were computed in artifact-free 4 s epochs. For each patient, connectivity analyses were performed on 57 data epochs (3.8 min), corresponding to the smallest number of epochs

retained across all subjects. This approach was applied to avoid potential confounds based on including different amounts of data.

wPLI Connectivity Analysis

To measure changes in brain connectivity induced by the two-weeks TOCT, especially related to phase synchronisation, wPLI (Vinck et al., 2011) of the alpha-band was considered, as previous studies in MS patients reported a frequency-specific decrease in alpha-range connectivity relative to healthy subjects (Cover et al., 2006; Leocani et al., 2000).

wSMI Connectivity Analysis

To measure changes in brain connectivity, mostly related to non-linear dynamics induced by the two-weeks TOCT paradigm, wSMI (King et al., 2013) was computed. This metric evaluates the extent to which two EEG signals present non-random joint fluctuations, suggesting sharing of information. We chose the kernel k to be 3, implying that the symbols are constituted of three elements amounting to six different potential symbols in total, and the temporal separation of elements that constitute a symbol to be $\tau = 4ms$ (1 time - sample), to include frequencies up to 45 Hz. For wSMI, surface-Laplacian (i.e. CSD) transform (Kayser and Tenke, 2006) was applied instead of average reference. Connectivity was computed across all frequencies (i.e., 1 - 45 Hz) (King et al., 2013).

4.2.5 The effects of TOCT on brain connectivity

A single index of 'global' (whole - brain) connectivity strength was calculated for both wPLI and wSMI. First, the connectivity measure was computed for all potential channel combinations. Then, the mean value of all these pairs was defined as global connectivity strength for wPLI (Vinck et al., 2011), while the median was considered instead for wSMI (King et al., 2013). Of note, since previous studies suggested that MS patients may show prevalent alterations of inter-hemispheric (INTERH) (Cover et al., 2006) or antero-posterior (AP) connectivity (Leocani et al., 2000),

we also computed two additional indices to specifically investigate the possible relevance of INTERH and AP regional interactions by considering the mean connectivity of all electrodes to their contralateral corresponding sensors along the left-right (INTERH) and the anterior-posterior (AP) axes, respectively.

To further explore the potential predictive role of the brain functional organization on post-training performance improvement, we performed additional graph-based analyses of the network global efficiency, based on wPLI (i.e., the average inverse shortest path length in the network). In fact, complex and highly integrated networks have shorter path lengths than random networks, allowing for efficient information transfer (Rubinov and Sporns, 2010).

Specifically, for each subject, the respective wPLI connectivity matrices were considered as adjacency matrices with channels representing nodes and connectivity values between them representing edges. Those weighted undirected networks were thresholded to include different percentages of strongest edges. The network global efficiency (Latora and Marchiori, 2001) was calculated as the Area under the Curve (AUC) across 5 different thresholds representing different subsets of strongest edges (i.e., from 30% to 70% strongest nodes with 10% steps) using the Brain Connectivity Toolbox (Rubinov and Sporns, 2010).

To evaluate the relationship between performance improvement as measured by changes in TUG and connectivity values at T0 or T1, or connectivity variations T1 - T0 (positive values represent higher degree of connectivity after training), partial correlation analysis was employed including patients' age as confounding variable. All reported p - values are results of two - tailed tests if not explicitly stated otherwise.

Of note, Shapiro-Wilk test was employed to verify whether, T0, T1 and ΔT EEG connectivity metrics were normally distributed and when the assumption of normality was violated, partial correlation analyses were based on the non-parametric Spearman's Rho test, while for all the other measures Pearson's correlation coefficient was employed.

4.3 Results

Power Analysis

No significant correlations were noted between ΔTUG and power in all tested frequency ranges (delta, theta, alpha, beta), either at T0, T1, or for T1–T0 variation.

4.3.1 wPLI Connectivity

Results obtained for wPLI connectivity are summarized in Table 1. A significant correlation was observed between the alpha-band wPLI connectivity at T0 and the behavioural measure ΔTUG (Fig. 25A; r = 0.61; p = 0.017). This effect appeared to be mainly explained by antero-posterior (AP) wPLI connectivity at T0 (Fig. 25B; r = 0.54; p = 0.038), rather than by inter-hemispheric (INTERH) T0 connectivity (r = 0.45; p = 0.089).

In line with these observations, wPLI network's global efficiency at T0 (r = 0.50; $p_{one-tail}$ = 0.030) and T1 (r = 0.47; $p_{one-tail}$ = 0.045) was found to be positively correlated with ΔTUG. No significant correlations were observed between T1 - T0 variations in connectivity (r = -0.019, p = 0.47) and ΔTUG.

Importantly, when removing the two PP subjects all tests remain significant, except for the relationship between antero-posterior wPLI connectivity at T0 and ΔTUG (r = 0.54; p = 0.058), and wPLI efficiency at T1 and ΔTUG (r = 0.50; p = 0.051; see Table 1).

4.3.2 wSMI Connectivity

Results obtained for wSMI connectivity are summarized in Table 2. The whole - brain wSMI connectivity was found to be correlated with ΔTUG at T1 (rho = 0.775; p = 0.001; Fig. 25C) but not at T0 (r = 0.23; p = 0.421). For wSMI, the correlation appeared to be explained by both AP-wSMI connectivity (r = 0.68; p = 0.008) and INTERH wSMI connectivity (rho = 0.67; p = 0.01). Crucially, a significant correlation was also observed between the T1-T0 variation in wSMI connectivity and ΔTUG, with r =

Table 1: Correlations between TUG at T0, T1, ΔTUG and wPLI. MS-RR stands for relapsing-remitting multiple sclerosis, while MS-PP stands for primary progressive multiple sclerosis. Depending on the outcome of the Shapiro-Wilk-Test, Pearson product-moment correlation values (r) or Spearman's rho (ρ) correlation tests were performed between EEG measures and ΔTUG. All significant effects are marked in bold and with an asterisk ($*$). All reported p-values are two-tailed, except for p_{ot}, which is a one-tailed p-value.

		MS-RR and MS-PP Patients			**Only MS-RR Patients**		
		T0	T1	**Diff. (T1-T0)**	T0	T1	**Diff. (T1-T0)**
wPLI	r	**0.606**	0.47	-0.256	**0.628**	0.445	-0.201
	p	**0.017***	0.09	0.378	**0.022***	0.147	0.531
AP wPLI	r (ρ)	**0.538**	0.524	0.061	0.538	0.54	0.063
	p	**0.038***	0.053	0.836	0.580	0.70	0.845
INTERH wPLI	r	0.455	0.148	-0.176	0.461	0.25	-3.799
	p	8.89	0.614	0.548	0.113	0.423	0.908
wPLI efficiency	r	**0.5**	**0.47**	-0.019	**0.52**	0.496	0.151
	p_{ot}	**0.029***	**0.045***	0.474	**0.034***	0.05	0.32

0.70 (p = 0.005; Fig. 25D), implying that an increase in behavioural performance was correlated to an increase in wSMI connectivity.

However, neither the T1-T0 difference in AP-wSMI connectivity (r = 0.53; p = 0.052) nor the T1-T0 difference in INTERH wSMI connectivity were correlated to ΔTUG (r = 0.38; p = 0.180). Importantly, when removing the two PP subjects, all tests remain significant, except for interhemispheric wSMI connectivity at T1 (r = 0.49; p = 0.108; see Table 2).

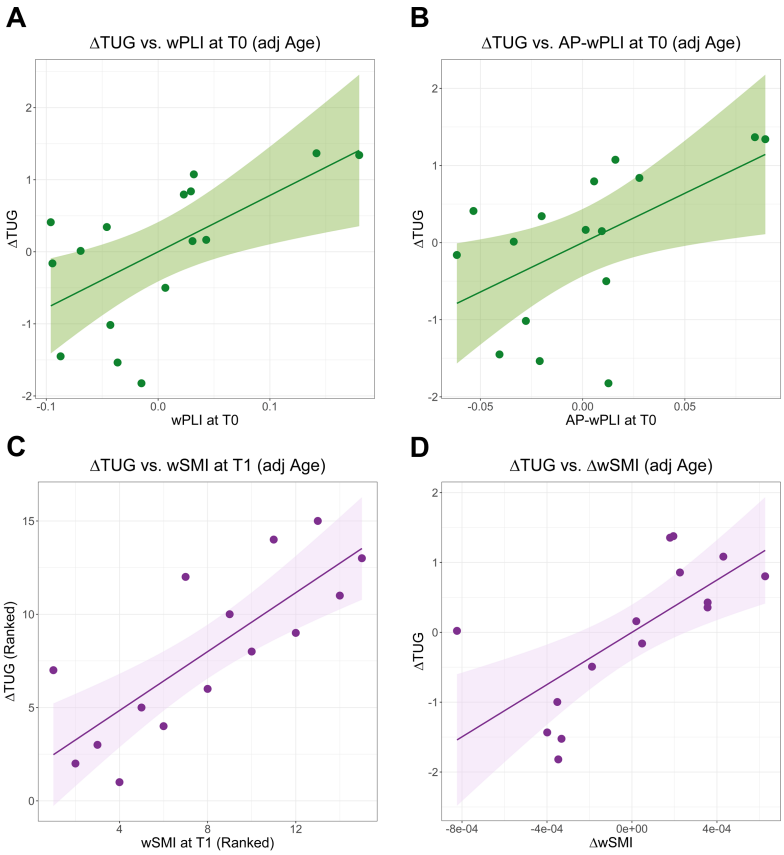

Figure 25: Panel A shows correlation between alpha-band wPLI connectivity and ΔTUG at T0 (r = 0.61; p = 0.017), while Panel B depicts the relationship between anteroposterior-alpha-band wPLI connectivity and ΔTUG at T0 (r = 0.54; p = 0.038). Panel C and D illustrate the correlation between broadband wSMI connectivity at T1 and ΔTUG (rho = 0.78; p = 0.001), and between T1-T0 wSMI connectivity variation and ΔTUG (r = 0.70; p = 0.005), respectively.

Table 2: Correlations between TUG at T0, T1, ΔTUG and wSMI. MS-RR stands for relapsing-remitting multiple sclerosis, while MS-PP stands for primary progressive multiple sclerosis. Depending on the outcome of the Shapiro-Wilk-Test, Pearson product-moment correlation values (r) or Spearman's rho (ρ) correlation tests were performed between EEG measures and ΔTUG. All significant effects are marked in bold and with an asterisk ($*$). All reported p-values are two-tailed.

		MS-RR and MS-PP Patients			**Only MS-RR Patients**		
		T0	T1	**Diff. (T1-T0)**	T0	T1	**Diff. (T1-T0)**
wSMI	r (ρ)	0.225	**0.775**	**0.700**	0.15	**0.632**	**0.699**
	p	0.42	**0.001***	**0.005***	0.608	**0.028***	**0.011***
AP wSMI	r	0.267	**0.676**	0.529	0.162	**0.644**	0.482
	p	0.337	**0.008***	0.051	0.59	**0.024***	0.112
INTERH wSMI	r (ρ)	0.216	**0.665**	0.38	0.327	0.487	0.338
	p	0.44	**0.01***	0.18	0.27	0.108	0.281

4.4 Discussion

In this study, the aim was to test whether EEG-based connectivity metrics could be used to predict and/or track functional recovery related to a specific gait rehabilitation protocol (TOCT) in MS patients.
Specifically, we hypothesized that

- pre-training connectivity metrics may predict the success of the intervention, and
- clinical improvement induced by the intervention may be associated to a brain functional reorganization that is captured by EEG-based connectivity metrics.

Consistent with these hypotheses, pre-training alpha-band wPLI connectivity was found to correlate with changes in behavioural performance as measured using the Timed Up and Go (TUG) index, while wSMI connectivity was able to track relative TUG changes associated with the gait rehabilitation protocol TOCT.

The strength and efficiency of alpha-band wPLI connectivity at T0 was positively correlated with the clinical improvement measured by ΔTUG. This relationship was also characterized by a relative topographical specificity, as the strongest relationship between connectivity and performance improvement was identified for for antero-posterior rather than inter-regional interactions. Of note, previous work showed that MS patients typically show a decreased alpha-band-connectivity with respect to healthy control subjects (Cover et al., 2006; Leocani et al., 2000). In this perspective, our results suggest that patients with less disrupted alpha-band connectivity may profit more from a two-week training intervention.

While alpha-band wPLI seem to reflect the potential of a patient to profit from treatment, it does not account well for changes that occur in neural activity based on the treatment itself. In fact, these changes may be better captured by wSMI connectivity, fundamentally rooted in information theory. Indeed, we observed a positive correlation between T1-T0 changes in broadband wSMI connectivity (ΔwSMI) and variations in motor performance (ΔTUG). Given that wSMI at T1, but not at T0, was also found to correlate with ΔTUG, changes in broadband wSMI connectivity may reflect compensatory functional adaptations (increase in system complexity): i.e., the implementation or the unmasking of mechanisms that were not 'active' in patients before treatment (no correlation at T0).

In line with this view, previous studies suggested that MS patients may have lower chaotic activity (Kotini et al., 2007), or decreased brain functional complexity (Carrubba et al., 2012). For instance, Kotini et al. (Kotini et al., 2007) found that the number of independent variables required to describe a dynamical system is lower for MEG activity in MS patients relative to healthy control subjects. Similarly, using recurrence quantification analysis, Carrubba et al. (Carrubba et al., 2012) found that

the probability that a specific state will recur was greater in MS patients. The wSMI as a weighted measure of mutual information may thus be well suited to track relative changes in the complexity of brain activity through the two-week treatment. We hypothesize that an increase in wSMI in patients from T0 to T1 could be related to an increase in 'healthy-brain-like' nonlinear system properties.

To our knowledge, this is the first study to account for changes in non-linear dynamics induced by treatment in MS patients, and our results suggest that methods investigating such dynamics may provide valuable information regarding the impact of rehabilitation strategies based on motor training.

Intriguingly, classical metrics of lesion volume based on the analysis of MRI data, were not associated with motor recovery after TOCT training in our sample. These data confirm that adaptive brain plasticity can occur in MS patients, despite a high burden of cerebral pathology and disability (Tomassini et al., 2012a), and may suggest that the brain plastic reorganization induced by the training could be better captured by functional, rather than structural, indices.

Limitations of this study include the comparatively small sample size (n=16) and the lack of a control group. These limitations inevitably reduced the statistical power of the analyses and the generalisability of the findings. Moreover, our sample contained two subsets of individuals with distinct MS phenotypes (RR for 14 out of 16 and PP for 2 out of 16 patients) and featured a relatively wide range in the Expanded Disability Status Scale EDSS score (3.5-5.5) and of age (27-67).

We carefully evaluated the possible presence of outliers, which are likely to affect correlation analyses when the number of patients is limited, and no evidence of outliers was found in our sample for the EEG connectivity and primary behavioural outcome measures. In addition, age was controlled for by regressing out the effect of this variable on performed analyses, and all principal results remained significant after the exclusion of the two PP phenotype patients.

4.5 Conclusions

In conclusion, our study showed that changes in brain connectivity related to phase synchronization (i.e., alpha-band wPLI connectivity) correlate with functional recovery after specific gait training in mildly impaired MS patients. Moreover, changes in brain connectivity related to non-linear dynamics (i.e., broadband wSMI) may represent a promising measure to account for behavioural changes induced by the treatment and may reflect functional compensatory brain plasticity.

These results offer a preliminary indication regarding the potential value of EEG-based connectivity metrics for predicting and tracking the impact of motor rehabilitation strategies in MS patients.

Chapter 5

Conclusions

The works included in this thesis allowed to demonstrate that the functional connectivity metrics wPLI and wSMI have a different sensitivity for distinct types of brain interaction dynamics and may thus account for different functional processes. The findings presented here indicate that the combined use of these two methods may provide a better and more complete characterization of brain functional dynamics within and across distinct physiological and pathological states.

Indeed, using simulated, yet highly realistic high-density EEG data, we showed that while wPLI displays an optimal sensitivity for interaction dynamics with linear and nonlinear components, wSMI has a higher sensitivity for exclusively nonlinear dynamics.

This finding may have significant implications for the analysis of functional connectivity in different vigilance stages. Specifically, we found that the combined use of power- and FC-based features better describes changes in brain activity across wakefulness, N2, N3 and REM sleep relative to individual feature sets alone.

Moreover, we investigated FC in vigilance stages associated with different probabilities of occurrences of conscious experiences. Previous observations in states characterized by altered levels of consciousness, including unresponsive wakefulness syndrome and anaesthesia, identified delta- and alpha-connectivity as potential markers of consciousness. However, here we found that alpha-FC does not significantly contribute to distinguishing between states characterized by a higher probability of conscious experiences (wakefulness and REM sleep) as compared to states associated with a lower probability of conscious experiences (N2 and N3 sleep).

Instead, we found alpha-FC to represent the best FC-feature for distinguishing between Wakefulness and REM sleep, a state typically characterized by vivid conscious experiences and by a relative sensory disconnection with respect to the external world. In this light, our results suggest that FC changes in the alpha range could mark disengagement from the external environment rather than the current level of consciousness.

Sigma-FC (but not sigma power) was found to strongly contribute to the differentiation between states characterized by higher and lower levels of consciousness. The study of this parameter as a potential marker of consciousness in sleep will certainly deserve further investigations.

Finally, we have also used the same FC metrics in EEG recordings of multiple sclerosis (MS) patients to evaluate their potential ability to track or predict behavioural performance enhancement induced by a rehabilitative motor training. This study confirmed that wPLI and wSMI account for different brain functional dynamics, and identify distinct aspects of training-related functional changes. Alpha-band wPLI resulted as a good indicator of whether a patient will positively respond to treatment, but was not able to track treatment-based changes in neural activity. On the contrary, broadband-wSMI was found to correlate with changes induced by the treatment (increase in system complexity), likely reflecting the implementation or unmasking of (compensatory) mechanisms that are not active in patients before treatment.

In conclusion, results of these works highlight the importance of taking into account the relative sensitivity of applied connectivity methods to different types of inter-regional interaction dynamics and provide a strong support to the combined use of multiple metrics for obtaining a more accurate description of functional connectivity across different conditions or groups. wPLI and wSMI are especially interesting due to their similar robustness to volume conduction confounds and to their different sensitivities to linear and nonlinear dynamics. The combined application of these two metrics may thus represent a powerful tool for the evaluation of brain connectivity in physiological and pathological conditions.

References

Allefeld, C., Görgen, K., and Haynes, J.-D. (2016). Valid population inference for information-based imaging: From the second-level t-test to prevalence inference. *Neuroimage*, 141:378–392. 73, 74

Allen, B., Stacey, B., and Bar-Yam, Y. (2017). Multiscale information theory and the marginal utility of information. *Entropy*, 19(6):273. 81

Andrillon, T., Nir, Y., Staba, R. J., Ferrarelli, F., Cirelli, C., Tononi, G., and Fried, I. (2011). Sleep spindles in humans: insights from intracranial eeg and unit recordings. *Journal of Neuroscience*, 31(49):17821–17834. 87

Arnhold, J., Grassberger, P., Lehnertz, K., and Elger, C. E. (1999). A robust method for detecting interdependences: application to intracranially recorded eeg. *Physica D: Nonlinear Phenomena*, 134(4):419–430. 34

Aserinsky, E., Kleitman, N., et al. (1953). Regularly occurring periods of eye motility, and concomitant phenomena, during sleep. *Science*, 118(3062):273–274. 57

Bastos, A. M. and Schoffelen, J.-M. (2016). A tutorial review of functional connectivity analysis methods and their interpretational pitfalls. *Frontiers in systems neuroscience*, 9:175. 3, 7

Bernardi, G., Betta, M., Cataldi, J., Leo, A., Haba-Rubio, J., Heinzer, R., Cirelli, C., Tononi, G., Pietrini, P., Ricciardi, E., et al. (2019a). Visual imagery and visual perception induce similar changes in occipital slow waves of sleep. *Journal of neurophysiology*, 121(6):2140–2152. 28, 59

Bernardi, G., Betta, M., Ricciardi, E., Pietrini, P., Tononi, G., and Siclari, F. (2019b). Regional delta waves in human rapid eye movement sleep. *Journal of Neuroscience*, 39(14):2686–2697. 57

Bernardi, G., Siclari, F., Yu, X., Zennig, C., Bellesi, M., Ricciardi, E., Cirelli, C., Ghilardi, M. F., Pietrini, P., and Tononi, G. (2015). Neural and behavioral correlates of extended training during sleep deprivation in humans: evidence for local, task-specific effects. *Journal of neuroscience*, 35(11):4487–4500. 94

Berthomier, C., Drouot, X., Herman-Stoïca, M., Berthomier, P., Prado, J., Bokar-Thire, D., Benoit, O., Mattout, J., and d'Ortho, M.-P. (2007). Automatic analysis of single-channel sleep eeg: validation in healthy individuals. *Sleep*, 30(11):1587–1595. 85

Blain-Moraes, S., Lee, U., Ku, S., Noh, G., and Mashour, G. A. (2014). Electroencephalographic effects of ketamine on power, cross-frequency coupling, and connectivity in the alpha bandwidth. *Frontiers in systems neuroscience*, 8:114. 19, 53, 87

Bonnet, M. H. and Moore, S. E. (1982). The threshold of sleep: perception of sleep as a function of time asleep and auditory threshold. *Sleep*, 5(3):267–276. 59, 137

Borbély, A. A. (1982). A two process model of sleep regulation. *Hum neurobiol*, 1(3):195–204. 28

Bullmore, E. and Sporns, O. (2009). Complex brain networks: graph theoretical analysis of structural and functional systems. *Nature reviews neuroscience*, 10(3):186–198. 2

Buysse, D. J., Reynolds, C. F., Monk, T. H., Berman, S. R., Kupfer, D. J., et al. (1989). The pittsburgh sleep quality index: a new instrument for psychiatric practice and research. *Psychiatry res*, 28(2):193–213. 59

Canales-Johnson, A., Billig, A., Olivares, F., Gonzalez, A., del Carmen Garcia, M., Silva, W., Vaucheret, E., Ciraolo, C., Mikulan, E., Ibanez, A., et al. (2017). Integration and differentiation of neural information dissociate between conscious percepts. *bioRxiv*, page 133801. 7, 15, 50

Carrubba, S., Minagar, A., Chesson, A. L., Frilot, C., and Marino, A. A. (2012). Increased determinism in brain electrical activity occurs in association with multiple sclerosis. *Neurological research*, 34(3):286–290. 101

Casali, A. G., Gosseries, O., Rosanova, M., Boly, M., Sarasso, S., Casali, K. R., Casarotto, S., Bruno, M.-A., Laureys, S., Tononi, G., et al. (2013). A theoretically based index of consciousness independent of sensory processing and behavior. *Science translational medicine*, 5(198):198ra105–198ra105. 11, 16

Cash, S. S., Halgren, E., Dehghani, N., Rossetti, A. O., Thesen, T., Wang, C., Devinsky, O., Kuzniecky, R., Doyle, W., Madsen, J. R., et al. (2009). The human k-complex represents an isolated cortical down-state. *Science*, 324(5930):1084–1087. 88

Chennu, S., Annen, J., Wannez, S., Thibaut, A., Chatelle, C., Cassol, H., Martens, G., Schnakers, C., Gosseries, O., Menon, D., et al. (2017). Brain networks predict metabolism, diagnosis and prognosis at the bedside in disorders of consciousness. *Brain*, 140(8):2120–2132. 7, 10, 11, 12, 15, 16, 17, 50, 54

Chennu, S., Finoia, P., Kamau, E., Allanson, J., Williams, G. B., Monti, M. M., Noreika, V., Arnatkeviciute, A., Canales-Johnson, A., Olivares, F., et al. (2014). Spectral signatures of reorganised brain networks in disorders of consciousness. *PLoS computational biology*, 10(10):e1003887. 7, 10, 11, 12, 15, 16, 17, 50, 53, 54, 58, 85, 87

Chennu, S., OâĂŹConnor, S., Adapa, R., Menon, D. K., and Bekinschtein, T. A. (2016). Brain connectivity dissociates responsiveness from drug exposure during propofol-induced transitions of consciousness. *PLoS computational biology*, 12(1):e1004669. 7, 10, 11, 12, 15, 16, 17, 19, 50, 53, 58, 87

Chisari, C., Venturi, M., Bertolucci, F., Fanciullacci, C., and Rossi, B. (2014). Benefits of an intensive task-oriented circuit training in multiple sclerosis patients with mild disability. *NeuroRehabilitation*, 35(3):509–518. 92, 93

Cohen, M. X. (2014). *Analyzing neural time series data: theory and practice*. MIT press. 3, 4, 6, 7, 32, 61

Cohen, M. X. (2015). Effects of time lag and frequency matching on phase-based connectivity. *Journal of neuroscience methods*, 250:137–146. 8, 15, 50

Colclough, G. L., Woolrich, M. W., Tewarie, P., Brookes, M. J., Quinn, A. J., and Smith, S. M. (2016). How reliable are meg resting-state connectivity metrics? *Neuroimage*, 138:284–293. 21

Comsa, I. M., Bekinschtein, T. A., and Chennu, S. (2019). Transient topographical dynamics of the electroencephalogram predict brain connectivity and behavioural responsiveness during drowsiness. *Brain topography*, 32(2):315–331. 7, 12, 15, 17, 19, 50, 53, 87

Cover, K. S., Vrenken, H., Geurts, J. J., van Oosten, B. W., Jelles, B., Polman, C. H., Stam, C. J., and van Dijk, B. W. (2006). Multiple sclerosis patients show a highly significant decrease in alpha band interhemispheric synchronization measured using meg. *Neuroimage*, 29(3):783–788. 66, 91, 92, 95, 101

Darracq, M., Funk, C. M., Polyakov, D., Riedner, B., Gosseries, O., Nieminen, J. O., Bonhomme, V., Brichant, J.-F., Boly, M., Laureys, S., et al. (2018). Evoked alpha power is reduced in disconnected consciousness during sleep and anesthesia. *Scientific reports*, 8(1):16664. 59, 88, 136, 137

David, O., Cosmelli, D., and Friston, K. J. (2004). Evaluation of different measures of functional connectivity using a neural mass model. *Neuroimage*, 21(2):659–673. 11, 16, 50

Delorme, A. and Makeig, S. (2004). Eeglab: an open source toolbox for analysis of single-trial eeg dynamics including independent component analysis. *Journal of neuroscience methods*, 134(1):9–21. 29, 46, 60, 94

Delorme, A., Mullen, T., Kothe, C., Acar, Z. A., Bigdely-Shamlo, N., Vankov, A., and Makeig, S. (2011). Eeglab, sift, nft, bcilab, and erica: new tools for advanced eeg processing. *Computational intelligence and neuroscience*, 2011:10. 49, 94

Dement, W. and Kleitman, N. (1957). Cyclic variations in eeg during sleep and their relation to eye movements, body motility, and dreaming. *Electroencephalography and clinical neurophysiology*, 9(4):673–690. 57

Demertzi, A., Tagliazucchi, E., Dehaene, S., Deco, G., Barttfeld, P., Raimondo, F., Martial, C., Fernández-Espejo, D., Rohaut, B., Voss, H., et al. (2019). Human consciousness is supported by dynamic complex patterns of brain signal coordination. *Science advances*, 5(2):eaat7603. 87

Donhauser, P. W., Florin, E., and Baillet, S. (2018). Imaging of neural oscillations with embedded inferential and group prevalence statistics. *PLoS computational biology*, 14(2):e1005990. 73, 74

Duda, R. O., Hart, P. E., and Stork, D. G. (2012). *Pattern classification*. John Wiley & Sons. 63

Efron, B. (1992). Bootstrap methods: another look at the jackknife. In *Breakthroughs in statistics*, pages 569–593. Springer. 61

Engemann, D. A., Raimondo, F., King, J.-R., Rohaut, B., Louppe, G., Faugeras, F., Annen, J., Cassol, H., Gosseries, O., Fernandez-Slezak, D., et al. (2018). Robust eeg-based cross-site and cross-protocol classification of states of consciousness. *Brain*, 141(11):3179–3192. 89

Evans, A. C., Collins, D. L., Mills, S., Brown, E., Kelly, R., and Peters, T. M. (1993). 3d statistical neuroanatomical models from 305 mri volumes. In *1993 IEEE conference record nuclear science symposium and medical imaging conference*, pages 1813–1817. IEEE. 17

Fries, P. (2005). A mechanism for cognitive dynamics: neuronal communication through neuronal coherence. *Trends in cognitive sciences*, 9(10):474–480. 3

Friston, K., Holmes, A., and Worsley, K. (1999). How many subjects constitute a study? *NeuroImage*, 10(1):1. 74

Friston, K. J. (1994). Functional and effective connectivity in neuroimaging: a synthesis. *Human brain mapping*, 2(1-2):56–78. 2

Gollo, L. L., Mirasso, C., Sporns, O., and Breakspear, M. (2014). Mechanisms of zero-lag synchronization in cortical motifs. *PLoS computational biology*, 10(4):e1003548. 5, 8, 15

Gratiy, S. L., Halnes, G., Denman, D., Hawrylycz, M. J., Koch, C., Einevoll, G. T., and Anastassiou, C. A. (2017). From maxwell's equations to the theory of current-source density analysis. *European Journal of Neuroscience*, 45(8):1013–1023. 6

Hagmann, P., Cammoun, L., Gigandet, X., Meuli, R., Honey, C. J., Wedeen, V. J., and Sporns, O. (2008). Mapping the structural core of human cerebral cortex. *PLoS biology*, 6(7). 2

Halász, P. (2016). The k-complex as a special reactive sleep slow wave–a theoretical update. *Sleep medicine reviews*, 29:34–40. 88

Hämäläinen, M., Hari, R., Ilmoniemi, R. J., Knuutila, J., and Lounasmaa, O. V. (1993). MagnetoencephalographyâĂŤtheory, instrumentation, and applications to noninvasive studies of the working human brain. *Reviews of modern Physics*, 65(2):413. 6

Haufe, S. and Ewald, A. (2016). A simulation framework for benchmarking eeg-based brain connectivity estimation methodologies. *Brain topography*, pages 1–18. 17, 18, 20, 33, 38, 43, 50

Haus, H. A. and Melcher, J. R. (1989). *Electromagnetic fields and energy*, volume 107. Prentice Hall Englewood Cliffs, NJ. 6

Hénon, M. (1976). A two-dimensional mapping with a strange attractor. In *The Theory of Chaotic Attractors*, pages 94–102. Springer. 20, 21

Hipp, J. F., Hawellek, D. J., Corbetta, M., Siegel, M., and Engel, A. K. (2012). Large-scale cortical correlation structure of spontaneous oscillatory activity. *Nature neuroscience*, 15(6):884. 8, 15

Honey, C. J., Kötter, R., Breakspear, M., and Sporns, O. (2007). Network structure of cerebral cortex shapes functional connectivity on multiple time scales. *Proceedings of the National Academy of Sciences*, 104(24):10240–10245. 2

Horwitz, B. (2003). The elusive concept of brain connectivity. *Neuroimage*, 19(2):466–470. 1

Huang, Y., Parra, L. C., and Haufe, S. (2016). The new york headâĂŤa precise standardized volume conductor model for eeg source localization and tes targeting. *NeuroImage*, 140:150–162. 17

Huber, R., Ghilardi, M. F., Massimini, M., and Tononi, G. (2004). Local sleep and learning. *Nature*, 430(6995):78. 31

Iber, C. (2007). The aasm manual for the scoring of sleep and associated events: Rules. *Terminology and Technical Specification*. 29, 60

Ikeda, K. (1979). Multiple-valued stationary state and its instability of the transmitted light by a ring cavity system. *Optics communications*, 30(2):257–261. 20, 21

Imperatori, L. S., Betta, M., Cecchetti, L., Canales-Johnson, A., Ricciardi, E., Siclari, F., Pietrini, P., Chennu, S., and Bernardi, G. (2019). Eeg functional connectivity metrics wpli and wsmi account for distinct types of brain functional interactions. *Scientific Reports*, 9(1):8894. viii, 14, 57, 58, 61, 73, 85, 92

Ince, R. A. (2017). The partial entropy decomposition: Decomposing multivariate entropy and mutual information via pointwise common surprisal. *arXiv preprint arXiv:1702.01591*. 67

Ince, R. A., Giordano, B. L., Kayser, C., Rousselet, G. A., Gross, J., and Schyns, P. G. (2017). A statistical framework for neuroimaging data analysis based on mutual information estimated via a gaussian copula. *Human brain mapping*, 38(3):1541–1573. 4, 11, 16, 66

Iriarte, J., Urrestarazu, E., Valencia, M., Alegre, M., Malanda, A., Viteri, C., and Artieda, J. (2003). Independent component analysis as a tool to eliminate artifacts in eeg: a quantitative study. *Journal of clinical neurophysiology*, 20(4):249–257. 60

James, R. G., Ellison, C. J., and Crutchfield, J. P. (2018). dit: a python package for discrete information theory. *J. Open Source Software*, 3(25):738. 81

Jobst, B. M., Hindriks, R., Laufs, H., Tagliazucchi, E., Hahn, G., Ponce-Alvarez, A., Stevner, A. B., Kringelbach, M. L., and Deco, G. (2017). Increased stability and breakdown of brain effective connectivity during slow-wave sleep: mechanistic insights from whole-brain computational modelling. *Scientific reports*, 7(1):4634. 53

Johns, M. W. (1991). A new method for measuring daytime sleepiness: the epworth sleepiness scale. *sleep*, 14(6):540–545. 59

Kayser, J. and Tenke, C. E. (2006). Principal components analysis of laplacian waveforms as a generic method for identifying erp generator patterns: I. evaluation with auditory oddball tasks. *Clinical neurophysiology*, 117(2):348–368. 22, 61, 95

Khadem, A. and Hossein-Zadeh, G.-A. (2014). Quantification of the effects of volume conduction on the eeg/meg connectivity estimates: an index of sensitivity to brain interactions. *Physiological measurement*, 35(10):2149. 7, 15

King, J.-R., Sitt, J. D., Faugeras, F., Rohaut, B., El Karoui, I., Cohen, L., Naccache, L., and Dehaene, S. (2013). Information sharing in the brain indexes consciousness in noncommunicative patients. *Current Biology*, 23(19):1914–1919. 7, 8, 9, 10, 11, 12, 15, 16, 17, 21, 22, 50, 53, 54, 57, 58, 61, 62, 95

Köbbert, C., Apps, R., Bechmann, I., Lanciego, J. L., Mey, J., and Thanos, S. (2000). Current concepts in neuroanatomical tracing. *Progress in neurobiology*, 62(4):327–351. 2

Koley, B. and Dey, D. (2012). An ensemble system for automatic sleep stage classification using single channel eeg signal. *Computers in biology and medicine*, 42(12):1186–1195. 85

Kotini, A., Anninos, P., Tamiolakis, D., and Prassopoulos, P. (2007). Differentiation of meg activity in multiple sclerosis patients with the use of nonlinear analysis. *Journal of integrative neuroscience*, 6(02):233–240. 101

Kurtzke, J. F. (1983). Rating neurologic impairment in multiple sclerosis: an expanded disability status scale (edss). *Neurology*, 33(11):1444–1444. 93

Kvålseth, T. O. (1991). The relative useful information measure: Some comments. *Information sciences*, 56(1-3):35–38. 9

Lachaux, J.-P., Rodriguez, E., Martinerie, J., and Varela, F. J. (1999). Measuring phase synchrony in brain signals. *Human brain mapping*, 8(4):194–208. 4

Langheim, F. J., Murphy, M., Riedner, B. A., and Tononi, G. (2011). Functional connectivity in slow-wave sleep: identification of synchronous cortical activity during wakefulness and sleep using time series analysis of electroencephalographic data. *Journal of sleep research*, 20(4):496–505. 57

Latora, V. and Marchiori, M. (2001). Efficient behavior of small-world networks. *Physical review letters*, 87(19):198701. 96

Lau, T. M., Gwin, J. T., McDowell, K. G., and Ferris, D. P. (2012). Weighted phase lag index stability as an artifact resistant measure to detect cognitive eeg activity during locomotion. *Journal of neuroengineering and rehabilitation*, 9(1):47. 7, 10, 15, 50

Laurino, M., Menicucci, D., Piarulli, A., Mastorci, F., Bedini, R., Allegrini, P., and Gemignani, A. (2014). Disentangling different functional roles of evoked k-complex components: mapping the sleeping brain while quenching sensory processing. *Neuroimage*, 86:433–445. 88

Laurino, M., Piarulli, A., Menicucci, D., and Gemignani, A. (2019). Local gamma activity during non-rem sleep in the context of sensory 1 evoked k-complexes. *Frontiers in neuroscience*, 13:1094. 88

Learmonth, Y. C., Paul, L., McFadyen, A. K., Mattison, P., and Miller, L. (2012). Reliability and clinical significance of mobility and balance assessments in multiple sclerosis. *International Journal of Rehabilitation Research*, 35(1):69–74. 94

Lee, M., Sanders, R. D., Yeom, S.-K., Won, D.-O., Kim, H.-J., Lee, B.-R., Seo, K.-S., Kim, H. J., Tononi, G., and Lee, S.-W. (2017a). Change in functional networks for transitions between states of consciousness during midazolam-induced sedation. In *2017 39th Annual International Conference of the IEEE Engineering in Medicine and Biology Society (EMBC)*, pages 958–961. IEEE. 7, 10, 11, 12, 15, 17, 50, 53, 54, 58, 85, 87, 139

Lee, M., Sanders, R. D., Yeom, S.-K., Won, D.-O., Seo, K.-S., Kim, H. J., Tononi, G., and Lee, S.-W. (2017b). Network properties in transitions of consciousness during propofol-induced sedation. *Scientific reports*, 7(1):16791. 7, 10, 11, 12, 15, 16, 17, 50, 53, 54, 58, 85, 87, 139

Lehembre, R., Bruno, M.-A., Vanhaudenhuyse, A., Chatelle, C., Cologan, V., Leclercq, Y., Soddu, A., Macq, B., Laureys, S., and Noirhomme, Q. (2012). Resting-state eeg study of comatose patients: a connectivity and frequency analysis to find differences between vegetative and minimally conscious states. *Functional neurology*, 27(1):41. 54

Leocani, L., Locatelli, T., Martinelli, V., Rovaris, M., Falautano, M., Filippi, M., Magnani, G., and Comi, G. (2000). Electroencephalographic coherence analysis in multiple sclerosis: correlation with clinical, neuropsychological, and mri findings. *Journal of Neurology, Neurosurgery & Psychiatry*, 69(2):192–198. 91, 92, 95, 101

Li, T., Zhu, S., and Ogihara, M. (2006). Using discriminant analysis for multi-class classification: an experimental investigation. *Knowledge and information systems*, 10(4):453–472. 63

Lorenz, E. N. (1963). The mechanics of vacillation. *Journal of the atmospheric sciences*, 20(5):448–465. 20, 21

Ma, Y., Shi, W., Peng, C.-K., and Yang, A. C. (2018). Nonlinear dynamical analysis of sleep electroencephalography using fractal and entropy approaches. *Sleep medicine reviews*, 37:85–93. 54

Maiwald, T. et al. (2008). Mathematical methods in signal processing and digital image analysis, eds. r. dahlhaus et al. 26

Maksimow, A., Kaisti, K., Aalto, S., Mäenpää, M., Jääskeläinen, S., Hinkka, S., Martens, S., Särkelä, M., Viertiö-Oja, H., and Scheinin, H. (2005). Correlation of eeg spectral entropy with regional cerebral blood flow during sevoflurane and propofol anaesthesia. *Anaesthesia*, 60(9):862–869. 19, 33

Maris, E. and Oostenveld, R. (2007). Nonparametric statistical testing of eeg-and meg-data. *Journal of neuroscience methods*, 164(1):177–190. 32

Martuzzi, R., Ramani, R., Qiu, M., Rajeevan, N., and Constable, R. T. (2010). Functional connectivity and alterations in baseline brain state in humans. *Neuroimage*, 49(1):823–834. 19, 33

Marzano, C., Moroni, F., Gorgoni, M., Nobili, L., Ferrara, M., and De Gennaro, L. (2013). How we fall asleep: regional and temporal differences in electroencephalographic synchronization at sleep onset. *Sleep medicine*, 14(11):1112–1122. 56

Massimini, M., Ferrarelli, F., Huber, R., Esser, S. K., Singh, H., and Tononi, G. (2005). Breakdown of cortical effective connectivity during sleep. *Science*, 309(5744):2228–2232. 53, 87

Massimini, M., Huber, R., Ferrarelli, F., Hill, S., and Tononi, G. (2004). The sleep slow oscillation as a traveling wave. *Journal of Neuroscience*, 24(31):6862–6870. 54, 73, 85

Mazziotta, J., Toga, A., Evans, A., Fox, P., Lancaster, J., Zilles, K., Woods, R., Paus, T., Simpson, G., Pike, B., et al. (2001). A probabilistic atlas and reference system for the human brain: International consortium for brain mapping (icbm). *Philosophical Transactions of the Royal Society of London. Series B: Biological Sciences*, 356(1412):1293–1322. 17

Migliorelli, C., Bachiller, A., Andrade, A. G., Alonso, J. F., Mañanas, M. A., Borja, C., Giménez, S., Antonijoan, R. M., Varga, A. W., Osorio, R. S., et al. (2019). Alterations in eeg connectivity in healthy young adults provide an indicator of sleep depth. *Sleep*, 42(6):zsz081. 57, 85, 86

Miller, G. (1955). Note on the bias of information estimates. *Information theory in psychology: Problems and methods*. 66

Muller, L., Piantoni, G., Koller, D., Cash, S. S., Halgren, E., and Sejnowski, T. J. (2016). Rotating waves during human sleep spindles organize global patterns of activity that repeat precisely through the night. *Elife*, 5:e17267. 87

Nichols, T. E. and Holmes, A. P. (2002). Nonparametric permutation tests for functional neuroimaging: a primer with examples. *Human brain mapping*, 15(1):1–25. 31

Nir, Y., Massimini, M., Boly, M., and Tononi, G. (2013). Sleep and consciousness. In *Neuroimaging of consciousness*, pages 133–182. Springer. 12, 17

Nir, Y. and Tononi, G. (2010). Dreaming and the brain: from phenomenology to neurophysiology. *Trends in cognitive sciences*, 14(2):88–100. 58, 59, 137

Nolte, G., Bai, O., Wheaton, L., Mari, Z., Vorbach, S., and Hallett, M. (2004). Identifying true brain interaction from eeg data using the imaginary part of coherency. *Clinical neurophysiology*, 115(10):2292–2307. 10

Nolte, G., Ziehe, A., Nikulin, V. V., Schlögl, A., Krämer, N., Brismar, T., and Müller, K.-R. (2008). Robustly estimating the flow direction of information in complex physical systems. *Physical review letters*, 100(23):234101. 10

Nunez, P. L., Srinivasan, R., et al. (2006). *Electric fields of the brain: the neurophysics of EEG*. Oxford University Press, USA. 7, 22, 61

Ogilvie, R. D. (2001). The process of falling asleep. *Sleep medicine reviews*, 5(3):247–270. 56

Oostenveld, R., Fries, P., Maris, E., and Schoffelen, J.-M. (2011). Fieldtrip: open source software for advanced analysis of meg, eeg, and invasive electrophysiological data. *Computational intelligence and neuroscience*, 2011:1. 22, 62

Ortiz, E., Stingl, K., Münßinger, J., Braun, C., Preissl, H., and Belardinelli, P. (2012). Weighted phase lag index and graph analysis: preliminary investigation of functional connectivity during resting state in children. *Computational and mathematical methods in medicine*, 2012. 7, 10, 15, 50

Palva, S. and Palva, J. M. (2012). Discovering oscillatory interaction networks with m/eeg: challenges and breakthroughs. *Trends in cognitive sciences*, 16(4):219–230. 8, 15

Parra, M., Mikulan, E., Trujillo, N., Della Sala, S., Lopera, F., Manes, F., Starr, J., and Ibanez, A. (2017). Brain information sharing during visual short-term memory binding yields a memory biomarker for familial alzheimer's disease. *Current Alzheimer Research*, 14(12):1335–1347. 7, 10, 15, 50

Peraza, L. R., Asghar, A. U., Green, G., and Halliday, D. M. (2012). Volume conduction effects in brain network inference from electroencephalographic recordings using phase lag index. *Journal of neuroscience methods*, 207(2):189–199. 8, 9, 10, 15

Pigorini, A., Sarasso, S., Proserpio, P., Szymanski, C., Arnulfo, G., Casarotto, S., Fecchio, M., Rosanova, M., Mariotti, M., Russo, G. L., et al. (2015). Bistability breaks-off deterministic responses to intracortical stimulation during non-rem sleep. *Neuroimage*, 112:105–113. 53, 88

Pizzella, V., Marzetti, L., Della Penna, S., de Pasquale, F., Zappasodi, F., and Romani, G. L. (2014). Magnetoencephalography in the study of brain dynamics. *Functional neurology*, 29(4):241. 5

Plonsey, R. and Heppner, D. B. (1967). Considerations of quasi-stationarity in electrophysiological systems. *The Bulletin of mathematical biophysics*, 29(4):657–664. 6

Polman, C. H., Reingold, S. C., Edan, G., Filippi, M., Hartung, H.-P., Kappos, L., Lublin, F. D., Metz, L. M., McFarland, H. F., O'Connor, P. W., et al. (2005). Diagnostic criteria for multiple sclerosis: 2005 revisions to the âĂIJmcdonald criteriaâĂİ. *Annals of Neurology: Official Journal of the American Neurological Association and the Child Neurology Society*, 58(6):840–846. 93

Quiroga, R. Q., Kraskov, A., Kreuz, T., and Grassberger, P. (2002). Performance of different synchronization measures in real data: a case study on electroencephalographic signals. *Physical Review E*, 65(4):041903. 34

Rechtschaffen, A., Hauri, P., and Zeitlin, M. (1966). Auditory awakening thresholds in rem and nrem sleep stages. *Perceptual and motor skills*, 22(3):927–942. 53

Reddy, H., Narayanan, S., Arnoutelis, R., Jenkinson, M., Antel, J., Matthews, P., and Arnold, D. (2000). Evidence for adaptive functional changes in the cerebral cortex with axonal injury from multiple sclerosis. *Brain*, 123(11):2314–2320. 92

Riedner, B. A., Vyazovskiy, V. V., Huber, R., Massimini, M., Esser, S., Murphy, M., and Tononi, G. (2007). Sleep homeostasis and cortical synchronization: Iii. a high-density eeg study of sleep slow waves in humans. *Sleep*, 30(12):1643–1657. 73

Robinson, S. E. and Mandell, A. J. (2015). Mutual information in a meg complexity measure suggests regional hyper-connectivity in schizophrenic probands. *Neuropsychopharmacology*, 40(1):251. 7, 10, 15, 50

Rocca, M. A., Colombo, B., Falini, A., Ghezzi, A., Martinelli, V., Scotti, G., Comi, G., and Filippi, M. (2005). Cortical adaptation in patients with ms: a cross-sectional functional mri study of disease phenotypes. *The Lancet Neurology*, 4(10):618–626. 92

Roelfsema, P. R., Engel, A. K., König, P., and Singer, W. (1997). Visuomotor integration is associated with zero time-lag synchronization among cortical areas. *Nature*, 385(6612):157. 5, 8, 15

Romero, S., Mananas, M., Clos, S., Gimenez, S., and Barbanoj, M. (2003). Reduction of eeg artifacts by ica in different sleep stages. In *Proceedings of the 25th*

Annual International Conference of the IEEE Engineering in Medicine and Biology Society (IEEE Cat. No. 03CH37439), volume 3, pages 2675–2678. IEEE. 60

Rosenfalck, P. (1969). Intra-and extracellular potential fields of active nerve and muscle fibres. *Acta Phisiologica Scandinavica*, 321. 6

Rössler, O. (1979). An equation for hyperchaos. *Physics Letters A*, 71(2-3):155–157. 20, 21

Rubinov, M. and Sporns, O. (2010). Complex network measures of brain connectivity: uses and interpretations. *Neuroimage*, 52(3):1059–1069. 96

Rusterholz, T., Achermann, P., Dürr, R., Koenig, T., and Tarokh, L. (2017). Global field synchronization in gamma range of the sleep eeg tracks sleep depth: Artifact introduced by a rectangular analysis window. *Journal of neuroscience methods*, 284:21–26. 57

Sadaghiani, S. and Kleinschmidt, A. (2016). Brain networks and α-oscillations: structural and functional foundations of cognitive control. *Trends in cognitive sciences*, 20(11):805–817. 20

Sakkalis, V. (2011). Review of advanced techniques for the estimation of brain connectivity measured with eeg/meg. *Computers in biology and medicine*, 41(12):1110–1117. 4

Salinas, E. and Sejnowski, T. J. (2001). Correlated neuronal activity and the flow of neural information. *Nature reviews neuroscience*, 2(8):539. 3

Sarasso, S., Rosanova, M., Casali, A. G., Casarotto, S., Fecchio, M., Boly, M., Gosseries, O., Tononi, G., Laureys, S., and Massimini, M. (2014). Quantifying cortical eeg responses to tms in (un) consciousness. *Clinical EEG and neuroscience*, 45(1):40–49. 87

Sassenhagen, J. and Draschkow, D. (2019). Cluster-based permutation tests of meg/eeg data do not establish significance of effect latency or location. *Psychophysiology*, 56(6):e13335. 32

Scherg, M., Berg, P., Nakasato, N., and Beniczky, S. (2019). Taking the eeg back into the brain: The power of multiple discrete sources. *Frontiers in neurology*, 10:855. 5

Schoffelen, J.-M. and Gross, J. (2009). Source connectivity analysis with meg and eeg. *Human brain mapping*, 30(6):1857–1865. 8, 15

Schreiber, T. (2000). Measuring information transfer. *Physical review letters*, 85(2):461. 3

Schubert, D., Kötter, R., and Staiger, J. F. (2007). Mapping functional connectivity in barrel-related columns reveals layer-and cell type-specific microcircuits. *Brain Structure and Function*, 212(2):107–119. 2

Siclari, F., Baird, B., Perogamvros, L., Bernardi, G., LaRocque, J. J., Riedner, B., Boly, M., Postle, B. R., and Tononi, G. (2017). The neural correlates of dreaming. *Nature neuroscience*, 20(6):872. 53, 58, 88, 89

Siclari, F., Bernardi, G., Cataldi, J., and Tononi, G. (2018). Dreaming in nrem sleep: a high-density eeg study of slow waves and spindles. *Journal of Neuroscience*, 38(43):9175–9185. 58, 88, 89

Siclari, F., Bernardi, G., Riedner, B. A., LaRocque, J. J., Benca, R. M., and Tononi, G. (2014). Two distinct synchronization processes in the transition to sleep: a high-density electroencephalographic study. *Sleep*, 37(10):1621–1637. 56, 60

Siclari, F., LaRocque, J. J., Postle, B. R., and Tononi, G. (2013). Assessing sleep consciousness within subjects using a serial awakening paradigm. *Frontiers in psychology*, 4:542. 58, 87, 137

Simor, P., van der Wijk, G., Gombos, F., and Kovacs, I. (2018). Sharpening the paradox of rem sleep: cortical oscillations, synchronization and topographical aspects during phasic and tonic rem microstates. In *JOURNAL OF SLEEP RESEARCH*, volume 27. WILEY 111 RIVER ST, HOBOKEN 07030-5774, NJ USA. 7, 15, 50

Singer, W. (1993). Synchronization of cortical activity and its putative role in information processing and learning. *Annual review of physiology*, 55(1):349–374. 3

Singh, S. P. (2014). Magnetoencephalography: basic principles. *Annals of Indian Academy of Neurology*, 17(Suppl 1):S107. 7

Sitt, J. D., King, J.-R., El Karoui, I., Rohaut, B., Faugeras, F., Gramfort, A., Cohen, L., Sigman, M., Dehaene, S., and Naccache, L. (2014). Large scale screening of neural signatures of consciousness in patients in a vegetative or minimally conscious state. *Brain*, 137(8):2258–2270. 8, 9, 10, 11, 12, 15, 17, 22, 50, 53, 54, 62

Sporns, O. (2007). Brain connectivity. *Scholarpedia*, 2(10):4695. 1

Sporns, O. (2011). The human connectome: a complex network. *Annals of the New York Academy of Sciences*, 1224(1):109–125. 1

Sporns, O. (2015). Cerebral cartography and connectomics. *Philosophical Transactions of the Royal Society B: Biological Sciences*, 370(1668):20140173. 2

Srinivasan, R., Winter, W. R., Ding, J., and Nunez, P. L. (2007). Eeg and meg coherence: measures of functional connectivity at distinct spatial scales of neocortical dynamics. *Journal of neuroscience methods*, 166(1):41–52. 7, 15

Stam, C. J. (2005). Nonlinear dynamical analysis of eeg and meg: review of an emerging field. *Clinical neurophysiology*, 116(10):2266–2301. 1, 50, 54

Stam, C. J., Nolte, G., and Daffertshofer, A. (2007). Phase lag index: assessment of functional connectivity from multi channel eeg and meg with diminished bias from common sources. *Human brain mapping*, 28(11):1178–1193. 8, 15

Theiler, J., Eubank, S., Longtin, A., Galdrikian, B., and Farmer, J. D. (1992). Testing for nonlinearity in time series: the method of surrogate data. *Physica D: Nonlinear Phenomena*, 58(1-4):77–94. 26

Theiler, J., Galdrikian, B., Longtin, A., Eubank, S., and Farmer, J. D. (1991). Using surrogate data to detect nonlinearity in time series. Technical report, Los Alamos National Lab., NM (United States). 26

Timme, N. M. and Lapish, C. (2018). A tutorial for information theory in neuroscience. *eNeuro*, 5(3). 4

Tomassini, V., Johansen-Berg, H., Jbabdi, S., Wise, R. G., Pozzilli, C., Palace, J., and Matthews, P. M. (2012a). Relating brain damage to brain plasticity in patients with multiple sclerosis. *Neurorehabilitation and neural repair*, 26(6):581–593. 92, 102

Tomassini, V., Matthews, P. M., Thompson, A. J., Fuglø, D., Geurts, J. J., Johansen-Berg, H., Jones, D. K., Rocca, M. A., Wise, R. G., Barkhof, F., et al. (2012b). Neuroplasticity and functional recovery in multiple sclerosis. *Nature Reviews Neurology*, 8(11):635. 92

Tononi, G. and Massimini, M. (2008). Why does consciousness fade in early sleep? *Annals of the New York Academy of Sciences*, 1129(1):330–334. 88

Tramonti, C., Imperatori, L. S., Fanciullacci, C., Lamola, G., Lettieri, G., Bernardi, G., Cecchetti, L., Ricciardi, E., and Chisari, C. (2018). Predictive value of eeg connectivity measures for motor training outcome in multiple sclerosis: an observational longitudinal study. *European journal of physical and rehabilitation medicine*. viii, 8, 10, 15, 50, 91

Van der Meer, M., Tewarie, P., Schoonheim, M., Douw, L., Barkhof, F., Polman, C., Stam, C., and Hillebrand, A. (2013). Cognition in ms correlates with resting-state oscillatory brain activity: An explorative meg source-space study. *NeuroImage: Clinical*, 2:727–734. 92

Vanhaudenhuyse, A., Demertzi, A., Schabus, M., Noirhomme, Q., Bredart, S., Boly, M., Phillips, C., Soddu, A., Luxen, A., Moonen, G., et al. (2011). Two distinct neuronal networks mediate the awareness of environment and of self. *Journal of cognitive neuroscience*, 23(3):570–578. 19, 33

Vanhaudenhuyse, A., Noirhomme, Q., Tshibanda, L. J.-F., Bruno, M.-A., Boveroux, P., Schnakers, C., Soddu, A., Perlbarg, V., Ledoux, D., Brichant, J.-F., et al. (2009). Default network connectivity reflects the level of consciousness in non-communicative brain-damaged patients. *Brain*, 133(1):161–171. 19, 33

Varela, F., Lachaux, J.-P., Rodriguez, E., and Martinerie, J. (2001). The brainweb: phase synchronization and large-scale integration. *Nature reviews neuroscience*, 2(4):229. 2

Vecchio, F., Miraglia, F., Gorgoni, M., Ferrara, M., Iberite, F., Bramanti, P., De Gennaro, L., and Rossini, P. M. (2017). Cortical connectivity modulation during sleep onset: a study via graph theory on eeg data. *Human brain mapping*, 38(11):5456–5464. 53, 57

Vinck, M., Oostenveld, R., Van Wingerden, M., Battaglia, F., and Pennartz, C. M. (2011). An improved index of phase-synchronization for electrophysiological data in the presence of volume-conduction, noise and sample-size bias. *Neuroimage*, 55(4):1548–1565. 7, 8, 11, 15, 16, 21, 22, 50, 57, 61, 62, 95

Wang, H. E., Bénar, C. G., Quilichini, P. P., Friston, K. J., Jirsa, V. K., and Bernard, C. (2014). A systematic framework for functional connectivity measures. *Frontiers in neuroscience*, 8:405. 21

West, T., Farmer, S., Berthouze, L., Jha, A., Beudel, M., Foltynie, T., Limousin, P., Zrinzo, L., Brown, P., and Litvak, V. (2016). The parkinsonian subthalamic network: measures of power, linear, and non-linear synchronization and their relationship to l-dopa treatment and off state motor severity. *Frontiers in human neuroscience*, 10:517. 11, 16

Williams, P. L. and Beer, R. D. (2010). Nonnegative decomposition of multivariate information. *arXiv preprint arXiv:1004.2515*. 67

Winkler, A. M., Ridgway, G. R., Webster, M. A., Smith, S. M., and Nichols, T. E. (2014). Permutation inference for the general linear model. *Neuroimage*, 92:381–397. 26

Xing, M., Tadayonnejad, R., MacNamara, A., Ajilore, O., DiGangi, J., Phan, K. L., Leow, A., and Klumpp, H. (2017). Resting-state theta band connectivity and graph analysis in generalized social anxiety disorder. *NeuroImage: Clinical*, 13:24–32. 8, 10, 15, 50

Zhong, J., Nantes, J. C., Holmes, S. A., Gallant, S., Narayanan, S., and Koski, L. (2016). Abnormal functional connectivity and cortical integrity influence dominant hand motor disability in multiple sclerosis: a multimodal analysis. *Human brain mapping*, 37(12):4262–4275. 92

Zoubek, L., Charbonnier, S., Lesecq, S., Buguet, A., and Chapotot, F. (2007). Feature selection for sleep/wake stages classification using data driven methods. *Biomedical Signal Processing and Control*, 2(3):171–179. 85

Appendices

Appendix A

Quantitative EEG analysis of Sleep and Wakefulness

A.1 Electroencephalography

It is currently not possible to measure non-invasively, in real time, the activity of individual neurons in human brains. The best approximation to this ideal situation is provided by intracranial recordings. However, this technique requires brain surgery and can therefore only be applied to patients with severe health conditions (e.g., epilepsy (Téllez-Zenteno et al., 2005)) that undergo brain surgery for the remediation of their conditions.

For research on large samples of healthy individuals, an alternative window into brain functioning is necessary. The voltage differences on the scalp resulting from the electrical communication among neurons in the brain have first been measured in 1924 by Hans Berger (Berger, 1929) on human participants. Models suggest that the EEG records postsynaptic potentials generated synchronously in cell assemblies (Da Silv, 2005).

Power and connectivity analyses can be computed directly on the signals recorded by individual scalp electrodes, i.e. in the sensor space, or in the source space, i.e. after the application of source reconstruction algorithms that can be used to estimate the location of brain sources underlying the EEG signal. While source reconstruction algorithms should

allow to make more specific inferences about brain dynamics, they are not always reliable (Schoffelen and Gross, 2009; Hassan et al., 2014), especially if no structural magnetic resonance imaging dataset is available to perform the mapping.

Magnetoencephalography (MEG) combines the great temporal resolution (millisecond-level) of EEG with a better spatial brain source resolution; however, its application involves greater practical difficulties, especially for the investigation of physiological stages of vigilance and also for the investigation of pathological conditions, as it requires remaining still and is not very comfortable for the patient/participant during an extended period of time. Moreover, MEG, as well as the functional imaging alternatives of functional magnetic resonance imaging (fMRI), and positron emission tomography (PET) are considerably costlier.

Therefore, the EEG provides an easy and efficient solution that can be used during sleep recordings and in pathological conditions.

A.2 Spectral Methods

The most prominent feature of the human scalp EEG is the presence of oscillations with peaks at specific frequencies. The canonical frequency bands historically used to describe the EEG are denoted by Greek letters: alpha (8-12 Hz), beta (13-30 Hz), gamma (above 30 Hz), delta (below 4 Hz), theta (4-7 Hz).

In sleep, the sigma band is especially relevant, as it tracks the occurrence and properties of sleep spindles (12-16 Hz). The exact source of each rhythms is not always fully clear and, sometimes, multiple unrelated sources produce rhythms of similar frequency which are difficult to disentangle (Sadaghiani and Kleinschmidt, 2016).

A.2.1 Spectral Power

A comprehensive picture of the spectral architecture of the EEG can be obtained using frequency decomposition algorithms such as the Fourier transform. The discrete Fourier transform produces the representation

of a signal from time domain to frequency domain by expressing it as a sum of sinusoids, thereby providing the power at N frequencies of interest: $s\left(f_k\right) = \sum_{i=0}^{N-1} s\left(t_i\right) e^{-j2\pi f_k t_i} \left(t_{i+1} - t_i\right), \quad k \in \{0, 1, \ldots, N-1\}$, where $s(t)$ is the waveform to be decomposed into a sum of sinusoids and $S(f)$ is the Fourier transform of $s(t)$.

The fast Fourier transform provides a computationally efficient algorithm for this purpose (Brigham, 1988). Notably, a disadvantage of the Fourier transform is that it requires a window of data, assumed to be generated by a stationary and linear system, to compute the power spectrum, thereby producing a temporal resolution inferior to that of the original signal.

A.2.2 Spectral Power in Distinct Stages of Vigilance

The alpha rhythm represents a typical marker of relaxed wakefulness observed most prominently over the posterior, especially occipital, areas of the scalp. In healthy adults, eye closing results in bursts of alpha waves easily visible in the EEG (Barry et al., 2007). Its origin is considered to be cortical; however, there is some debate on the functional meaning of the alpha rhythm (Klimesch, 2012; Niedermeyer et al., 2005).

As the subject becomes drowsy and approaches sleep, the alpha rhythm fades, while lower-frequency oscillations in theta and delta band appear in the EEG (Ogilvie, 2001).

Light sleep is characterized by the appearance of spindles in the sigma frequency (12-16 Hz) and K-complexes in the delta range (< 2 Hz). In deep sleep, slower frequency oscillations are present, including large-amplitude slow waves, which reflect a cyclical hyperpolarisation and depolarisation of the membrane potential in cortical neurons (Steriade et al., 1993a,b), also referred to as up and down states (Steriade et al., 2001).

Historically, spectral power is the most well-established method for analysing the EEG and extensive literature exists on its relationship with a wide range of cognitive processes and states (Hanslmayr et al., 2011; Klimesch, 2012).

However, as there are a plethora of interactions across the whole-brain network, analysing the power spectrum by itself is not satisfactory in the quest for understanding the neural correlates of complex physiological and pathological conditions.

A.3 Connectivity Metrics in Different Stages of Vigilance

A review of the literature has been performed to investigate how brain connectivity change between wakefulness and sleep, as well as between the different sleep stages. In spite of the different methodological approaches reported in the literature, some common aspects emerged. A detailed overview of the current research can be found in Table 3.

A.3.1 Overall Connectivity Differences

The findings that are most consistent across previous publications are as following.

The overall delta-connectivity is higher in NREM and REM sleep as compared to wakefulness, specifically inter-hemispheric (INTERH) connectivity. The same applies to to the theta band. However, the overall alpha-connectivity is higher in wakefulness as compared to all sleep stages.

While sigma-connectivity is higher in NREM-Sleep as compared to wakefulness, it has not been investigated in REM-Sleep as compared to wakefulness. However, there is higher inter- and intra-hemispheric sigma-connectivity in NREM-Sleep as compared to REM-Sleep. The highest beta-connectivity seems to occur in REM-Sleep as compared to NREM-Sleep. There are mixed results regarding differences in beta-connectivity between sleep stages as compared to wakefulness. Gamma-connectivity is higher in NREM-Sleep as compared to Wakefulness; however, there are also mixed results regarding the differences between REM- and NREM-Sleep.

Notably, many of the studies have a very small number of electrodes (e.g., < 10 channels (Achermann and Borbély, 1998; Guevara et al., 1995)), number of subjects and use coherence as a method of choice. The problem with coherence is its great sensitivity to volume conduction confounds.

At a local level, the thalamus (accompanied by several other brain regions throughout the cortex, the limbic lobe, the caudate nucleus, as well as midbrain structures, such as the mammillary body/hypothalamus) has been shown to have reduced activity during NREM sleep across all sleep stages (Kaufmann et al., 2005). Moreover, decreased thalamic activity was recorded at sleep onset (Kaufmann et al., 2005), temporally preceding the deactivation of the cortex (Magnin et al., 2010).

Using slow bold FC, thalamocortical connectivity has been shown to be sharply reduced in the transition from wakefulness to light sleep (Spoormaker et al., 2010). However, cortico-cortical connectivity was found to increase with a breakdown of cortico-cortical connectivity in Slow-Wave-Sleep (SWS). (Spoormaker et al., 2010). Both intra- and inter-hemispheric thalamic connectivity measured from functionally defined thalamic subdivisions strengthened during the progression into sleep. The largest increases have been shown during N2 sleep (especially in sensorimotor cortices) (Hale et al., 2016). The global thalamo-cortical connectivity has been shown to increase on awakening (Tsai et al., 2014).

Thalamocortical synchrony has been suggested to underlie global field synchronization, a metric that has been employed to find differences between stages of vigilance (Achermann et al., 2016) (see Table 3). Several studies point to altered thalamocortical FC during light sleep (Hale et al., 2016; Picchioni et al., 2014; Spoormaker et al., 2010).

In general, bivariate connectivity metrics such as coherence, wPLI and wSMI, are easier to understand, implement, visualise and to statistically quantify as compared to multivariate methods. Moreover, the most relevant types of connections for many cognitive functions are also bivariate (Cohen, 2014). However, if the network structure is actually multivariate, they can inflate or misrepresent estimates of relationships. Multivariate network analyses rely fundamentally on graph theory.

A.3.2 Graph-Theoretic Analyses

Theoretical Background

Graph theory attempts to answer the question how a system as a whole can emerge from the properties of its constituents. For example, it can enable us to understand how magnetism emerges from the collective behavior of millions of spins, or how quantum particles lead to phenomena as Bose-Einstein condensation or superfluidity (Albert and Barabási, 2002).

Graph theory defines the study of mathematical structures used to model pairwise relations between objects. A graph or network [1] is a collection of vertices or nodes connected by lines called edges or links. A graph may be undirected, meaning that there is no distinction between the two vertices associated with each edge, or it may be directed, which means that its edges are directed from one vertex to another. Nodes correspond to entities in a network and links to the connections between them.

In the graph-representation, nodes are all the same, whereas a weight (numerical value) can be assigned to each link of the network to make the model more realistic. Hence, the focus is on relationships between entities rather than the entities themselves.

[1] The term 'graph' is primarily used in mathematics and the term 'networks' predominantly in physics.

Network-Level Changes in Sleep

The overall network organization of the EEG slow-wave synchronization during sleep has been shown to feature characteristic of small-world networks (high average clustering coefficient combined with a low average-path-length) (Ferri et al., 2007). Moreover, all other sleep stages have been shown to demonstrate small-world organisation (Ferri et al., 2008).

There was increased neocortical connectivity as well as increased small-world properties on specific frequency bands (Dimitriadis et al., 2009; Ferri et al., 2007, 2008). Specifically anterior and posterior brain areas have been shown to become more isolated from one another during REM-Sleep (Dimitriadis et al., 2009).

Sleep deprivation is often used in experimental designs to learn more about the restorative effects of sleep. The alpha-clustering-coefficient (local integration) was decreased and theta-path-length (global integration) was increased in wakefulness after total sleep deprivation (Verweij et al., 2014).

Global network properties in the alpha, theta and gamma band have been demonstrated to move to a more random network after sleep deprivation compared to after sleep (Koenis et al., 2013).

Continued on next page

	Delta	Theta	Alpha	Sigma	Beta	Gamma	All
REM compared to wakefulness	higher INTERH correlations for slow (<0.1 Hz) fluctuations (Nir et al., 2008); higher INTERH correlation than W (Guevara et al., 1995)	higher INTERH correlation than W (Guevara et al., 1995)	Higher in wakefulness (wPLI (Simor et al., 2018); phase coherence (Voss et al., 2009); Highest global field synchronization wakefulness (Achermann et al., 2016); significant decrease in the fronto-occipital as well as in the inter-frontal coherence values in the alpha range (Cantero et al., 1999); higher inter- and INTRAH correlation in W (Corsi-Cabrera et al., 1996; Guevara et al., 1995)			INTERH coherence in cats only in wakefulness, no coherence in REM (Castro et al., 2014, 2013); coherence (30–48 and 52–100 Hz) smaller in REM than NREM and W in rats (Cavelli et al., 2015); decrease in correlation spectra (27–48 Hz, 2s epochs) INTRAH frontal-perceptual cortical ROIs in REM (Pérez-Garci et al., 2001); coherence decreases during REM compared with W; during lucid dreaming, coherence values are intermediate between W and REM sleep (Voss et al., 2009); increase in INTERH synchrony (Corsi-Cabrera et al., 2014; Pérez-Garci et al., 2001)	Highest global field synchronization in REM (Achermann et al., 2016)
REM: phasic vs. tonic		INTRAH WPLI in tonic REM higher for 5–6 Hz (Simor et al., 2018)	long-range inter- and INTRAH WPLI higher in tonic REM (Simor et al., 2018)	INTRAH WPLI in tonic REM higher for 13-16 Hz (Simor et al., 2018)	long-range inter- and INTRAH WPLI higher in tonic REM (Simor et al., 2018))	Short-range WPLI higher in phasic REM (frontal) (Simor et al., 2018)	low EEG synchronization for F7–F8 and T3–T4, especially in tonic REM sleep. (Landwehr and Jowaed, 2012)

NREM vs. Wakefulness	higher INTERH correlations during N2 for slow (<0.1 Hz) fluctuations (Nir et al., 2008); coherence between GP and fronto-central cortex and GP and parieto-occipital cortex (Salih et al., 2009); higher INTERH correlation for S2 and S4 than W (Guevara et al., 1995); nonlinear mechanisms (Terry et al., 2004); based on MI SWA propagated predominantly between adjacent cortical areas in EcoG recordings in focal epilepsy (Hangya et al., 2011)	FP wPLI peaks before and after LOR in N1/N2 (Comsa et al., 2019); higher INTERH correlation for S2 and S4 than W (Guevara et al., 1995)); parietal and fronto-parietal precedes behavioural microsleep (Toppi et al., 2012))	Highest global field synchronization in wakefulness (Achermann et al., 2016); Decrease in wPLI in N1/N2 (Comsa et al., 2019); coherent between fronto-central and parieto-occipital cortex in N3 (Salih et al., 2009)); Regional coherence during SWS is differentially distributed with a 14 Hz component in central and posterior regions and a 10 Hz component in frontal and central regions (Duckrow and Zaveri, 2005); higher INTRAH correlation for S2 and S4 than W (Guevara et al., 1995)	Highest global field synchronization in NREM (Achermann et al., 2016); lateralized left fronto-temporal network of positively correlated synchronous EEG potentials (Langheim et al., 2011)); coherence between GP and fronto-central cortex and GP and parieto-occipital cortex from 9.5 to 17 Hz in N2 and N3 (Salih et al., 2009); higher inter- and INTRAH correlation for S2 and S4 than W (Guevara et al., 1995); spherical harmonics in light sleep (Sivakumar et al., 2016)	Higher proportion of recurrent increases in synchronisation based on pointwise transinformation events during wakefulness, light sleep, and REM sleep than in SWS (Landwehr et al., 2014)	INTRAH coherence may be higher in SWS than W. (Pérez-Garci et al., 2001); hypercorrelated activity in NREM sleep (Bola et al., 2018)	Higher pointwise transinformation in N2 and N3 than in R, W, and N1. (Landwehr and Jowaed, 2012)); phase-amplitude coupling between spindles and broadband $> 20Hz$ activity, spindle-beta coupling greater during frontally defined up states relative to down states (Cox et al., 2014)
REM vs. NREM	Increased coherence in the low delta band in NREM (Achermann and Borbély, 1998)		Higher anterior INTERH in NREM (Achermann and Borbély, 1998); higher INTERr and INTRAr in NREM than REM (Guevara et al., 1995)	Higher INTRAH coherence in NREM (Achermann and Borbély, 1998); Higher inter- and INTRAH correlation in N2 vs REM (Corsi-Cabrera et al., 2003); higher INTERr and INTRAr in NREM than REM (Guevara et al., 1995)	Higher coherence in REM (Achermann and Borbély, 1998); Higher INTRAH corr in N2 vs REM, lower INTERH corr (Corsi-Cabrera et al., 2003))	No differences in coherence (Cantero et al., 2004); similar low inter-hemispheric homotopic coherence (Castro et al., 2014), reduction of rhinal-hippocampal coherence (Fell et al., 2003)	No difference in posterior INTERH coherence (Achermann and Borbély, 1998); mean INTERH coherence (delta, theta, alpha, beta) higher in stage 2, 4, REM than in W (Nielsen et al., 1990)

Table 3: Review on Connectivity in Wakefulness and Sleep

Appendix B

Metrics for the Study of Consciousness

B.1 Definition of Consciousness

Consciousness is probably one of the most difficult phenomena to clearly define - in a philosophical and scientific way. In the context of our everyday experience, we can define it as what is lost when we fall into a dreamless sleep and what returns when we wake up again (Searle, 1993; Seth, 2009).

There are differences in the level of consciousness, ranging from brain-death to alert wakefulness, and in the content of consciousness, referring to the composition of a given conscious scene at any non-zero conscious level (Seth, 2009). Conscious contents typically consist of phenomenal aspects ('qualia') such as perceptual experiences (e.g. 'redness'), bodily sensations (e.g. pain), emotional reactions (e.g. happiness) and moods (e.g. boredom; Haugeland (1985)). Morever, thoughts, inner speech, a sense of agency, self and a subjective first-person perspective on the world (the 'I') also represent conscious contents. The underlying idea is that the greater the conscious level, the greater the range of possible contents (Seth, 2009).

B.2 A Selection of Theories of Consciousness

There are many different theories that attempt to build an explanatory bridge between the subjective experience of consciousness and neural activity. Here, we focus on the two theories that are currently the most discussed in the scientific community: Dehaene's neuronal global workspace theory and Tononi's integrated information theory.

The global workspace theory (Baars, 1993) is based on the observation that consciousness encompasses a momentarily unified collection of information processed by specialised 'mental modules'. Highly-specialised modules perform different, intrinsically unconscious computations that can momentarily become part of the 'global workspace' and share information with other modules of the brain. We are then conscious of the globally shared content.

A neural implementation of the global workspace theory, the "neuronal global workspace", has been suggested by Dehaene et al. (2003). The underlying idea is that cortical areas, that code for certain contents of consciousness (e.g., sensory areas), "broadcast" their information in a global neuronal workspace that consists of highly recurrent frontoparietal areas, thereby making these contents globally available for use by other areas. The theory predicts that conscious awareness is a nonlinear function of stimulus salience; i.e., a gradual increase in stimulus visibility is accompanied by a sudden transition in conscious awareness.

Starting from phenomenology itself, e.g. the experience that every conscious scene is both integrated (i.e. experienced 'all of a piece') and differentiated (i.e. composed of many different parts and therefore one among a large number of possible experiences; Tononi (2004)), the integrated information theory (Oizumi et al., 2014; Tononi, 2004) attempts to bridge the gap between the first-person experience and the underlying causal mechanisms that can generate it.

It proposes a set of axioms that describe conscious experience, e.g. that it consists as a composition of multiple elements that are experienced at the same time, that it is informative due to its distinctiveness from any other possible experience, is integrated and irreducible to the

sum of its components, and exclusive of other simultaneous conscious experiences (Oizumi et al., 2014).

IIT proposes an information integration metric of consciousness called Φ, that is computed based on the causal structure of a system. Systems with $\Phi > 0$ are conscious, while a system with $\Phi = 0$ is unconscious. For example, Φ is always greater than zero in recurrent systems (they are always conscious) and always equal to zero in feedforward systems (they are never conscious; Oizumi et al. (2014)), as they do not generate cause and effect as a whole. [1]

In line with the idea of consciousness depending on the brain's ability to support complex activity patterns that are, at the same time, distributed among interacting cortical areas (integrated) and differentiated in space and time (information-rich), a practical proxy of Φ, the Perturbational Complexity Index (PCI; see Table 5), has been found to be low in coma, intermediate in minimally conscious states, and maximal during wakefulness (Casali et al., 2013).

B.3 How to quantify different levels of consciousness?

Differences in the level of consciousness are mostly studied by comparing conscious states with unconscious (or less conscious) states. Two very popular ways of studying the difference between consciousness and unconsciousness is through investigating the loss of consciousness induced by anaesthesia and the decrease in the level of consciousness induced by traumatic brain injuries in patients with disorders of consciousness (DoC).

One of the fundamental problems of considering patients with disorders of consciousness regarding testing the accuracy of different metrics of consciousness is that there is a misdiagnosis rate of almost 40% (Schnakers et al., 2009). Unfortunately, there is no standardized diagnos-

[1] However, different mathematical formulations of IIT's axioms lead to different predictions about which systems are conscious, and for each system that provides evidence for IIT, there are other possible systems that falsify it (Doerig et al., 2019).

tic tool for establishing the state of consciousness of a patient. One of the more advanced assessments in addition to the standard clinical examinations is based on the Coma Recovery Scale-Revised (CRS-R), that tests behavioural awareness in these patient. It is designed to find differences between patients that show reflexive responses only (UWS) and those who show a degree of awareness with/without command following (MCS-/MCS+ respectively). Any studies of consciousness in patients with disorders of consciousness suffer from the confound of lacking the knowledge of the ground-truth regarding which state any particular patient is in.

Another popular paradigm is the investigation of pharmacologically-induced differences in the level of consciousness due to anaesthesia. However, the mechanisms through which the extremely diverse group of general anaesthetics drugs (ranging from very potent intravenous anaesthetics, such as propofol, to less potent gaseous agents, such as nitrous oxide) cause reversible loss of consciousness are still not fully understood (Franks, 2008) and once in every $1000 - 2000$ operations a patient may temporarily regain consciousness or even remain conscious during surgery (Sebel et al., 2004). However, despite different mechanisms and sites of action, most anaesthetic agents seem to cause unconsciousness by targeting, directly or indirectly, a posterior lateral corticothalamic complex centered around the inferior parietal lobe, and potentially also a medial cortical core (Alkire et al., 2008).

The key confound for studying either pathologically-induced differences in consciousness or pharmacologically-induced differences in consciousness is that disconnection from the environment, unresponsiveness and unconsciousness are hard to separate from each other - within the same paradigm. In anaesthesia, we can experience the loss of consciousness as well as disconnected consciousness; however, these states are mostly induced by different anaesthetic agents, and anaesthesia is not promptly reversible. After undergoing ketamine anaesthesia, subjects mostly report vivid dream-like experiences consistent with disconnected consciousness, while in propofol anaesthesia most subjects experience a loss of consciousness (Darracq et al., 2018). During physiological sleep,

when we dream, we have vivid conscious experiences, but are unresponsive because inhibition by the brainstem induces muscle paralysis (Hobson et al., 2000), especially during REM-sleep, and we are disengaged from the external environment (Bonnet and Moore, 1982; Darracq et al., 2018; Nir and Tononi, 2010). Conscious sleep can be directly compared with wakefulness. Moreover, within the same sleep stage, we can compare connected consciousness with disconnected consciousness using a serial awakening paradigm (Siclari et al., 2013).

B.3.1 wPLI and wSMI in anaesthesia and DoC patients

wPLI and wSMI have both been suggested to allow the identification of variations in functional integration accompanying changes in the level of consciousness (Chennu et al., 2017, 2014, 2016; King et al., 2013; Lee et al., 2017a,b; Sitt et al., 2014). Both of them mostly represent metrics of integration, while wSMI has been especially designed in the context of Integrated Information Theory.

King and colleagues (King et al., 2013) found that wSMI connectivity between centro-posterior areas and other brain regions is higher in healthy conscious individuals as compared to patients with unresponsive wakefulness syndrome (UWS) or in a minimally conscious state (MCS).

Moreover, alpha-band wPLI-based functional networks differ between healthy individuals and patients with disorders of consciousness (UWS, MCS) (Chennu et al., 2017, 2014). In line with this, previous studies (Chennu et al., 2016; Lee et al., 2017b) also showed that propofol sedation in healthy individuals is associated with a decrease in alpha-band wPLI (Chennu et al., 2016) and a relative increase in delta-band wPLI connectivity (Lee et al., 2017b).

These observations across different conditions characterized by altered levels of consciousness are particularly interesting, as they suggest that wPLI and wSMI may offer general, relatively simple and reproducible indices of the current level of consciousness of an individual (Casali et al., 2013).

A review of the literature has been performed to identify differences in functional integration in conditions that are known to be associated with different levels of consciousness, i.e. in patients with disorders of consciousness (unresponsive wakefulness syndrome (UWS) vs. minimally conscious state (MCS)) and in anaesthesia (see Table 4).

A more general overview of several metrics that have been suggested to allow tracking changes in the level of consciousness can be found in Table 5.

Abbreviations: F: Frontal; P: Parietal; FP: Frontoparietal; UnC: Unconsciousness: CS; Conscious; RES: Responsiveness; TRANS: Transition; SAPD: Spatial Analytic Phase Difference

	Delta	Theta	Alpha	Sigma	Beta	Gamma	All
Unresponsive Wakefulness Syndrome/ Minimally Conscious State / (Severe Neurocognitive Disorder)		wPLI increased (Chennu et al., 2014); wSMI decreased mainly in P or AP (King et al., 2013; Sitt et al., 2014); higher frontal-to-posterior PLI and imaginary coherence in MCS as compared to UWS (Lehembre et al., 2012)	Decrease in FP-wPLI (Chennu et al., 2017); lower wSMI in VS as compared to MCS and CS patients (Sitt et al., 2014); higher PLI INTERH connectivity (Lehembre et al., 2012), richer GC for SND than MCS (Leon-Carrion et al., 2012)		Stronger GC from all areas to frontal region in SND vs. MCS (Pollonini et al., 2010), richer GC for SND than MCS (Leon-Carrion et al., 2012))		Reduced connectivity in MCS vs. SND, particularly of frontal regions from other regions (Pollonini et al., 2010)
Sedation / Anaesthesia compared to Wakefulness	Increased P and PF wPLI (Propofol/Midazolam) Lee et al. (2017a,b) ; drop in sub-delta band phase coherence (0.05-1.5 Hz) slow-wave coherence between frontal, occipital, and frontal-occipital electrode pairs (Wang et al., 2014); higher integrated information, higher average degree (wPLI) in anesthesia, lower number of modules (Kim et al., 2018) (Ketamine, Propofol)	SAPD increase (Murphy et al., 2011) (Propofol), Higher coherence in Propofol than baseline (Akeju et al., 2014); higher integrated information (Ketamine, Propofol), lower number of modules in anesthesia (Kim et al., 2018)	Decrease, especially in FP (PLI) and F-to-P (dPLI) (Blain-Moraes et al., 2014) (Ketamine); Decrease in wPLI (Chennu et al., 2016) (mild and moderate propofol sedation); SAPD increase (Murphy et al., 2011) (Propofol); Lower P wPLI (Lee et al., 2017a); Higher coherence in propofol than dexmedetomidine sedation and baseline (Akeju et al., 2014); lower integrated information, lower average degree (wPLI) in anesthesia, higher number of modules (Kim et al., 2018) (Ketamine, Propofol)	F-wPLI higher in UnC (Lee et al., 2017a,b); higher coherence in dexmedetomidine sedation than propofol or baseline) (Akeju et al., 2014)	High wPLI in transitions of RES over F, P, and FP (Lee et al., 2017b) (Propofol)	High wPLI in UnRES; higher during TRANS to RES than UnC (Lee et al., 2017b); hypercorrelated activity in Propofol anaesthesia (Bola et al., 2018); SAPD increase (Murphy et al., 2011)	Phase Lag Entropy reliably distinguished between consciousness and its loss in anaesthesia (8-30Hz; (Lee et al., 2017a); Decrease in coherence (John et al., 2001)

Table 4: Review on Connectivity in Anaesthesia and Disorders of Consciousness

Measures of Consciousness

General Overview

Key Considerations

Name	Functional or Effective (F/E)	Undirected or Directed (U/D)	Kind	Algorithm	Methodology	Preprocessing	Assumptions	Advantages	Limitations	References
wPLI	F	U	S-P	Weighted Phase Lag Index estimates, for a particular frequency, to what extent the phase leads and lags between signals from two sensors are not equiprobable, irrespective of the magnitude of the phase leads and lags, weighting the contribution of observed phase leads and lags by the magnitude of the imaginary component of the cross-spectrum.	EEG, LFP, MEG	Data has to be Fourier- or Hilbert-transformed.	Quasi-stationarity required ; Observed data modelled as linear mixture of source activities, assuming quasi-stationary description of the Maxwell equations for the EEG/MEG/LFP frequencies of interest; therefore not valid for order of kHz (spike-waveforms)	Comparatively reduced wPLI graph-theoretic network efficiency found in the alpha band in DoC patients as compared to healthy controls.		(Chennu et al., 2014; Vinck et al., 2011)
Spectral Coherence	F	U	S-F	Cross-spectral density divided by autospectral densities of two different electrodes; computed using nonparametric spectral estimation techniques, e.g. Fourier or wavelet transform.	EEG	Test for weak-sense stationarity; use single trial data such that detailed non-stationary interactions can be appropriately quantified.	Requirements of linearity and stationarity; assuming (weak-sense) stationarity means that the autocorrelation structure of a signal is not dependent on the reference time point.	Loss of gamma-band coherence has been reported to be associated with LOC; Well understood and studied, computationally fast, relatively robust against noise and allows an easy overview over relevant coherent frequencies in the data.	Can be increased during loss of consciousness induced by propofol anesthesia; spectral coherence sensitive to amplitude correlation values.	(John et al., 2002)

Abbreviations: S - Spectral; IT: Information-Theoretic; B - Baysian; P - Phase; F - Frequency; T - Time; Continued on next page

Approximate Entropy	F	U	IT-T	Quantify the amount of regularity and the unpredictability of fluctuations over time-series data	EEG	Choose vector length, filter factor, number of included data points of segment.	Stationarity required; High ApEN: random, unpredictable; Low ApEN: regular, predictable	Differences in different states of sleep can be computed using short data sets.	Tends to show group-level differences between specific conditions in which consciousness is absent or present, but is less reliable at detecting reproducible and graded changes.	(Burioka et al., 2005)
Bispectral Index	F	U	IT-T/F	The BIS index is based on the power distribution of the Fourier transform of the EEG signal, and quantifies the phase coupling between different EEG frequencies	EEG	Detrend epochs by mean, high-pass-filter and notch filter of 50Hz.	More suitable for the analysis of stationary signals; EEG is assumed to have multiple discrete oscillatory peaks.	One of the most popular EEG-based commercial monitor systems in hospitals.	Widely variable among subjects and anesthetic agents; no theoretical or mechanistic link proposed between neural network physiology in the cerebral cortex and the intrafrequency coupling notion of the BIS.	(Iselin-Chaves et al., 1998)
Complexity measures	F	U	IT-F	Lempel-Ziv Complexity, amplitude coalition entropy, synchrony coalition entropy. LZc counts the number of distinct patterns in the concatenated observations, or equivalently computes how incompressible the data matrix is, while ACE and SCE are based on the average surprise (entropy) of a single $nx1$ observation drawn at random from the matrix (n being the number of time series).	hdEEG	Reject channels with artefacts, remove electronic frequency artefacts, spatially filter by computing Surface Laplacian. Perform linear de-trending and baseline subtraction.	More suitable for the analysis of stationary signals	Robustly distinguish loss-of-consciousness (LOC) from wakeful resting (WR) on the broad-band signal, giving higher mean values for WR as compared to LOC across subjects. On analyses restricted to specific frequency bands, the discriminative power of the complexity measures is highest for low and high frequency bands (delta, beta, gamma), and lower for intermediate bands (theta, alpha). ACE and LZc can also discriminate mild sedation (MS) from WR.	LZc, SCE and ACE, when applied to multi-dimensional EEG recordings of brain activity, may only cautiously be considered to also correlate with integration in EEG dynamics, and therefore to track complexity in the sense of simultaneous differentiation and integration.	(Schartner et al., 2015)
wSMI	F	U	IT-T	Weighted symbolic mutual information evaluates the extent to which two EEG signals present nonrandom joint fluctuations, suggesting sharing of information.	hd-EEG		No stationarity required	wSMI increases with consciousness state, particularly across distant sites; distinguishes patients in vegetative state (VS), minimally conscious state (MCS), and conscious state (CS); observed regardless of etiology and delay since insult.	wSMI does not lead to reliable results for average referencing.	(King et al., 2013)

Abbreviations: S - Spectral; IT: Information-Theoretic; B - Baysian; P - Phase; F - Frequency; T - Time; Continued on next page

Perturbational complexity index (PCI)	E	U	IT-T	Perturb the cortex with TMS to engage distributed interactions in the brain (integration) and compress the spatiotemporal pattern of these electrocortical responses to measure their algorithmic complexity (information).	TMS-EEG	Identify primary sources by source modelling.	No stationarity in data required; however, perturbation must trigger significant response; Need to apply many TMS pulses to compute a single PCI value (relevant for minimally conscious patients in whom consciousness fluctuates over time or for the real-time monitoring of anesthesia).	Can be used to measure the level of consciousness in single individuals during wakefulness, sleep, and anesthesia, as well as in patients who had emerged from coma and recovered a minimal level of consciousness; Theoretical Foundation is Integrated Information Theory.	PCI values are comparable across different conditions such as slow-wave sleep, anaesthetic-induced unconsciousness and unresponsive wakefulness syndrome; although PCI does not depend on the cortical site of stimulation in healthy brains, it may be inaccurate in brain-injured patients when applied to a structurally damaged portion of the cortical surface.	(Casali et al., 2013)
Granger Causality	F	D	IT-T/F	A time series X is said to Granger-cause Y if X values provide statistically significant information about future values of Y.	EEG, source space EEG, fMRI	Needs to be modified for ERP-EEG.	Covariance stationary or window technique; Vulnerable to producing spurious results as a result of its linear interpretation, sensitivity to noise and band pass filtering and inaccurate inferences in cases where two signals are mutually influenced by a third independent source; Random fluctuations assumed to be serially independent (show no temporal correlations and fluctuate at very fast timescales), even if neuronal fluctuations in the brain are produced by neuronal systems that have the same time constants as the system studied	Granger causality can be applied directly to any given time series to detect the coupling among empirically sampled neuronal systems; useful in identifying distributed networks for subsequent analyses of effective connectivity; Granger causality can be used in source space (Brainstorm).	Need to specify a model for the signals and their interactions; can actually be increased during loss of consciousness induced by propofol anesthesia	(Friston, 2011; Nalatore et al., 2007)

Abbreviations: S - Spectral; IT: Information-Theoretic; B - Baysian; P - Phase; F - Frequency; T - Time; Continued on next page

Directed Transfer Function	F	D	IT-F	Frequency domain analog of the concept of Granger causality	EEG	Should be limited to subtraction of the mean, division by the variance and digital filtering. Filtering must not influence phases of signals, e.g. filter forward and backward (Matlab filtfilt). The signals should be referenced to a "neutral" derivation; Use linear inverse procedure to estimate current density waveforms in each ROI; Apply DTF to cortical waveforms related to the ROIs.	Quasi-stationary only required for short-time DTF. Requires a multivariate autoregressive model to be estimated simultaneously from all the time series.	Very robust to noise; perform quite well even in case of non-linear signals.	Decreased SNR and length impairs the accuracy of the connectivity pattern estimation obtained by the DTF; DTF performs significantly better in bivariate than multivariate case.	(Winterhalder et al., 2005)
Phase Slope Index	F	D	IT-P	If the speed at which different waves travel is similar, then the phase difference between sender and recipient increases with frequency, leading to a positive slope of the phase spectrum.	EEG	For estimating cross-spectral density, divide into epochs, use Hanning windows, Fourier-transform data.	No stationarity required; PSI indicates temporal order of two signals. For bidirectional coupling, A drives B does not imply B cannot have an impact on A.	Can estimate the direction of causal relations from time series' based on the phase slope of the cross-spectra; insensitive to arbitrary mixtures of independent source	Substantial intersubject variation, similar to alpha peak power.	(Nolte et al., 2008)

Abbreviations: S - Spectral; IT: Information-Theoretic; B - Baysian; P - Phase; F - Frequency; T - Time; Continued on next page

Transfer Entropy	F	D	IT-T	Transfer entropy is conditional mutual information, with the history of the influenced variable as condition.	EEG, MEG, fMRI, LFP		TE should only be used on data of sufficient length that show at most weak non-stationarities; TE may not accurately measure the underlying causal structure in all situations, as causal interactions can also serve the purposes of information storage and modification. Assume pairwise interactions, although a fully multivariate extension is possible.	Detect purely non-linear interactions in a model-free manner; robust for a wide distribution of interaction delays	No information on the type of interaction, i.e. TE analysis is difficult to interpret when signals have a different physical origin such as for example a chemical concentration and an electric field; high sensitivity for all types of depedencies between two time-series; susceptible to producing spurious results due to a source that mutually influences the signals of interest.	(Schreiber, 2000; Lindner et al., 2011)
Dynamic Causal Modelling	E	D	B-T	Bayesian model comparison procedure that rests on comparing models of how data were generated.	ERP-EEG, fMRI		Assuming linearity and stationarity model's biophysical parameters prescribe the cross-spectral density of responses. DCM assumes a bilinear state space model with nonlinear interactions and requires a priori knowledge about the underlying connectivity and comparisons of several competing models with respect to the observed data; Three sub-populations in each neuronal source (spiny stellate input cells, deep pyramidal output cells and inhibitory interneurons) with forward connections (targeting spiny stellate cells), backward connections (targeting pyramidal cells and inhibitory interneurons with slower kinetics) and lateral connections (targeting all subpopulations).	Biophysically plausible generative model of the measured data; in EEG-based DCM models will potentially allow the characterisation of receptor-specific contributions to brain connectivity (important in pharmacological and clinical settings)	DCM can currently not be implemented in spontaneous EEG recordings and requires prior knowledge of connectivity.	(Moran et al., 2009, 2011)

Table 5: Review on Suggested Metrics for Tracking Consciousness

Appendix C

The Application of Mutual Information in ECoG-Data

C.1 Introduction

I undertook this project during my Erasmus+ traineeship with Dr Robin Ince at the University of Glasgow.

This is a new analysis of electrocorticography (ECoG) data, that has already been used in a previous publication (Komatsu et al., 2015) and of unpublished ECoG data of a work that is currently in preparation.

The goal of our analysis was to find whether the changes between standard and deviant tones is marked by a difference across all frequencies in a broadband-manner or whether this was due to changes in particular oscillations.

In the predictive coding framework, the brain constantly generates and updates a mental model of sensory input. In each region of the neural sensory processing network, the propagated model is compared to the current sensory input. If they do not match, a prediction error is sent back up the network and the model is revised (Clark, 2013).

The underlying neural mechanisms of prediction error are typically studied by presenting a series of "standard" stimuli with intermittently occurring deviant stimuli, also called "oddballs", and by contrasting brain

responses between these stimuli categories (Lumaca et al., 2019). This way, event-related potentials (ERP) and a range of neural oscillations have been identified as neural markers of prediction error.

The most widely studied deviance ERP is auditory mismatch negativity (MMN) – a negative deflection of electrical event related potential recorded on the scalp or cortical surface using electrocorticography (ECoG) (Näätänen et al., 2007). MMN originates from the primary auditory cortex (Edwards et al., 2005), and it peaks around 150-200 ms in humans, whilst the peak latencies below 100 ms are typically reported in monkeys (Komatsu et al., 2015). In addition to MMN, prediction error responses are observed in neural oscillations in a variety of frequency ranges including theta (3-8 Hz), alpha (8-12 Hz), beta (14-30 Hz) and gamma (> 30 Hz) ranges (MacLean and Ward, 2014). Especially, Broadband High-frequency Activity (BHA; 70-150 Hz), also known as "high gamma" has been used to study neuronal population responses in auditory processes (Mesgarani and Chang, 2012; Tang et al., 2017). Here, we investigated whether all any frequency bands involved in the mismatch negativity response contain the overlapping or complementary information regarding the prediction error.

C.2 Methods

C.2.1 Experimental Model

Three adult male common marmosets (Callithrix jacchus) that weighed 320-380 g were included in this study. Monkeys were implanted with ECoG electrode array under general anaesthesia, and all efforts were made to minimize suffering. All surgical and experimental procedures were performed in accordance with the National Institutes of Health Guidelines for the Care and Use of Laboratory Animals and approved by the RIKEN Ethical Committee (No. H26-2-202).

C.2.2 ECoG arrays

Chronically implanted, customized multichannel ECoG electrode arrays (Cir-Tech Inc., Japan) were used for neural recordings (Komatsu et al., 2017, 2015). One monkey had 32 implanted electrodes in the epidural space of the the left hemisphere (monkey Fr), while the other two monkeys had 64 implanted electrodes (the right hemispheres of monkey Go and Kr) in the epidural space. In all monkeys, the electrode-array covered the frontal, parietal, occipital, and temporal cortices, including the primary auditory area.

C.2.3 Stimuli and task

Based on a roving oddball paradigm (Cowan et al., 1993), trains of 3, 5, or 11 repetitive single-tones of 20 different frequencies (250–6727 Hz with intervals of 1/4 octave) were pseudo-randomly presented.

Tones were identical within each tone-train, but differed between tone-trains. Because tone-trains followed on from one another continuously, the first tone of a train was considered to be an unexpected deviant tone, because it was of a different frequency from that of the preceding train. The final tone was considered to be an expected standard tone, because it was preceded by several repetitions of this same tone.

To avoid analytical artefacts stemming from differences in the number of standard and deviant stimuli, only the last tone of a train was considered as standard.

Standards and deviants were presented 240 times in a single recording session. Pure sinusoidal tones lasted 64 ms (7 ms rise/fall), and stimulus onset asynchrony was 503 ms. Stimulus presentation was controlled by MATLAB (MathWorks Inc., Natick, MA, USA) using the Psychophysics Toolbox extensions (Pelli and Vision, 1997). Tones were presented through two audio speakers (Fostex, Japan) with an average intensity of 60 dB SPL around the animal's ear.

C.2.4 ECoG recording and preprocessing

ECoG recordings were taken in the passive listening condition while monkeys were awake. In each recording session, the monkey Fr was held in a drawstring pouch, which was stabilized in a dark room, and the monkeys Go and Kr sat on a primate chair in a dimly lit room.

The length of a single session was about 15min: the first 3min of data were used for many standard stimuli and the remaining 12min of data were used for the roving oddball sequences. For monkey Fr, data from 3 sessions were used for analysis, which resulted in 720 (=240 × 3) standard and deviant presentations.

For monkeys Go and Kr, data from 6 sessions were used for analysis, which resulted in 1440 (=240 × 6) standard and deviant presentations. ECoG signals were recorded at a sampling rate of 1kHz per channel. In the signal preprocessing, those signals were re-referenced using an average reference montage, and high-pass filtered above $1Hz$. Datasets were segmented from -903 to 400ms relative to the onset of the unexpected tone, so that each segment would include a pair of a deviant and a standard immediately preceding the deviant, as well as a baseline of 400ms preceding the standard tone.

The segments were then divided into standard epochs and deviant epochs (-400 ms to 400ms). Parts of the dataset are shared in the public server Neurotycho.org (http://neurotycho.org/; (Nagasaka et al., 2011)). ECoG electrode-of-interested was identified functionally by contrastic time frequency charts between standard and deviant stimuli (0-350 ms), separately for each electrode.

Hilbert transforms were applied every 10 Hz and z-scored with respect to the baseline period (-100 ms to 0 ms). One electrode with the largest high-gamma difference between the standard and deviant tones (MacLean and Ward, 2014) was selected for each monkey for further analyses. In all three monkeys, the selected electrode-of-interest was located in the auditory cortex.

C.2.5 Mutual Information Analysis

Stockwell-Transform

The recorded ECoG data from the channel best representing the auditory cortex in each individual monkey was transformed in time-frequency-space using Stockwell transforms (Stockwell, 2007).

The filter is a Gaussian window function in frequency domain. Therefore, when the input frequency is low, it has a better clarity in the frequency as compared to the time domain, while when the input frequency is high, it has a better clarity in the time domain as compared to the frequency domain.

Binned Mutual Information

The binned mutual information (MI, NBin=2; NBin = number of bins) that each frequency bin contains regarding the difference between standard and deviant tones was computed across all available trials for each monkey and for each individual time point.

Redundancy Analysis

To find the redundancy between different frequencies with respect to each other (frequency-frequency redundancy), two different information-theoretic frameworks were used: a) II or Co-Information (Bell, 2003; McGill, 1954) and b) partial information decomposition (PID) analysis (Allen et al., 2017; James et al., 2018).

The time-point of interest selected here was obtained based on computing the maximum possible mean information content across all pairs of frequencies.

Explanation C.2.1: Interaction Information

Co-Information or Interaction Information answers the question whether the joint information between any two variables X_1 and X_2 and a third variable Y, specifically $I(\{X_1, X_2\}, Y)$, is greater or smaller than the information that any variable contains about Y individually, e.g. $I(\{X_1\}, Y)$. Mathematically, this is experessed as following:

$$II = I(\{X_1, X_2\}; Y) - (I(X_1; Y) + I(X_2; Y)), \tag{C.1}$$

where $I(X_1, Y)$ represents the information that X_1 contains about Y and $I(\{X_1, X_2\}, Y)$ represents the joint information that X_1 and X_2 contain about Y. If the co-information is positive, this implies that X_1 and X_2 contain more information about Y, when they are considered together as compared to individually (**synergy**). If the co-information is negative, X_1 and X_2 share overlapping information about Y (**redundancy**).
However, it is not clear how much more/less information they contain together as compared to individually due to the phenomenon of redundancy-synergy cancelling (Chicharro et al., 2018).

Explanation C.2.2: Partial Information Decomposition

Based on considering the joint information $I(\{X_1, X_2\}, Y)$, partial information decomposition allows us to disentangle the following questions from each other:

- what information overlap about Y exists between X_1 and X_2 (**redundancy**, $R(X_1, X_2; Y)$),
- what information does X_1 provide about Y, that X_2 does not, and vice versa (**unique information**, $U1(X_1, X_2; Y)$, $U2(X_1, X_2; Y)$),
- what additional information do X_1 and X_2 provide about Y when both are known simultaneously (**synergy**, $S(X_1, X_2; Y)$).

$$I(\{X_1, X_2\}; Y) = S(X_1, X_2; Y) + R(X_1, X_2; Y) + U1(X_1, X_2; Y) + U2(X_1, X_2; Y) \tag{C.2}$$

$$I(X_1, Y) = R(X_1, X_2; Y) + U1(X_1, X_2; Y) \tag{C.3}$$

$$I(X_2, Y) = R(X_1, X_2; Y) + U2(X_1, X_2; Y) \tag{C.4}$$

While the mutual information (MI) expressions in eqs. (C.2) to (C.4) can be calculated within the standard mutual information framework, it is not possible to derive mathematical expressions for the synergy, redundancy, and unique information without any further measures (Timme and Lapish, 2018).
Several candidate measures for redundancy have been proposed. Here, we used a metric of redundancy that quantifies the common change in surprisal shared between variables at the local or pointwise level (Ince, 2017) in the dit package in Python (Allen et al., 2017; James et al., 2018).

C.3 Results

A clear pattern of frequency redundancy above $70Hz$ can be observed for all three monkeys. While co-information shows different clusters of redundancy (figs. 26, 28 and 30), PID shows most of the oddball response is marked by redundancy in the Broadband High-frequency Activity (figs. 27, 29 and 31).

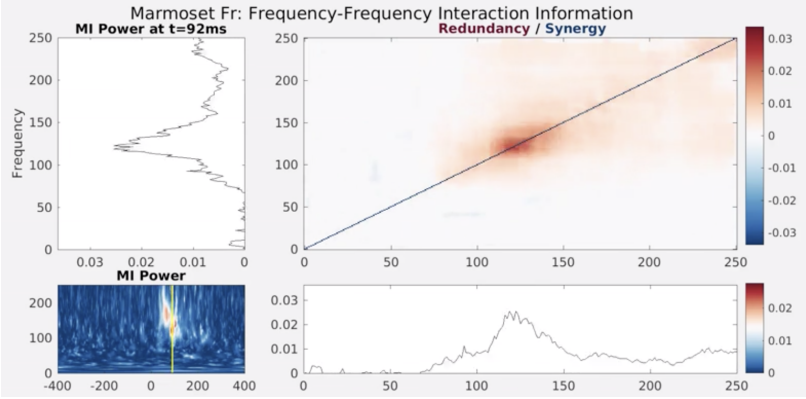

Figure 26: The top right plot shows the inverse of the Interaction Information between any two frequencies (x- and y-axis) for Monkey Fr. Positive values are shown in red and represent redundancy, while negative values are shown in blue and represent synergy. The top left and bottom right plot show the individual frequency-resolved mutual information of the oddball response, while the bottom left plot shows the time-frequency resolution of the mutual information computed on the spectral power during the whole trial (-400ms to 400ms). Here, 0 along the x-axis marks the onset of the stimulus and the associated color bar is at the bottom right. Higher values are shown in red and lower values are shown in blue. Videos of the changes occurring during the whole trial are available on request.

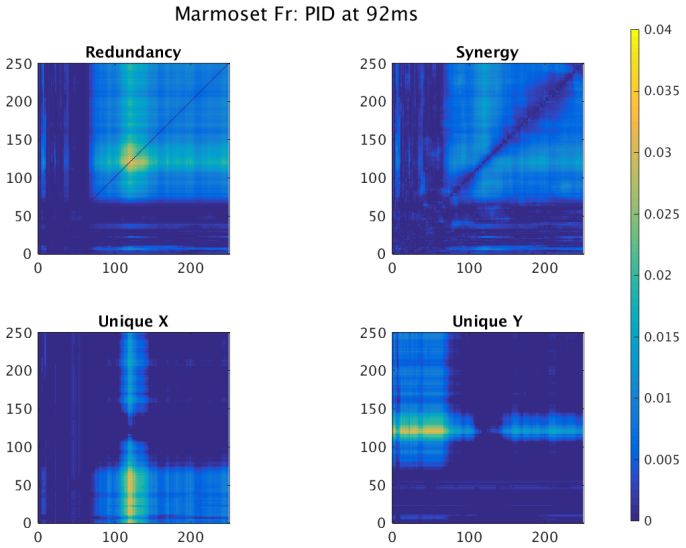

Figure 27: Partial Information Decomposition between any two frequency bins (x- and y-axis) for Monkey Fr. The redundancy, synergy as well as the unique information for X and Y are shown for the interactions between all pairs of frequencies. Videos of the changes occurring during the whole trial are available on request.

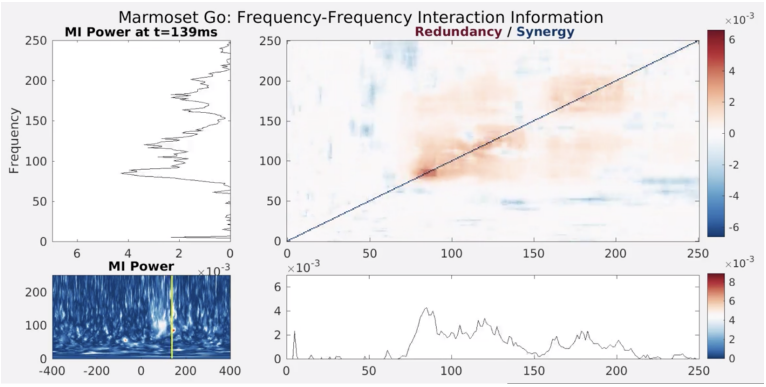

Figure 28: Interaction Information between all pairs of frequencies for Monkey Go. A detailed explanation of the subplots can be found in the caption of Figure 26.

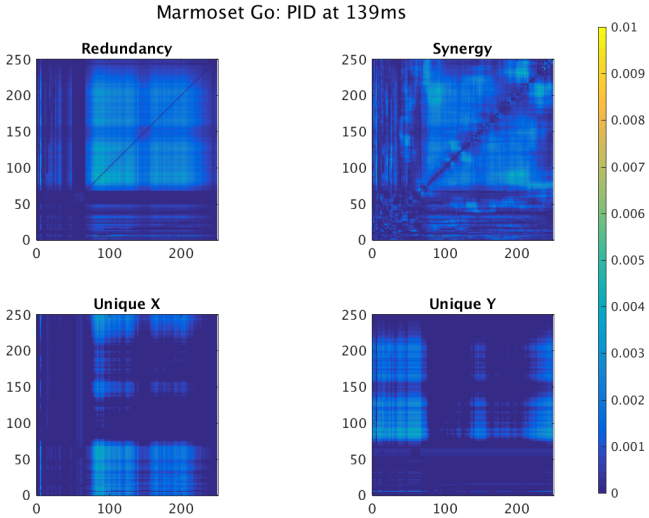

Figure 29: Partial Information Decomposition of Frequencies for Monkey Go. A detailed explanation of the subplots can be found in the caption of Figure 27.

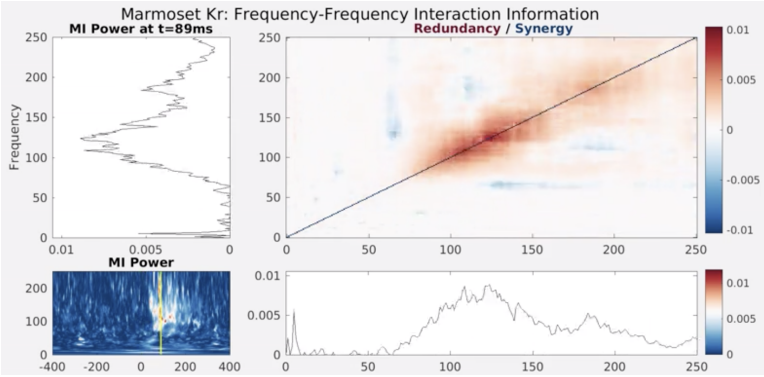

Figure 30: Interaction Information between all pairs of frequencies for Monkey Kr. A detailed explanation of the subplots can be found in the caption of Figure 26.

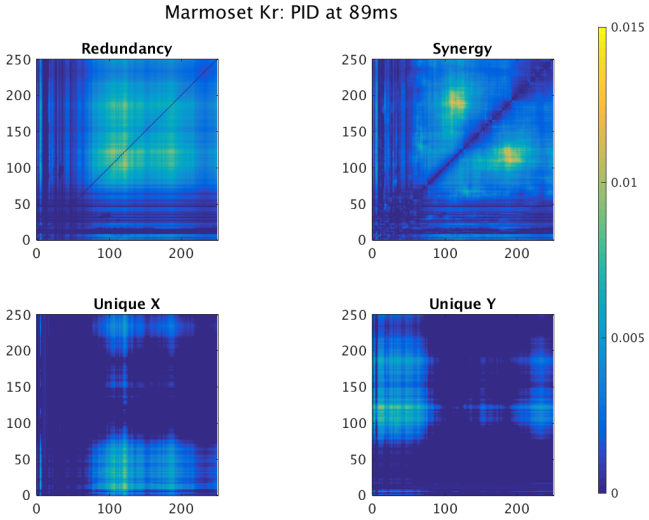

Figure 31: Partial Information Decomposition for all pairs of frequencies for Monkey Kr. A detailed explanation of the subplots can be found in the caption of Figure 27.

C.4 Conclusions

This study represents the first time partial information decomposition analysis has been applied in the frequency domain.

Interestingly, PID reveals a different perspective to co-information. While co-information shows different clusters of redundancy, PID shows most of the oddball response is marked by redundancy in the broadband high-frequency activity (BHA). From a methodological point of view, this finding shows that redundacy-synergy cancellation is possible (Chicharro et al., 2018). From a physiological point of view, it shows that the activity at all frequencies in the BHA-range is not only co-occurring at the same time, but also redundant with itself. Future studies should test whether this redundancy effect in the high frequencies is limited to the auditory cortex or whether it represents a whole-brain effect.

References of Appendices

Achermann, P. and Borbély, A. (1998). Temporal evolution of coherence and power in the human sleep electroencephalogram. *Journal of sleep research*, 7(S1):36–41.

Achermann, P., Rusterholz, T., Dürr, R., König, T., and Tarokh, L. (2016). Global field synchronization reveals rapid eye movement sleep as most synchronized brain state in the human eeg. *Royal Society open science*, 3(10):160201.

Akeju, O., Westover, M. B., Pavone, K. J., Sampson, A. L., Hartnack, K. E., Brown, E. N., and Purdon, P. L. (2014). Effects of sevoflurane and propofol on frontal electroencephalogram power and coherence. *Anesthesiology: The Journal of the American Society of Anesthesiologists*, 121(5):990–998.

Albert, R. and Barabási, A.-L. (2002). Statistical mechanics of complex networks. *Reviews of modern physics*, 74(1):47.

Alkire, M. T., Hudetz, A. G., and Tononi, G. (2008). Consciousness and anesthesia. *Science*, 322(5903):876–880.

Allen, B., Stacey, B., and Bar-Yam, Y. (2017). Multiscale information theory and the marginal utility of information. *Entropy*, 19(6):273. 81

Baars, B. J. (1993). *A cognitive theory of consciousness*. Cambridge University Press.

Barry, R. J., Clarke, A. R., Johnstone, S. J., Magee, C. A., and Rushby, J. A. (2007). Eeg differences between eyes-closed and eyes-open resting conditions. *Clinical Neurophysiology*, 118(12):2765–2773.

Bell, A. J. (2003). The co-information lattice. In *Proceedings of the Fifth International Workshop on Independent Component Analysis and Blind Signal Separation: ICA*, volume 2003.

Berger, H. (1929). Über das elektrenkephalogramm des menschen. *European archives of psychiatry and clinical neuroscience*, 87(1):527–570.

Blain-Moraes, S., Lee, U., Ku, S., Noh, G., and Mashour, G. A. (2014). Electroencephalographic effects of ketamine on power, cross-frequency coupling, and connectivity in the alpha bandwidth. *Frontiers in systems neuroscience*, 8:114. 19, 53, 87

Bola, M., Barrett, A. B., Pigorini, A., Nobili, L., Seth, A. K., and Marchewka, A. (2018). Loss of consciousness is related to hyper-correlated gamma-band activity in anesthetized macaques and sleeping humans. *NeuroImage*, 167:130–142.

Brigham, E. O. (1988). 6 the discrete fourier transform. *The fast Fourier transform and its applications*.

Burioka, N., Miyata, M., Cornélissen, G., Halberg, F., Takeshima, T., Kaplan, D. T., Suyama, H., Endo, M., Maegaki, Y., Nomura, T., et al. (2005). Approximate entropy in the electroencephalogram during wake and sleep. *Clinical EEG and neuroscience*, 36(1):21–24.

Cantero, J. L., Atienza, M., Madsen, J. R., and Stickgold, R. (2004). Gamma eeg dynamics in neocortex and hippocampus during human wakefulness and sleep. *Neuroimage*, 22(3):1271–1280.

Cantero, J. L., Atienza, M., Salas, R. M., and Gómez, C. M. (1999). Alpha eeg coherence in different brain states: an electrophysiological index of the arousal level in human subjects. *Neuroscience Letters*, 271(3):167–170.

Casali, A. G., Gosseries, O., Rosanova, M., Boly, M., Sarasso, S., Casali, K. R., Casarotto, S., Bruno, M.-A., Laureys, S., Tononi, G., et al. (2013). A theoretically based index of consciousness independent of sensory processing and behavior. *Science translational medicine*, 5(198):198ra105–198ra105. 11, 16

Castro, S., Cavelli, M., Vollono, P., Chase, M. H., Falconi, A., and Torterolo, P. (2014). Inter-hemispheric coherence of neocortical gamma oscillations during sleep and wakefulness. *Neuroscience letters*, 578:197–202.

Castro, S., Falconi, A., Chase, M. H., and Torterolo, P. (2013). Coherent neocortical 40-hz oscillations are not present during rem sleep. *European Journal of Neuroscience*, 37(8):1330–1339.

Cavelli, M., Castro, S., Schwarzkopf, N., Chase, M. H., Falconi, A., and Torterolo, P. (2015). Coherent neocortical gamma oscillations decrease during rem sleep in the rat. *Behavioural brain research*, 281:318–325.

Chennu, S., Annen, J., Wannez, S., Thibaut, A., Chatelle, C., Cassol, H., Martens, G., Schnakers, C., Gosseries, O., Menon, D., et al. (2017). Brain networks predict metabolism, diagnosis and prognosis at the bedside in disorders of consciousness. *Brain*, 140(8):2120–2132. 7, 10, 11, 12, 15, 16, 17, 50, 54

Chennu, S., Finoia, P., Kamau, E., Allanson, J., Williams, G. B., Monti, M. M., Noreika, V., Arnatkeviciute, A., Canales-Johnson, A., Olivares, F., et al. (2014). Spectral signatures of reorganised brain networks in disorders of consciousness. *PLoS computational biology*, 10(10):e1003887. 7, 10, 11, 12, 15, 16, 17, 50, 53, 54, 58, 85, 87

Chennu, S., OâĂŹConnor, S., Adapa, R., Menon, D. K., and Bekinschtein, T. A. (2016). Brain connectivity dissociates responsiveness from drug exposure during propofol-induced transitions of consciousness. *PLoS computational biology*, 12(1):e1004669. 7, 10, 11, 12, 15, 16, 17, 19, 50, 53, 58, 87

Chicharro, D., Pica, G., and Panzeri, S. (2018). The identity of information: how deterministic dependencies constrain information synergy and redundancy. *Entropy*, 20(3):169.

Clark, A. (2013). Whatever next? predictive brains, situated agents, and the future of cognitive science. *Behavioral and brain sciences*, 36(3):181–204.

Cohen, M. X. (2014). *Analyzing neural time series data: theory and practice*. MIT press. 3, 4, 6, 7, 32, 61

Comsa, I. M., Bekinschtein, T. A., and Chennu, S. (2019). Transient topographical dynamics of the electroencephalogram predict brain connectivity and behavioural responsiveness during drowsiness. *Brain topography*, 32(2):315–331. 7, 12, 15, 17, 19, 50, 53, 87

Corsi-Cabrera, M., Guevara, M. A., Arce, C., and Ramos, J. (1996). Inter and intrahemispheric eeg correlation as a function of sleep cycles. *Progress in Neuro-Psychopharmacology and Biological Psychiatry*, 20(3):387–405.

Corsi-Cabrera, M., Miró, E., del Rıo-Portilla, Y., Pérez-Garci, E., Villanueva, Y., and Guevara, M. (2003). Rapid eye movement sleep dreaming is characterized by uncoupled eeg activity between frontal and perceptual cortical regions. *Brain and Cognition*, 51(3):337–345.

Corsi-Cabrera, M., Sifuentes-Ortega, R., Rosales-Lagarde, A., Rojas-Ramos, O., and Del Río-Portilla, Y. (2014). Enhanced synchronization of gamma activity between frontal lobes during rem sleep as a function of rem sleep deprivation in man. *Experimental brain research*, 232(5):1497–1508.

Cowan, N., Winkler, I., Teder, W., and Näätänen, R. (1993). Memory prerequisites of mismatch negativity in the auditory event-related potential (erp). *Journal of Experimental Psychology: Learning, Memory, and Cognition*, 19(4):909.

Cox, R., van Driel, J., de Boer, M., and Talamini, L. M. (2014). Slow oscillations during sleep coordinate interregional communication in cortical networks. *Journal of Neuroscience*, 34(50):16890–16901.

Da Silv, F. L. (2005). *Electroencephalography: basic principles, clinical applications, and related fields*. Lippencott Wlliams & Wilkins.

Dehaene, S., Sergent, C., and Changeux, J.-P. (2003). A neuronal network model linking subjective reports and objective physiological data during conscious perception. *Proceedings of the National Academy of Sciences*, 100(14):8520–8525.

Dimitriadis, S. I., Laskaris, N. A., Del Rio-Portilla, Y., and Koudounis, G. C. (2009). Characterizing dynamic functional connectivity across sleep stages from eeg. *Brain topography*, 22(2):119–133.

Doerig, A., Schurger, A., Hess, K., and Herzog, M. H. (2019). The unfolding argument: Why iit and other causal structure theories cannot explain consciousness. *Consciousness and cognition*, 72:49–59.

Duckrow, R. and Zaveri, H. (2005). Coherence of the electroencephalogram during the first sleep cycle. *Clinical neurophysiology*, 116(5):1088–1095.

Edwards, E., Soltani, M., Deouell, L. Y., Berger, M. S., and Knight, R. T. (2005). High gamma activity in response to deviant auditory stimuli recorded directly from human cortex. *Journal of neurophysiology*, 94(6):4269–4280.

Fell, J., Staedtgen, M., Burr, W., Kockelmann, E., Helmstaedter, C., Schaller, C., Elger, C. E., and Fernández, G. (2003). Rhinal–hippocampal eeg coherence is reduced during human sleep. *European Journal of Neuroscience*, 18(6):1711–1716.

Ferri, R., Rundo, F., Bruni, O., Terzano, M. G., and Stam, C. J. (2007). Small-world network organization of functional connectivity of eeg slow-wave activity during sleep. *Clinical neurophysiology*, 118(2):449–456.

Ferri, R., Rundo, F., Bruni, O., Terzano, M. G., and Stam, C. J. (2008). The functional connectivity of different eeg bands moves towards small-world network organization during sleep. *Clinical Neurophysiology*, 119(9):2026–2036.

Franks, N. P. (2008). General anaesthesia: from molecular targets to neuronal pathways of sleep and arousal. *Nature Reviews Neuroscience*, 9(5):370–386.

Friston, K. J. (2011). Functional and effective connectivity: a review. *Brain connectivity*, 1(1):13–36.

Guevara, M., Lorenzo, I., Arce, C., Ramos, J., and Corsi-Cabrera, M. (1995). Inter- and intrahemispheric eeg correlation during sleep and wakefulness. *Sleep*, 18(4):257–265.

Hale, J. R., White, T. P., Mayhew, S. D., Wilson, R. S., Rollings, D. T., Khalsa, S., Arvanitis, T. N., and Bagshaw, A. P. (2016). Altered thalamocortical and intra-thalamic functional connectivity during light sleep compared with wake. *NeuroImage*, 125:657–667.

Hangya, B., Tihanyi, B. T., Entz, L., Fabó, D., Eróss, L., Wittner, L., Jakus, R., Varga, V., Freund, T. F., and Ulbert, I. (2011). Complex propagation patterns characterize human cortical activity during slow-wave sleep. *Journal of Neuroscience*, 31(24):8770–8779.

Hanslmayr, S., Gross, J., Klimesch, W., and Shapiro, K. L. (2011). The role of alpha oscillations in temporal attention. *Brain research reviews*, 67(1-2):331–343.

Hassan, M., Dufor, O., Merlet, I., Berrou, C., and Wendling, F. (2014). Eeg source connectivity analysis: from dense array recordings to brain networks. *PloS one*, 9(8):e105041.

Haugeland, J. (1985). Artificial intelligence: The very idea, cambridge, ma, bradford.

Hobson, J. A., Pace-Schott, E. F., and Stickgold, R. (2000). Dreaming and the brain: toward a cognitive neuroscience of conscious states. *Behavioral and brain sciences*, 23(6):793–842.

Ince, R. (2017). Measuring multivariate redundant information with pointwise common change in surprisal. *Entropy*, 19(7):318.

Iselin-Chaves, I. A., Flaishon, R., Sebel, P. S., Howell, S., Gan, T. J., Sigl, J., Ginsberg, B., and Glass, P. S. (1998). The effect of the interaction of propofol and alfentanil on recall, loss of consciousness, and the bispectral index. *Anesthesia & Analgesia*, 87(4):949–955.

James, R. G., Ellison, C. J., and Crutchfield, J. P. (2018). dit: a python package for discrete information theory. *J. Open Source Software*, 3(25):738. 81

John, E., Prichep, L., Kox, W., Valdés-Sosa, P., Bosch-Bayard, J., Aubert, E., Tom, M., diMichele, F., and Gugino, L. (2002). Invariant reversible qeeg effects of anesthetics. *Consciousness and Cognition*, 11(1):138–138.

John, E., Prichep, L., Kox, W., Valdes-Sosa, P., Bosch-Bayard, J., Aubert, E., Tom, M., Gugino, L., et al. (2001). Invariant reversible qeeg effects of anesthetics. *Consciousness and cognition*, 10(2):165–183.

Kaufmann, C., Wehrle, R., Wetter, T., Holsboer, F., Auer, D., Pollmächer, T., and Czisch, M. (2005). Brain activation and hypothalamic functional connectivity during human non-rapid eye movement sleep: an eeg/fmri study. *Brain*, 129(3):655–667.

Kim, H., Hudetz, A. G., Lee, J., Mashour, G. A., Lee, U., Avidan, M. S., Bel-Bahar, T., Blain-Moraes, S., Golmirzaie, G., Janke, E., et al. (2018). Estimating the integrated information measure phi from high-density electroencephalography during states of consciousness in humans. *Frontiers in human neuroscience*, 12:42.

King, J.-R., Sitt, J. D., Faugeras, F., Rohaut, B., El Karoui, I., Cohen, L., Naccache, L., and Dehaene, S. (2013). Information sharing in the brain indexes consciousness in noncommunicative patients. *Current Biology*, 23(19):1914–1919. 7, 8, 9, 10, 11, 12, 15, 16, 17, 21, 22, 50, 53, 54, 57, 58, 61, 62, 95

Klimesch, W. (2012). Alpha-band oscillations, attention, and controlled access to stored information. *Trends in cognitive sciences*, 16(12):606–617.

Koenis, M. M., Romeijn, N., Piantoni, G., Verweij, I., Van der Werf, Y. D., Van Someren, E. J., and Stam, C. J. (2013). Does sleep restore the topology of functional brain networks? *Human brain mapping*, 34(2):487–500.

Komatsu, M., Sugano, E., Tomita, H., and Fujii, N. (2017). A chronically implantable bidirectional neural interface for non-human primates. *Frontiers in neuroscience*, 11:514.

Komatsu, M., Takaura, K., and Fujii, N. (2015). Mismatch negativity in common marmosets: whole-cortical recordings with multi-channel electrocorticograms. *Scientific reports*, 5:15006.

Landwehr, R. and Jowaed, A. (2012). Pointwise transinformation distinguishes a recurrent increase of synchronization in the rapid eye movement sleep electroencephalogram. *Journal of Clinical Neurophysiology*, 29(1):76–83.

Landwehr, R., Volpert, A., and Jowaed, A. (2014). A recurrent increase of synchronization in the eeg continues from waking throughout nrem and rem sleep. *ISRN neuroscience*, 2014.

Langheim, F. J., Murphy, M., Riedner, B. A., and Tononi, G. (2011). Functional connectivity in slow-wave sleep: identification of synchronous cortical activity during wakefulness and sleep using time series analysis of electroencephalographic data. *Journal of sleep research*, 20(4):496–505. 57

Lee, M., Sanders, R. D., Yeom, S.-K., Won, D.-O., Kim, H.-J., Lee, B.-R., Seo, K.-S., Kim, H. J., Tononi, G., and Lee, S.-W. (2017a). Change in functional networks for transitions between states of consciousness during midazolam-induced sedation. In *2017 39th Annual International Conference of the IEEE Engineering in Medicine and Biology Society (EMBC)*, pages 958–961. IEEE. 7, 10, 11, 12, 15, 17, 50, 53, 54, 58, 85, 87, 139

Lee, M., Sanders, R. D., Yeom, S.-K., Won, D.-O., Seo, K.-S., Kim, H. J., Tononi, G., and Lee, S.-W. (2017b). Network properties in transitions of consciousness during propofol-induced sedation. *Scientific reports*, 7(1):16791. 7, 10, 11, 12, 15, 16, 17, 50, 53, 54, 58, 85, 87, 139

Lehembre, R., Bruno, M.-A., Vanhaudenhuyse, A., Chatelle, C., Cologan, V., Leclercq, Y., Soddu, A., Macq, B., Laureys, S., and Noirhomme, Q. (2012). Resting-state eeg study of comatose patients: a connectivity and frequency analysis to find differences between vegetative and minimally conscious states. *Functional neurology*, 27(1):41. 54

Leon-Carrion, J., Leon-Dominguez, U., Pollonini, L., Wu, M.-H., Frye, R. E., Dominguez-Morales, M. R., and Zouridakis, G. (2012). Synchronization between the anterior and posterior cortex determines consciousness level in patients with traumatic brain injury (tbi). *Brain research*, 1476:22–30.

Lindner, M., Vicente, R., Priesemann, V., and Wibral, M. (2011). Trentool: A matlab open source toolbox to analyse information flow in time series data with transfer entropy. *BMC neuroscience*, 12(1):119.

Lumaca, M., Trusbak Haumann, N., Brattico, E., Grube, M., and Vuust, P. (2019). Weighting of neural prediction error by rhythmic complexity: A predictive coding account using mismatch negativity. *European Journal of Neuroscience*, 49(12):1597–1609.

MacLean, S. E. and Ward, L. M. (2014). Temporo-frontal phase synchronization supports hierarchical network for mismatch negativity. *Clinical Neurophysiology*, 125(8):1604–1617.

Magnin, M., Rey, M., Bastuji, H., Guillemant, P., Mauguière, F., and Garcia-Larrea, L. (2010). Thalamic deactivation at sleep onset precedes that of the cerebral cortex in humans. *Proceedings of the National Academy of Sciences*, 107(8):3829–3833.

McGill, W. (1954). Multivariate information transmission. *Transactions of the IRE Professional Group on Information Theory*, 4(4):93–111.

Mesgarani, N. and Chang, E. F. (2012). Selective cortical representation of attended speaker in multi-talker speech perception. *Nature*, 485(7397):233.

Moran, R. J., Stephan, K. E., Seidenbecher, T., Pape, H.-C., Dolan, R. J., and Friston, K. J. (2009). Dynamic causal models of steady-state responses. *Neuroimage*, 44(3):796–811.

Moran, R. J., Symmonds, M., Stephan, K. E., Friston, K. J., and Dolan, R. J. (2011). An in vivo assay of synaptic function mediating human cognition. *Current Biology*, 21(15):1320–1325.

Murphy, M., Bruno, M.-A., Riedner, B. A., Boveroux, P., Noirhomme, Q., Landsness, E. C., Brichant, J.-F., Phillips, C., Massimini, M., Laureys, S., et al. (2011). Propofol anesthesia and sleep: a high-density eeg study. *Sleep*, 34(3):283–291.

Näätänen, R., Paavilainen, P., Rinne, T., and Alho, K. (2007). The mismatch negativity (mmn) in basic research of central auditory processing: a review. *Clinical neurophysiology*, 118(12):2544–2590.

Nagasaka, Y., Shimoda, K., and Fujii, N. (2011). Multidimensional recording (mdr) and data sharing: an ecological open research and educational platform for neuroscience. *PloS one*, 6(7):e22561.

Nalatore, H., Ding, M., and Rangarajan, G. (2007). Mitigating the effects of measurement noise on granger causality. *Physical Review E*, 75(3):031123.

Niedermeyer, E. et al. (2005). The normal eeg of the waking adult. *Electroencephalography: Basic principles, clinical applications, and related fields*, 167:155–164.

Nielsen, T., Abel, A., Lorrain, D., and Montplaisir, J. (1990). Interhemispheric eeg coherence during sleep and wakefulness in left-and right-handed subjects. *Brain and cognition*, 14(1):113–125.

Nir, Y., Mukamel, R., Dinstein, I., Privman, E., Harel, M., Fisch, L., Gelbard-Sagiv, H., Kipervasser, S., Andelman, F., Neufeld, M. Y., et al. (2008). Interhemispheric correlations of slow spontaneous neuronal fluctuations revealed in human sensory cortex. *Nature neuroscience*, 11(9):1100.

Nolte, G., Ziehe, A., Nikulin, V. V., Schlögl, A., Krämer, N., Brismar, T., and Müller, K.-R. (2008). Robustly estimating the flow direction of information in complex physical systems. *Physical review letters*, 100(23):234101. 10

Ogilvie, R. D. (2001). The process of falling asleep. *Sleep medicine reviews*, 5(3):247–270. 56

Oizumi, M., Albantakis, L., and Tononi, G. (2014). From the phenomenology to the mechanisms of consciousness: integrated information theory 3.0. *PLoS Comput Biol*, 10(5):e1003588.

Pelli, D. G. and Vision, S. (1997). The videotoolbox software for visual psychophysics: Transforming numbers into movies. *Spatial vision*, 10:437–442.

Pérez-Garci, E., del Río-Portilla, Y., Guevara, M. A., Arce, C., and Corsi-Cabrera, M. (2001). Paradoxical sleep is characterized by uncoupled gamma activity between frontal and perceptual cortical regions. *Sleep*, 24(1):118–126.

Picchioni, D., Pixa, M. L., Fukunaga, M., Carr, W. S., Horovitz, S. G., Braun, A. R., and Duyn, J. H. (2014). Decreased connectivity between the thalamus and the neocortex during human nonrapid eye movement sleep. *Sleep*, 37(2):387–397.

Pollonini, L., Pophale, S., Situ, N., Wu, M.-H., Frye, R. E., Leon-Carrion, J., and Zouridakis, G. (2010). Information communication networks in severe traumatic brain injury. *Brain topography*, 23(2):221–226.

Sadaghiani, S. and Kleinschmidt, A. (2016). Brain networks and α-oscillations: structural and functional foundations of cognitive control. *Trends in cognitive sciences*, 20(11):805–817. 20

Salih, F., Sharott, A., Khatami, R., Trottenberg, T., Schneider, G., Kupsch, A., Brown, P., and Grosse, P. (2009). Functional connectivity between motor cortex and globus pallidus in human non-rem sleep. *The Journal of physiology*, 587(5):1071–1086.

Schartner, M., Seth, A., Noirhomme, Q., Boly, M., Bruno, M.-A., Laureys, S., and Barrett, A. (2015). Complexity of multi-dimensional spontaneous eeg decreases during propofol induced general anaesthesia. *PloS one*, 10(8):e0133532.

Schnakers, C., Vanhaudenhuyse, A., Giacino, J., Ventura, M., Boly, M., Majerus, S., Moonen, G., and Laureys, S. (2009). Diagnostic accuracy of the vegetative and minimally conscious state: clinical consensus versus standardized neurobehavioral assessment. *BMC neurology*, 9(1):35.

Schoffelen, J.-M. and Gross, J. (2009). Source connectivity analysis with meg and eeg. *Human brain mapping*, 30(6):1857–1865. 8, 15

Schreiber, T. (2000). Measuring information transfer. *Physical review letters*, 85(2):461. 3

Searle, J. R. (1993). The problem of consciousness. *Consciousness and cognition*, 2(4):310–319.

Sebel, P. S., Bowdle, T. A., Ghoneim, M. M., Rampil, I. J., Padilla, R. E., Gan, T. J., and Domino, K. B. (2004). The incidence of awareness during anesthesia: a multicenter united states study. *Anesthesia & Analgesia*, 99(3):833–839.

Seth, A. (2009). Explanatory correlates of consciousness: theoretical and computational challenges. *Cognitive Computation*, 1(1):50–63.

Simor, P., van der Wijk, G., Gombos, F., and Kovacs, I. (2018). Sharpening the paradox of rem sleep: cortical oscillations, synchronization and topographical aspects during phasic and tonic rem microstates. In *JOURNAL OF SLEEP RESEARCH*, volume 27. WILEY 111 RIVER ST, HOBOKEN 07030-5774, NJ USA. 7, 15, 50

Sitt, J. D., King, J.-R., El Karoui, I., Rohaut, B., Faugeras, F., Gramfort, A., Cohen, L., Sigman, M., Dehaene, S., and Naccache, L. (2014). Large scale screening of neural signatures of consciousness in patients in a vegetative or minimally conscious state. *Brain*, 137(8):2258–2270. 8, 9, 10, 11, 12, 15, 17, 22, 50, 53, 54, 62

Sivakumar, S. S., Namath, A. G., Tuxhorn, I. E., Lewis, S. J., and Galán, R. F. (2016). Decreased heart rate and enhanced sinus arrhythmia during interictal sleep demonstrate autonomic imbalance in generalized epilepsy. *Journal of neurophysiology*, 115(4):1988–1999.

Spoormaker, V. I., Schröter, M. S., Gleiser, P. M., Andrade, K. C., Dresler, M., Wehrle, R., Sämann, P. G., and Czisch, M. (2010). Development of a large-scale functional brain network during human non-rapid eye movement sleep. *Journal of Neuroscience*, 30(34):11379–11387.

Steriade, M., McCormick, D. A., and Sejnowski, T. J. (1993a). Thalamocortical oscillations in the sleeping and aroused brain. *Science*, 262(5134):679–685.

Steriade, M., Nunez, A., and Amzica, F. (1993b). A novel slow (< 1 hz) oscillation of neocortical neurons in vivo: depolarizing and hyperpolarizing components. *Journal of neuroscience*, 13(8):3252–3265.

Steriade, M., Timofeev, I., and Grenier, F. (2001). Natural waking and sleep states: a view from inside neocortical neurons. *Journal of neurophysiology*, 85(5):1969–1985.

Stockwell, R. (2007). Why use the s-transform. *Pseudo-differential operators: partial differential equations and time-frequency analysis*, 52:279–309.

Tang, C., Hamilton, L., and Chang, E. (2017). Intonational speech prosody encoding in the human auditory cortex. *Science*, 357(6353):797–801.

Téllez-Zenteno, J. F., Dhar, R., and Wiebe, S. (2005). Long-term seizure outcomes following epilepsy surgery: a systematic review and meta-analysis. *Brain*, 128(5):1188–1198.

Terry, J. R., Anderson, C., and Horne, J. A. (2004). Nonlinear analysis of eeg during nrem sleep reveals changes in functional connectivity due to natural aging. *Human brain mapping*, 23(2):73–84.

Timme, N. M. and Lapish, C. (2018). A tutorial for information theory in neuroscience. *eNeuro*, 5(3). 4

Tononi, G. (2004). An information integration theory of consciousness. *BMC neuroscience*, 5(1):42.

Toppi, J., Astolfi, L., Poudel, G. R., Babiloni, F., Macchiusi, L., Mattia, D., Salinari, S., and Jones, R. D. (2012). Time-varying functional connectivity for understanding the neural basis of behavioral microsleeps. In *2012 Annual International Conference of the IEEE Engineering in Medicine and Biology Society*, pages 4708–4711. IEEE.

Tsai, P.-J., Chen, S. C.-J., Hsu, C.-Y., Wu, C. W., Wu, Y.-C., Hung, C.-S., Yang, A. C., Liu, P.-Y., Biswal, B., and Lin, C.-P. (2014). Local awakening: regional reorganizations of brain oscillations after sleep. *Neuroimage*, 102:894–903.

Verweij, I. M., Romeijn, N., Smit, D. J., Piantoni, G., Van Someren, E. J., and van der Werf, Y. D. (2014). Sleep deprivation leads to a loss of functional connectivity in frontal brain regions. *BMC neuroscience*, 15(1):88.

Vinck, M., Oostenveld, R., Van Wingerden, M., Battaglia, F., and Pennartz, C. M. (2011). An improved index of phase-synchronization for electrophysiological data in the presence of volume-conduction, noise and sample-size bias. *Neuroimage*, 55(4):1548–1565. 7, 8, 11, 15, 16, 21, 22, 50, 57, 61, 62, 95

Voss, U., Holzmann, R., Tuin, I., and Hobson, A. J. (2009). Lucid dreaming: a state of consciousness with features of both waking and non-lucid dreaming. *Sleep*, 32(9):1191–1200.

Wang, K., Steyn-Ross, M. L., Steyn-Ross, D. A., Wilson, M. T., and Sleigh, J. W. (2014). Eeg slow-wave coherence changes in propofol-induced general anesthesia: experiment and theory. *Frontiers in systems neuroscience*, 8:215.

Winterhalder, M., Schelter, B., Hesse, W., Schwab, K., Leistritz, L., Klan, D., Bauer, R., Timmer, J., and Witte, H. (2005). Comparison of linear signal processing techniques to infer directed interactions in multivariate neural systems. *Signal processing*, 85(11):2137–2160.